Republic of Iraq
Ministry of Higher Education
And Scientific Research
University of Babylon
College of Materials Engineering
Department of Metallurgical Engineering

Enhancing the Corrosion Resistance of Ti+35wt%Nb Shape Memory Alloy used for Biomedical Applications.

A Dissertation
Submitted to the Council of the Collage of Materials Engineering / University of Babylon in Partial fulfillment of the Requirements for the Master Degree in Materials Engineering / Metallurgy

By

Zahraa Hussein Khalaf Salman

(B.Sc. In Metallurgical Engineering, 2016)

((DipHE. In Metallurgical Engineering, 2020)

Supervised by

Prof. Dr. Nawal Mohammed Dawood

Assit prof. Sundus Abbas Jasim

2023 A.D **1444 A.**

وزارة التعليم العالي والبحث العلمي
جامعة بابل
كلية هندسة المواد
قسم هندسة المعادن

تعزيز مقاومة التآكل لسبيكة (Ti+35wt%Nb) ذاكرة الشكل المستخدمة في التطبيقات الطبية

اطروحة

مقدمة إلى مجلس كلية هندسة المواد/ جامعة بابل وهي جزء من متطلبات نيل شهادة الماجستير في هندسة المواد/ المعادن

من قبل

زهراء حسين خلف سلمان

(بكالوريوس هندسة معادن٢٠١٦)

(دبلوم عالي هندسة معادن ٢٠٢٠)

باشراف

أ.د نوال محمد داوود

أ. م سندس عباس جاسم

٢٠٢٣م ١٤٤٤هـ

بسم الله الرحمن الرحيم

﴿نَرْفَعُ دَرَجَاتٍ مَنْ نَشَاءُ وَفَوْقَ كُلِّ
ذِي عِلْمٍ عَلِيمٌ﴾

صدق الله العظيم

سورة يوسف : الاية (٧٦)

Dedication

To:

The Spirit of my mother and My father

My husband and children

My sisters and brothers

To the present in our hearts absent from our eyes, my grandmother, may God bless her.

With love and respect

Zahraa

Acknowledgments

First of all, profusely all thanks be for ***ALLAH*** who enable me to achieve this work.

I would like to express my gratitude to my supervisors **Prof .Dr. Nawal Mohammed Dawood** ***and Assit. prof Sundus Abass Jassim*** for her enthusiasm and support. His suggestions, guidance and moral support in difficult times have been essential for completing this work. Special thanks are to my friend engineer Kalthoum Obeid to help me all the time.

also thank my department, Metallurgical Engineering and my College, Materials Engineering, for their help and good facilities.

Finally, I would like to thank the staff of the workshop materials lab. in Babylon University

Zahraa hussien

Supervisor Certificates

we am Certify that this thesis, entitled **(Enhancing the Corrosion Resistance of Ti+35wt %Nb Shape Memory Alloy used for Biomedical Applications**) was prepared by **(zahraa hussien khalaf)** under our supervision at the department of metallurgy engineering / College of Materials Engineering / University of Babylon in partial fulfillment of the requirements for the degree of Master of Science in Material's Engineering/ Metallurgical

Signature	Signature
Prof. Dr.Nawal Mohammed Dawood	Assist prof. Sundus Abbas Jasim
Date / /2023	Date / / 2023

وزارة التعليم العالي والبحث العلمي
استمارة مستخلص اطاريح الدراسات العليا للجامعات العراقية

رقم الاستمارة:	

الجامعة: جامعة بابل	الكلية: هندسة المواد
القسم: هندسة المعادن	التخصص الدقيق:

عنوان الرسالة او الأطروحة: تعزيز مقاومة التآكل لسبيكة(Ti+35wt%Nb) ذاكرة الشكل المستخدمة في التطبيقات الطبية	تاريخ تسجيل الرسالة او الاطروحة:	(١)طبيعة البحث:اكاديمي	الجهة المستفيدة:جامعة بابل تاريخ العقد:

(٢)اسم الطالب: زهراء حسين خلف سلمان	العمر: ٢٩ سنة	الجنس:انثى	(٤) جهة الانتساب:
تاريخ القبول: ٢٠٢٠-٢٠٢١		(٣) قناة القبول: عام	

اسم المشرف	الدرجة العلمية	الجنس	جهة الانتساب	العمر
١-نوال محمد داوود ٢-سندس عباس جاسم	١-استاذ ٢-استاذ مساعد	١-انثى ٢-انثى	وزارة التعليم العالي والبحث العلمي	١-٤٧ ٢-٥١

(١) تحديد طبيعة البحث اكاديمي او تطبيقي وفي حالة البحث التطبيقي يذكر اسم الجهة المستفيدة وتاريخ ابرام العقد.

(٢) يذكر الاسم الرباعي واللقب او كما ورد في الرسالة او الاطروحة.

(٣) تذكر قناة القبول(متميزين ، قبول مباشر ، وافدين ، حجز).

(٤) جهة الانتساب تذكر الوزارة او الجهة للطالب الموظف.

تاريخ صدور الأمر الجامعي:		الشهادة:	ماجستير	الاختصاص العام:		الاختصاص الدقيق:	

	الكلمات المفتاحية

المستخلص بلغة الاطروحة

. في هذة الدراسة تم تحضير جميع السبائك بواسطة تقنية المتلورجيا المساحيق ومن ثم اضافة عناصر السبك (الزركونيوم والسليكون)بنسب مختلفة (٢,٥و ٣,٥ و٤,٥) (٠,٤و٠,٨و(١,٢) نسب وزنية على التوالي الى سبائك الرئيسية من اجل دراسة تاثير هذه العناصر على الخصائص البنية المجهرية (EDS,XRD,SEM ,DSC,XRF) والمجهر الضوئي ،المسامية والخواص الكهروكيميائية (جهد الدائرة المفتوحة والاستقطاب) وخواص ميكانيكية (الضغط والصلادة واختبار البلى الجاف) لهذة السبائك تم تحديد الضغط على ان ٧٠٠ ميغا باسكال وتم التلبيد السبائك الخضراء عند ١١٠٠ درجة مئوية لمدة ست ساعات في الغاز الخامل الاركون ومن ثم تترك العينات لتبرد في الفرن وايضا تم دراسة تاثير المعاملة الحرارية على خصائص السبيكة Ti-35Nb تظهر النتائج ان نسبة المسامية تنخفض تدريجيا مع الزيادة في كل من Zr ,Si تضهر النتائج الاكس ري ان السبائك الاساسية بعد المعالجة الحرارية تتكون من مرحلتين هي بيتا والفا في درجة حرارة الغرفة .تتناقص شدة طور الفا تدريجيا مع زيادة محتوى Zr ,Si لانهما يعتبران من مثبتات طور بيتا .تقلل من درجة حرارة الانتقال عن طريق تثبيت طور بيتا .اضهرت نتائج اختبار الDSC ان درجات الحرارة للتحول ان درجات التحويل Ms انخفضت بعد عملية الاضافة وبعد عملية المعاملة الحرارية للسبيكة الاساسية كما اضهرت نتائج الSME تحسن بعد اضافة ال Zr , Si بعد عملية المعاملة الحرارية .تؤدي اضافة العناصر الى قيم صلادة عالية بلمقارنة بلسبائك الرئيسية .تزداد مقاومة التاكل عند اضافة كل من السليكون و الزركونيوم لكن مقاومة التالكل للسبائك الرئيسية عند اضافة الزركونيوم اعلى مقارنة بمقاومة التاكل عند اضافة السليكون .كما اضهرت نتائج اختبار الغمر في محاليل البلازما ان كمية تحرر ايون المعدن تنخفض بشكل كبير بعد اضافة ال Zr ,Si وبعد المعالجة الحرارية

توقيع المشرف على الرسالة او الاطروحة	توقيع المشرف على الدراسات العليا

Table of Content

Chapter Three: Experimental Part

Chapter Four Results and Discussion

Chapter Five: Conclusions & Recommendations

Examining Committee Certification

We certify that we have read this thesis **(Enhancing the Corrosion Resistance of Ti+35wt%Nb Shape Memory Alloy used for Biomedical Applications)** and examining committee, we have examined the student **(Zahraa Hussien Khalaf Salman)** in the content and that in our opinion it meets the stander of a thesis for the Master degree in Material Engineering / Metallurgical Engineering.

Signature

Prof. Dr. Abdulraheem K. Abid Ali

Date / /

Committee Chair

Signature
Assist prof Dr. Ali Mundher Mustafa
Date / / 2023
Committee Member

Signature

Prof. Dr. Haydar H. J.Jamal Al-Deen

Date: / / 2023
Committee Member

Signature
Prof . Dr.Nawal Mohammed Dawood
Date / /2023
Supervisor

Signature
Assist prof. Sundus Abbas Jasim
Date / / 2023
Supervisor

Approval of the Department Metallurgical Engineering

Head of Metallurgy Engineering Department

Approval of the College of Materials Engineering

Dean of the College of Materials Engineering

Signature
Prof. Dr. Saad Hameed Al-Shafaie
Date: / /2023

Signature
Prof. Dr. Imad Ali Disher
Date: / /2023

Abstract

In the present study, Ti-35wt%Nb alloy prepared by powder metallurgy technique, a various amounts of Zirconium (3.9, 5.4, and 6.9 wt%) and Silicon (0.2 ,0.4 ,0.6 wt %) added to the base alloy. The compact pressure was 700 MPa and the green compacts sintered at 1100°C for 6h in inert gas (Argon), then the specimens cooled in the furnace. The effect of heat treatment on the properties of Ti-35Nb shape memory alloy was studied. Also the microstructure was characterized using (scanning electron microscope combined with energy dispersive X-ray spectroscopy, X- Ray Diffraction Analysis, X ray Fluorescent Analysis, Differential Scanning Calorimeter and light Optical microscope). The mechanical properties (Compression, Hardness, and dry wear test), electrochemical (Open circuit, and Polarization tests), and toxicity (Static immersion test) was also study.

Results appear that the porosity percentage decreases gradually with increasing both (Zr and Si) additions. The XRD results show that the base alloys and base alloy after heat treatment consist of two phases (β phase) and (α-phase) at room temperature. The presence of both α and β phase is evident in an alloy with additive Zr and Si. The primary α phase diminishes gradually as the Zr and Si content increases because Zr and Si β stabilizers depress the transition temperature by stabilizing the β phase. The results of transformation temperatures DSC test showed that the transformation temperatures, Ms decreased after adding Zr, Si and after heat treatment for base alloy. The results of shape memory effect showed that the shape effect improved after adding (Zr and Si) and after heat treatment where the improvement ratio is (56.66, 76.36 and 70.44) % respectively.

The addition of Zr, and Si leads to higher values of hardness compared with the master alloy, where the improvement of percentage for highest percentage of addition of Zr, Si and after heat treatment process of base

alloy was (48.55%, 29.6%, 72.4%) respectively. The wear resistance increases with the addition of Zr and Si where the improvement of wear rate for C3 alloy at 10 N reached 73% and 50 % at load 15 N, respectively, while the improvement percentage for D3 was (86.5%) and (76.5 %) at load (10, 15) N, respectively. The compressive strength of Ti-35%wt Nb alloy increases with increases Zr, and Si elements addition, but the compressive strength of master alloys with Zr additives is higher compared with master alloys with Si additives, where the improvement ratio is (57.62%) for C3 alloy while it is equal (34.31%) for D3 alloy. After the heat treatment process the compression strength improves significantly where the percentage of improvement (50.40%).

Due to the formation of the inert protective layer on the surface of the metal after the heat treatment process and after the addition of the elements (Zr and Si) it improves in corrosion resistance of Ti-35Nb alloy in Simulated body fluid and Hank's solutions. It was shown that higher improvement with the addition of the 6.9 % wt. Zr, the improvement was reach (176.8%) in Hank's solution, while the higher improvement in Simulated body fluid was (53%) for 0.6 wt.% Si. Also the results of immersion test in Simulated body fluid and hanks solutions showed that the amount of metal ion release significantly decrease after Zr and Si additions and after the heat treatment. The contact angle of the specimen decreases dramatically after heat treatment and addition Zirconium and Silicon.

44-1288 Wavelength= 1.540598 C

β-Ti

Titanium

2θ	Int	h	k	l
38.482	100	1	1	0
55.543	12	2	0	0
69.607	17	2	1	1
82.447	4	2	2	0
94.927	5	3	1	0
107.628	1	2	2	2
121.308	6	3	2	1
137.462	1	4	0	0
162.567	4	4	1	1

Rad.: CuKa1 λ: 1.540598 Filter: d-sp: Calculated

Cut off: Int.: Calculated I/Icor.: 8.679

Ref: Calvert, L., Lakes Entrance, Victoria, Australia, Private Communication, (1993)

Sys.: Cubic S.G.: Im3m (229)

a: 3.3065 b: c: A: C:

α: β: γ: Z: 2 mp:

Ref: Eppelsheimer, D., Perman, R., Nature (London), 166, 960 (1950)

Dx: 4.401 Dm: SS/FOM: F_9 = 66(.0152, 9)

High temperature phase, stable above 1153 K. W type. PSC: cI2. Mwt: 47.90. Volume[CD]: 36.15.

44-1294 Wavelength= 1.54056

Ti

Titanium

Rad.: CuKa1 λ: 1.54056 Filter: Graph Mono d-sp: Diff.

Cut off: 15.0 Int.: Diffract. I/Icor.: 0.9

Ref: Sailer, R., McCarthy, G., North Dakota State University, Fargo, North Dakota, USA, ICDD Grant-in-Aid, (1993)

Sys.: Hexagonal S.G.: $P6_3/mmc$ (194)

a: 2.9505(1) b: c: 4.6826(3) A: C: 1.5871

α: β: γ: Z: 2 mp:

Ref: Ibid.

Dx: 4.506 Dm: SS/FOM: F_{17} = 387(.0026, 17)

Color: Gray
Peak height intensity. Sample was obtained from A.D. Mackay Inc. CAS #: 7440-32-6. Average relative standard deviation in intensity of the ten strongest reflections for three specimen mounts = 6.7%. Mg type. Silicon used as an internal stand. PSC: hP2. Validated by calculated pattern. To replace 5-682. Mwt: 47.90. Volume[CD]: 35.30.

2θ	Int	h	k	l
35.093	25	1	0	0
38.421	30	0	0	2
40.170	100	1	0	1
53.004	13	1	0	2
62.949	11	1	1	0
70.661	11	1	0	3
74.157	1	2	0	0
76.218	9	1	1	2
77.368	6	2	0	1
82.290	1	0	0	4
86.759	1	2	0	2
92.729	1	1	0	4
102.361	2	2	0	3
105.798	1	2	1	0
109.042	4	2	1	1
114.278	3	1	1	4
119.256	1	2	1	2

1.1. General View

Biomaterials are those materials intended to interface with biological systems, either to replace, reconstruct, enhance or support either tissues or tissue function. Biomaterials have typically been metallic, ceramic and polymeric. Metallic materials are being used for long for prostheses; ceramic specially hydroxyapatite has been used for bone reconstruction, and polymeric materials have been found for innumerable applications, from surgical sutures and surgical glues to contact lenses, heart valves, etc, [1]. Biomaterials are divided into two types: biological and biomedical biomaterials; every type can be divided into subdivision as shown in figure (1.1)

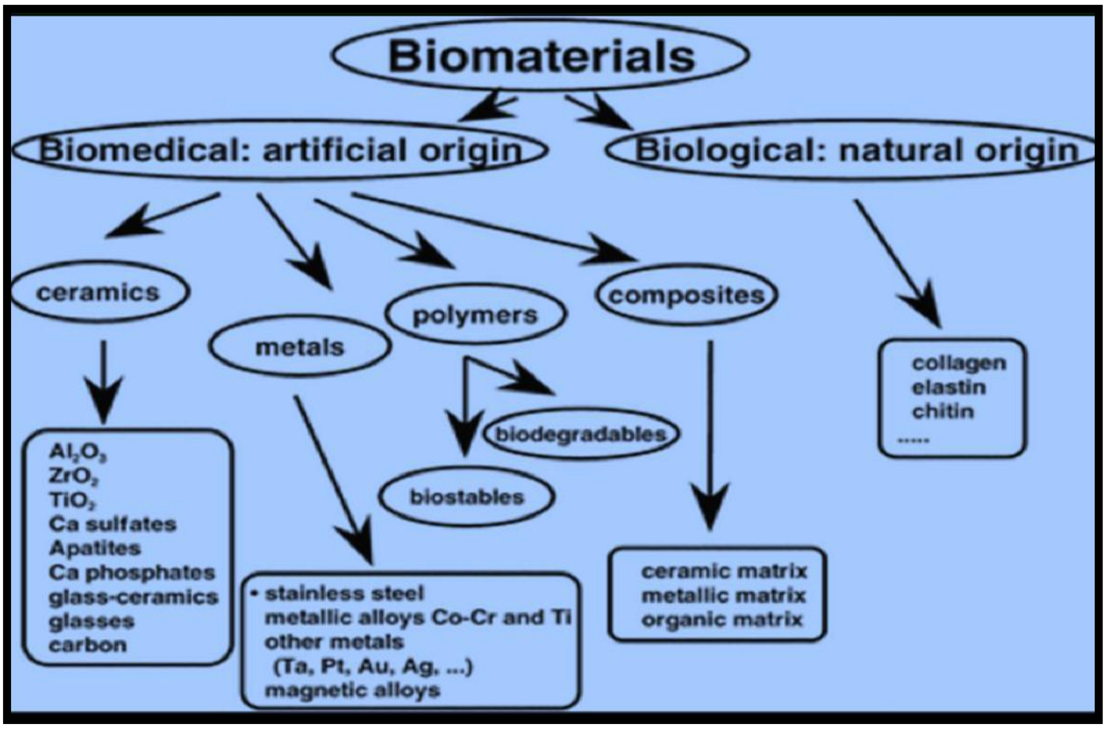

Figure (1.1) Types of Biomaterials [1].

In the past decade, β type titanium (Ti) alloys were widely investigated owing to their low Young's modulus, high strength, high corrosion resistance, and good biocompatibility. Non-toxic elements, such as niobium (Nb), molybdenum (Mo), zirconium (Zr), tantalum (Ta), and stannum (Sn), were added to achieve low Young's modulus and good mechanical properties [2-5]. These metastable β type Ti alloys with non-toxic and allergy-free elements become attractive since the allergic reactions of nickel (Ni) ions released from Ni–Ti alloy was eliminated [6].

Ti-Nb has considered being the most popular Ti-based alloy in many years ago because the appropriate properties: biocompatibility and pseudoelasticity are used for medical implant. Among Ti alloys, β alloys exhibit the lowest elastic modulus and wear resistance as well as a high hardenability [7]. Nb is a β phase stabilizer that increases ratio of the β/α phase and maintains advantageous mechanical characteristics [8, 9]. Ti-Nb based alloys draw a considerable attention for biomedical applications not only due to their non-toxicity, good corrosion behavior and biocompatibility, but also due to the presence of Nb that is reported as favorable for ontogenesis, cell adhesion, proliferation, and differentiation in vitro [10,11]. Table below show the properties of Ti-Nb alloy. In any case, the pseudoelasticity is in sufficient for the real applied usage. Consequently, the third element alloys was researched to prove some weakness of the former alloy. A variety of third-element alloys have been approved in many past decades for instance Ti-Nb- Zr[12], Ti-Nb-Ta[13] and Ti-Nb-Al [14].

Table (1.1) Show Titanium Niobium Alloy Properties

Compound Formula	TiNb
Molecular Weight	140.733
Appearance	Metallic solid in Various forms (plate, sheet, ingot, Custom parts)
Melting point	1900°C
Boiling point	N/A
Density	5.7g/cm3
Solubility in H2O	N/A
Specific Heat	0.427J/g.°C
Tensile strength	Ultimate :450 MPa (at RT)
Thermal conductivity	10 W/m.k
Thermal expansion	9.03 *10^-6/°C

1.2. Shape-memory alloys.

Shape-memory alloy (SMA) is a smart material that has the ability to return to its pre-deformed size and shape via either the application of heat, (because of shape memory effect), or elimination of the load, (because of super elastic effect) [15]. The capability of SMAs to regain their shape is due in part to the ordered crystalline structure between the phases of austenite and martensite that enables the material to undergo a displacement (diffusionless) martensitic phase transition as a result of temperature change or applied stress. Other microstructural features, like precipitate formation, dislocation development, and grain texturing also affect the properties of SMAs and encourage the shape recovery process. Super-elastic SMAs have been shown to develop a flag-shaped hysteresis under cyclic axial loading at a macroscopic level [16], which can provide both a more recent and supplementary energy dissipation as seen in figure (1.2) [17].

SMAs are extensively used in biomedical applications. Orthodontic wires, catheters and intravascular stents are particular examples of medical devices that benefit from the shape memory effect in these unique alloys [18].

NiTi alloys (Nitinol), are widely used as shape memory alloy The Ti-Ni alloys have been successfully applied as biomaterials such as orthodontic arch wires, guide wires and stents in addition to many engineering applications. Ti-Ni alloys are also considered as one of the attractive candidates for orthopedic implants, etc. However, it has been pointed out that pure Ni is a toxic element and causes Ni-hypersensitivity. Although the Ti-Ni alloys are considered as safe in the human body based on experience and scientific consideration, in order to solve the psychological problem on the risk of Ni hypersensitivity, Ni-free Ti-based SM and SE alloys have been recently developed, e.g., Ti-Nb-Sn, Ti-Nb-Al, Ti-Nb-Ta, Ti-Nb -Zr, Ti-Nb-O, Ti-Nb-Pt, Ti-Mo-Ga, Ta-Mo-Sn and Ti- (8-10) Mo -4Nb-2V-3Al. It has been found that Ti-Nb binary alloys exhibit SME and SE at room temperature, and their SE properties can be considerably improved by thermomechanical treatment. It has been also found that SE properties of Ti-Nb alloys can be improved by the addition of alloying elements such Zr, Ta, Pt and O.

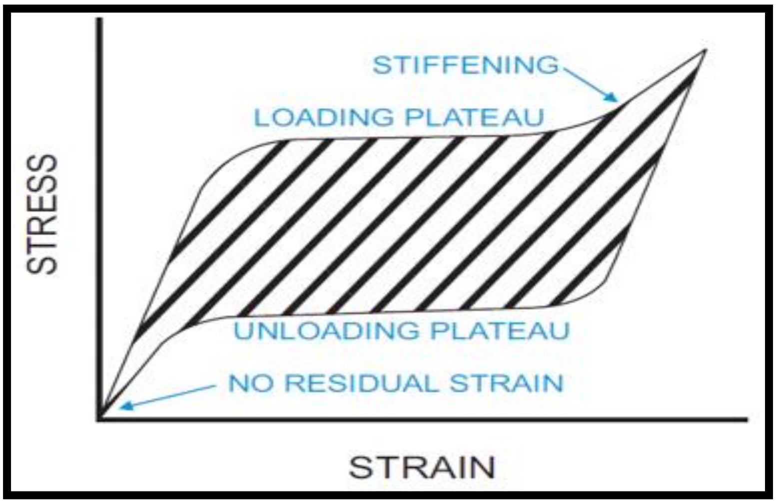

Figure (1.2): Idealized Superelastic Shape Memory Alloy Stress-Strain Behavior [4]

1.3 . Biomedical Applications of Shape Memory Alloys.

In recent years it became clear that the largest commercial successes of SMAs are linked to biomedical application. The combination of good biocompatibility, good strength and ductility with the specific functional properties such as shape memory effect and superelasticity creates a unique material for medical applications. Especially the superelastic effect of SMAs results in unique combination of high strength, high stiffness and high pliability; no other material or technology can offer this unique combination [19] . The followings, some medical applications of SMAs.

1.3.1. Cardiovascular application

• Angiography : A medical imaging procedure used to image the interior of the blood vessels and organs of the body, with a particular interest in the arteries, veins, and chambers of the heart, is angiography or arteriography. The procedure includes the application to the heart chamber or coronary artery of a radiopaque contrast medium through a catheter [20].

• **Angioplasty** is a form of treating an artery or blood vessel with stenosis or blockage to restore natural blood flow. Stents are the instruments used to "open" the narrowed artery or blood vessel. Also, stents are classified into two categories: expandable balloon stents and self-expandable stents, with the latter being more widely used. The SME plays an important role here because the martensitic stent is compressed to be directed to the desired position and recovers its original shape at the temperature of the inner body when released from the catheter, supporting the wall of the vessel and allowing normal circulation, as shown in figure (1.3) [21].

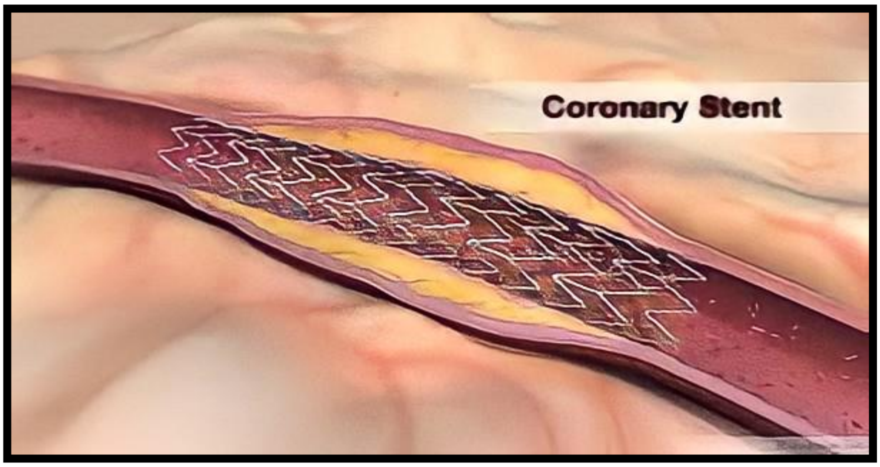

Figure (1.3): A stent that has been used to open the coronary artery [21]

• **Atrial Septal Defect**: is a situation where there is a hole or defect in the wall between the left and the right atria of the heart which consequently leads to oxygen-rich blood from the left side to mix with oxygen-poor blood on the right side thus depriving the organs and the brain from the proper amount of oxygen and in the long term this may be lethal [22].

1.3.2. Orthopedic applications

The devices developed for orthopedic applications are used to support injured, weakened or fractured bones. One such applications is the spinal vertebra spacer, see Figure. (1.4), which is used to provide local reinforcement to the Vertebrae and prevent motion during the healing process [23]. The device applies a constant force on the joint, hence will provide flexibility

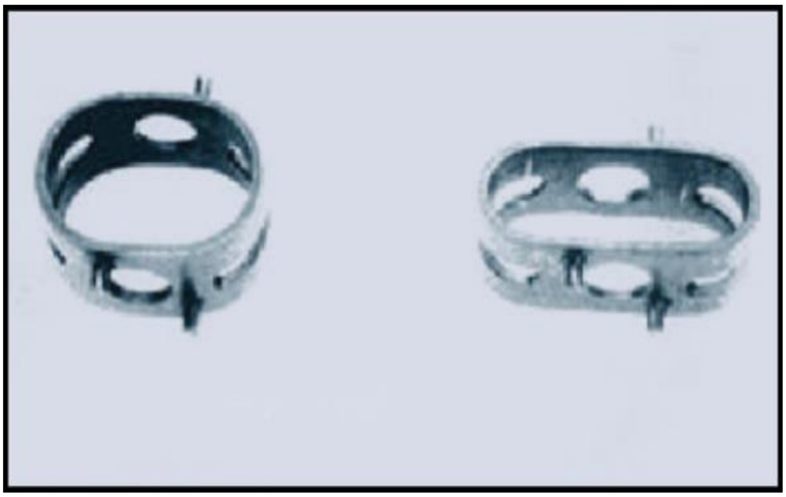

Fig. (1.4) Martensitic state shape memory spacers (left) and their original form (right) (right) [24].

In orthopedic applications, bone plate is used in surgical treatment of broken bones as shown in Figure. (1.5). The plates based on the SME have been developed to allow for a constant and uniform constraint on the two sections of the broken bone. The continuous pressure between the two parts of the bone encourages rapid healing as well as a quick recovery of mobility compared to traditional surgical techniques. Like synthetic bone plates, compression stables are used to set broken bones and promote healing. They are implanted directly into the area of the break to compress the two parts of the bone. Nails for marrow cavity stimulate the osteosynthesis where long bones, such as the femur, are broken [25].

The current surgical procedure to treat the break consists of hollowing out the bone marrow cavity of the two bone sections followed by the reconnection and insertion of a nail to allow the healing of the break. The nail is made of an SMA stem with soft polymer ends that completely fill the cavity and prevent relative movement of the bone. [2 6].

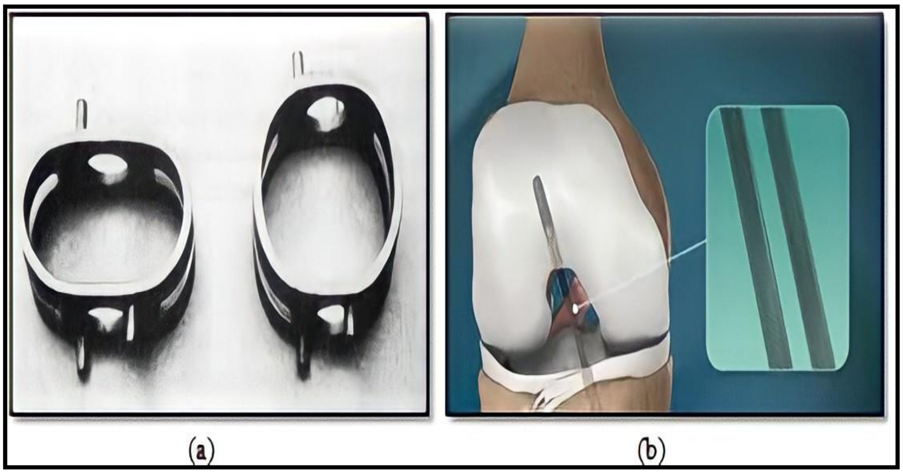

Fig. (1.5) Orthopedic plates [27].

The porous nature of the material enables the existing bone tissue to migrate inward, increasing bonding strength. Furthermore, the implant properties (Stiffness and porosity) can be engineered to match those of bone. [28,29].

1.3.3. Dentistry:

The range of applications for SMAs has grown over the years, a major area of development being dentistry. One example is the prevalence of dental braces using SMA technology to exert constant tooth-moving forces on the teeth; the nitinol archwire was developed in 1972 by orthodontist George Andreasen. This revolutionized clinical orthodontics and has also had an effect on fiber optic development. Andreasen's alloy has a patterned shape memory, expanding and contracting within given temperature ranges because of its geometric programming [30].

(a) the archwire (b) expanded palate

Figure (1.6): Orthodontic applications [31, 32].

1.3.4. Applications to surgical instruments

Medical industry lately, medicine and has concentrated on the notion of minimal invasive surgical procedures**.** These devices are useful in many interventional and endoscopic procedures. The basic applications for surgical instruments are: guide wires, devices for laparoscopy, catheters, snares and basket which is used for kidney and bladder stones removing [33.34].. Different type of endoscope showed in figure (1.7) [24].

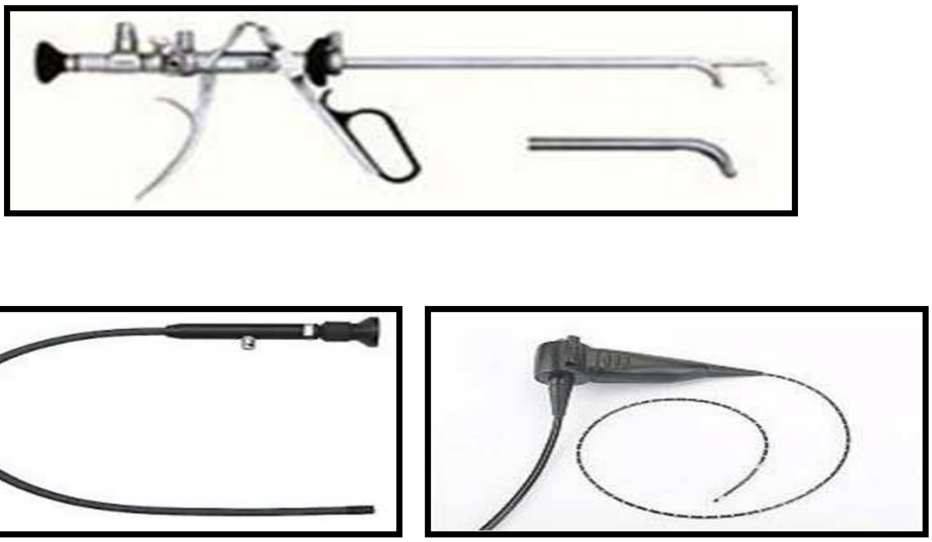

Fig. (1.7) a few types of endoscopic (a) stiff endoscopic, (b) Flexible endoscopy and (c) Semi–flexible endoscopy [24].

1.4. Objectives of the Work

The aim of this study are:

1- Study the effect of Zirconium and Silicon addition with different percentage on mechanical properties as hardness and wear resistance.

2-Modulus of elasticity was important for beta type Ti-Nb alloys so the effect of Zirconium and silicon addition with different percentage on modulus of elasticity of prepared alloy was studied

3-Corrosion rate and ion release of the prepared alloy was studied also.

4-Study the effect of heat treatment on physical , mechanical , modulus of elasticity and corrosion resistance of the prepared alloy.

5-Make a compartion between elements additions and heat treatment on properties of prepared alloy.

2.1. Introduction

This chapter covers a general view about titanium and its alloy used in implants and about bone structure. There will be a focus on their chemical compositions which will include biomaterials, mechanical properties, biocompatible, osseointegration and biology of wound healing following implant placement, corrosion behavior and types of corrosion, wear properties, shape memory alloy and properties of shape memory alloy, effects of alloy types of titanium alloys, phase diagram of Ti-Nb, alloying elements in Ti alloys such as zirconium Nibuom, and silicon, and titanium alloy processing are included casting and powder metallurgy blending and mixing of the powders, compacting and sintering). Finally, the end of this chapter will cover up some of the recent researches and studies about titanium alloys.

2.2. Requirements and Limitations of Biomaterials.

The selection of biomaterial must address at least three criteria. The first being biocompatibility in which the material must be able to function and perform with an appropriate host response in a specific situation [35] that is not harmful or toxic to the living tissues in the human body. Secondly, it should be strictly inert chemically to discourage passivation or corrosion that facilitates removal or revision surgery. Lastly, it depends on the intended medication application whether the implant should be resorbable over time or osseointegrate with the host bone, promoting bone ingrowth at the implant surface or securely linking the bone to the surface of the implant [36].

2.2.1. Mechanical Properties.

The mechanical properties like tensile strength, hardness, modulus, elongation (strain), fracture resistance and fatigue strength or life play an important role in material selection for application in the human body [36]. The material to replace bone is required to have stiffness matches the bone, which is shown in table (2.1). It is targeted to prevent inadequate strength or mismatch of stress (stress shielding) between the living bone and implant that lead to crack nucleation and fracture. The material aimed to replace bone is expected to have modulus ranges from 4 to 30 GPa within a variety of bone type and the angles or phases of measurement [37].

Table (2.1): Mechanical properties of human bones [38]

	Yield strength, MPa	Ultimate strength, MPa	Elastic Modulus, GPa	Elastic strain, %	Density, g/cm^3
Fibula	-	80-100	15.2-19.2	1.19-2.10	1.73-1.91
Humerus	-	149-151	15.6-16.1	1.90-2.20	1.72-1.77
Tibia	129	84-156.71	16.2-23.83	1.56-3.09	1.83-1.96
Femur	114.14	68-141	13.6-16.8	1.07-2.83	1.80-1.91

2.2.1.1 Stress Shielding

problem of current implant materials that is related to mechanical factor is of high stiffness. In this scenario, the implant shields the adjacent bones from the stress transferred, thereby preventing bone from functioning and thus causing bone resorption and consequently implant loosening. This phenomenon is called the stress shielding effect which leads to bone cells death [39]. Cases of stress shielding effect are normally observed in medial side of proximal femur after hip replacement, or under tibial implant [36]. Thus, selection of material with optimized coexistence of sufficient strength yet Young's modulus closest to bone is vital in promoting a good quality and durable implant. To avoid stress shielding, more flexible components have been proposed [40]. Current research has shown improvements especially in Young's modulus and strength/ductility balance of metallic biomaterials. However, a high flexible metal may create unsustainable interface stresses between bone and implants and eventually damage accumulation in cemented implants or failed ingrowth within cement less implants [36]. Young's modulus is most extensively researched because of its close connection to alleviate stress shielding that causes bone atrophy and poor bone remodelling [41]. Therefore, many scientists and engineers have been since developing materials with comparative Young's modulus to bones and sufficient structural strength to be used in prostheses.

2.2.1.2 Wear of Metallic Biomaterials.

Property of wear property can be defined as damage to a solid surface, including progressive loss of material because relative motion between that surface and a contacting substance or substances as shown in Figure (2.1). Recently main concern, for further development of metallic implant materials is among others, stress transmission between hard tissue and metallic implant components which are in contact since further bone degradation and bone adsorption should be avoided. Namely, a great difference between bone and metallic implant materials hardness and other mechanical and tribological characteristics may lead to further bone loss and degradation [42].

The process of wear can rupture the protective oxide film inherently present on the alloys surface, which can lead to accelerated attack in the presence of a corrosive environment [43]. .

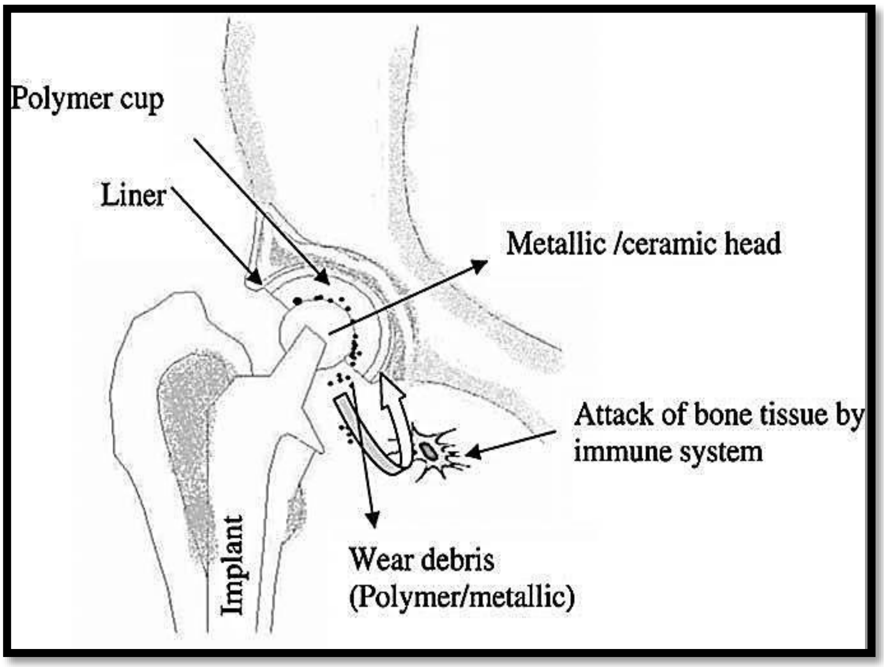

Figure (2.1): Wear of Total Joint Replacements

2.2.1.3. Wear Testing Methods ...

Given the aforementioned limitations, especially in terms of the tribological properties, it is important to characterize the wear and friction of developed biomaterials using a suitable test methodology. The methods that are most commonly used in the study of the wear behavior of metallic biomaterials are the pin-on-disc, block-on-disc and ball-on-disc [44]. Table (2.2) summarizes the advantages and disadvantages of various wear test configurations [45]

Table (2.2): Advantages and Disadvantages of Different Wear Test Configurations

Test	Advantages	Disadvantages	Test format
Pin-on-Disk	After run-in, surface pressure remains constant. Easy to determine wear volume and wear rate.	Difficult to stratify the pin. Suppose the pin does not stand perfectly vertical on the plate, the edge contact results. A very long run-in time is therefore necessary. The front edge of the pin can skim off lubricant. This makes a defined lubrication state impossible.	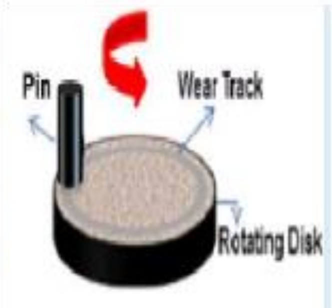
Ball-on-Disk	High surface pressures are possible. The ball skims off lubricant less than a pin does. The model is similar to a linear friction bearing and a radial friction bearing.	Minimal contact ratio: The contact surface of the ball is small compared to the sliding track on the disk. The contact area is enlarged by wear. Difficult to determine the wear volume of the ball.	
Block-on-disc	The model is capable of simulating a variety of harsh field conditions, e.g., high temperature, high speed, and high loading pressure.		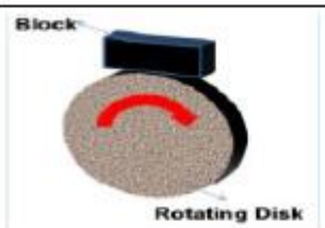

2.2.3.4. Wear Mechanisms

Understanding of wear mechanisms is very important so as to design materials which are suitable for the reduction of wear [46]. Wear mechanisms generally can be grouped into six generic types:

1- Adhesive Wear. The wear of adhesive is caused by the surface interaction and welding of the junctions at the sliding contact. This mechanism of wear is affected by the bonding type (metallic, ionic, covalent and van der Waals) in the contact junction. The weaker part of the materials in contact is removed and transferred to the counter surface if the bond in the junction is stronger than the bond in the bulk. Surface removal results in a rough appearance and a large volume of worn material, thereafter, severe wear [46].

2- Delamination Wear The debris is plates, the length to the thickness is ten times caused by forming and fracture such as a cylinder in internal combustion machining may by occur in abrasive wear. It is seen that the ductility increases the strength of material against delamination [45].

3- Fatigue Wear: The debris of wear is generated by cyclic loading of the contact. Fatigue wear can be characterized by crack formation and flaking of surface material [46].

4-Erosion Wear: Caused by impact of solid or liquid or gaseous particles form losses in weight or removal of particles in which the fluid carry the particles .it is depended on the kinetic energy for particles and the emission of the energy on the surface [46].

5-Tribochemical Wear: Tribochemical wear results from the removal of reaction products/layers formed in situation from the contacting surface [46].

6-Abrasive Wear. The remove of material by hard particles slide between two surfaces in relative motion. The surface deforms plastically and grooves are produced in the surface [47]. More than one type of mechanism can be involved in a wear situation. Also, these individual mechanisms can interact sequentially to form a more complex wear process. However, one mechanism generally is the controlling and primary mechanism. The relative importance or occurrence of individual mechanisms can change with changes in tribosystem parameters. Therefore, materials can exhibit transitions in wear behavior as a result of changes in other operational parameters, such as load, velocity, and friction [48].

2.2.2.Biocompatibility.

It is essential that the metallic biomaterials that are used in medical implants to be biocompatible, nontoxic and not causing any inflammatory or allergic responses in the body. An implant may cause alteration mechanically or chemically in its adjacent environment or systemically, such as materials degradation in vivo and the human body reaction towards the implant [49].

Three groups of responses from the human body towards biomaterials are biotolerant, bioactive and bioreabsorbable. The exposure of the implants to human tissues and fluids will result in reactions that will determine either the body system accept or reject the implant [50]. There are four reactions that happen more frequently than any other cases.

Firstly, the protein absorption, whereby protein immediately spread over the outer layer of the implant and controls the response of the host, including cells and tissues. Secondly is the degradation of material in whereby a metallic implant corrodes, a ceramic implant is resorbed or the occurrence of polymer hydrolysis. Thirdly, the evolution of local host response through initiation of inflammatory which is followed consequently by repair process until the reaction becomes stable. Lastly, the systemic effects that happen remotely at a distance from the implant via chemical and mass transport phenomena in which implants release small particles from wear or damage and induce interference that might be carcinogenic to our immunologic system [36].

Table (2.3) shows the biological impact of different elements. From the data given, there are four elements which are considered safe to our body system as no sign of toxicity or allergenic has been traced. The four elements are titanium (Ti), niobium (Nb), zirconium (Zr), and tantalum (Ta).

Table (2.3) : Biological impact of some common alloying elements for implantation [51]

Periodic position	Element	Biocompatible	Carcinogenic	Genotoxic	Mutagenic	Cytotoxic	Allergenic	Prone to corrosion	Other*
3d	Ti	Yes	No	No	No	Med	No	No	No
	V	No	Yes	Yes	Yes	High	Disputed	No	No
	Cr	No	Disputed	Yes	Yes	High	Yes	No	No
	Mn	No	No	Yes	No	High	No	Yes	No
	Fe	No	No	Yes	Disputed	Med	No	Yes	No
	Co	No	Yes	Yes	Yes	High	Yes	Yes	Yes
	Ni	No	Yes	Yes	Yes	High	Yes	Yes	Yes
	Cu	No	No	Yes	Yes	High	Yes	Yes	Yes
4d	Zr	Yes	No	No	No	Low	No	No	No
	Nb	Yes	No	No	No	Low	No	No	No
	Mo	No	Disputed	Yes	Yes	Low	Yes	Yes	Yes
	Tc	No	- Radioactive -						
	Ru	Yes	No	No	No	Med	No	No	Yes
	Rh	No	Yes	Yes	Yes	High	Unknown	No	No
	Pd	No	Yes	No	Disputed	Med	Yes	No	No
	Ag	No	No	No	No	High	Yes	No	Yes
5d	Hf	Unknown	Unknown	Unknown	Unknown	Med	No	No	Unknown
	Ta	Yes	No	No	No	Low	No	No	No
	W	No	Yes	Yes	No	Med	No	Yes	No
	Re	Unknown	Unknown	Unknown	Unknown	Unknown	No	No	Unknown
	Os	No	Unknown	Yes	Yes	High	No	Yes	No
	Ir	No	No	No	Yes	High	No	No	Yes
	Pt	No	Yes	Yes	Yes	High	Yes	No	No
	Au	Yes	No	No	No	High	No	No	No
Other	Al	No	No	Yes	No	Low	No	No	Yes
	Zn	No	No	No	No	High	No	No	Yes
	Sn	Yes	No	No	No	Low	No	No	Yes

2.2.3. Corrosion Behavior

Corrosion is a subversive attack on metallic materials when in contact with a chemical environment. Human body fluid pH in different tissues varies in the range from one to nine that may be considered an extremely corrosive environment for metallic materials, because the presence of a particular amount of NaCl and a series of acids. The presence of a high chlorides concentration is also considered to accelerate corrosion of metallic implants that ability lead to metal ion release. Additionally, most metallic implants are undergone to a static loading or a low frequency cyclic loading. While corrosion damages of the metallic biomaterials are found in many forms like crevice, pitting, fretting, galvanic, wear, intergranular and fatigue corrosion. The attack rate of general corrosion is very low due to the existence of spontaneous formation of passive surface layers on most metallic implants that are utilized at the present time [52].

2.2.3.1.Types of Corrosion

Pitting Corrosion localized corrosion attack made on resistant surface produces pitting corrosion. It commonly occurs on base metals which are protected by a naturally forming thin film of an oxide (for instance the firmly adherent over the surface) when the potential of the film exceeds the breakdown potential of the oxide in an aggressive environment. In the presence of given ions such as chlorides and sulphides, the film locally breaks down and rapid dissolution of underlying metal occurs in the form of pits [53].

Intergranular Corrosion this type of corrosion happens because of the technical errors and inhomogeneity that result in more reactive nature of boundaries of the grain, that the corrosion of intergranular happens adjacent to boundaries of grain with comparatively very little corrosion of grains [54].

Fretting Corrosion this is a form of from erosion corrosion and considered as the more important form of corrosion for implantology. Fretting corrosion is a degradation process resulting from the combined action of small movements between contacting parts and the corrosivity of the environment. This can lead to tissues inflammation caused by degradation of metallic materials used in prosthetic implants which will lead to failure of orthopedic surgical operations [54].

Galvanic Corrosion galvanic or two metal corrosion occurs when two different metals are in physical contact in an ionic conducting fluid medium like a serum or interstitial fluid. In much practical applications, the contact of dissimilar materials is unavoidable. In surgical implants, galvanic corrosion will occur if a bone plate and bone screw are made of dissimilar metals or alloys [55].

CreviceCorrosion occurs from the geometry of the implant/prostheses assembly. Corrosion of an alloy is greater in the small sheltered volume of the crevice created by contact with another material. The other metal could be part of the fastener of the same or different alloy, a sheltered crown, cement packing or implant prostheses joint [53].

Corrosion Fatigue is a fracture failure of metal that happens due to the combined interaction of electrochemical reactions and cyclic loading. Corrosion fatigue resistance is an important factor of consideration for load-bearing surgical implant metals or for metals used in cyclicmotion applications. Normally, a failure may not happen, but cracks can initiate from hidden imperfections, minute flaws, surface damage, chemical attack and other causes [56]. Types of corrosion can be summarized in the table below.

Table (2.4): Types of Corrosion in the Conventional Materials Used for Biomaterial Implants [57].

Type of Corrosion	Materials	Implant location
Pitting	304SS, cobalt-based alloy	An orthopaedic, dental Implant
Crevice	316L SS	Bone plate and screws
Stress corrosion	CoCrMo , 316LSS	Only in vitro
Fatigue corrosion	316 L , CoCrNi Fe	Bone cemnt
Fretting	Ti-5Al2.5Fe , CoCrSS	Ball joints
Galvanic	304،SS/316SS ،.CoCr+Ti5Al2.5Fe	Oral implants (Skrews and nuts
Selective Leaching	Mercury from gold	Oral implants

2.3. The Memory Alloys.

Mechanical properties of shape-memory alloys (SMAs) are typically represented by the characteristic stress–strain curve, which forms a hysteresis loop in a loading, unloading and shaperecovering process. To represent the deformation behavior of SMAs, various constitutive equations have been developed, and prediction of the macroscopic behavior has been possible using finite-element simulations. [58].

The atomistic behavior leading to the deformation and shape-recovery is explained on the basis of the phase transformation between austenite and martensite phases and the characteristics of the crystal structure. One well-known atomistic mechanism is illustrated in Fig. (2.2a). The stable phase depends on the temperature, and phases at high and low temperature are body-centered cubic (bcc or B2) and martensite, respectively. The martensitic phase consists of many *variants*, and each variant has a directional unit cell. In Fig.(2.2b), for example, a unit cell of the martensite is illustrated as a box leaning in the positive or negative direction along the *x*-axis. Cells leaning in the same direction constitute a layer, and the direction of the lean alternates between layers. the layer is called a variant, although a realistic variant is defined as a rather larger domain. The martensite phase is generated by cooling the B2 str ucture shown in Figure (2.2a). Randomly orientated variants are then generated, as shown in Figure (2.2b) some of the layers change their orientation, as shown in Figure (2.2c) This structural change induces macroscopic deformation. When the external shear load is released, the strain does not return to the original state except for slight elastic recovery. When the specimen is heated to the transformation temperature, the martensite transforms into the B2 structure, and martensite appears again with cooling of the specimen. Since the B2 structure is cubic, the shape of the unit cell is independent of the orientation of the martensite layers. Therefore, [59] the specimen macroscopically regains its original shape.

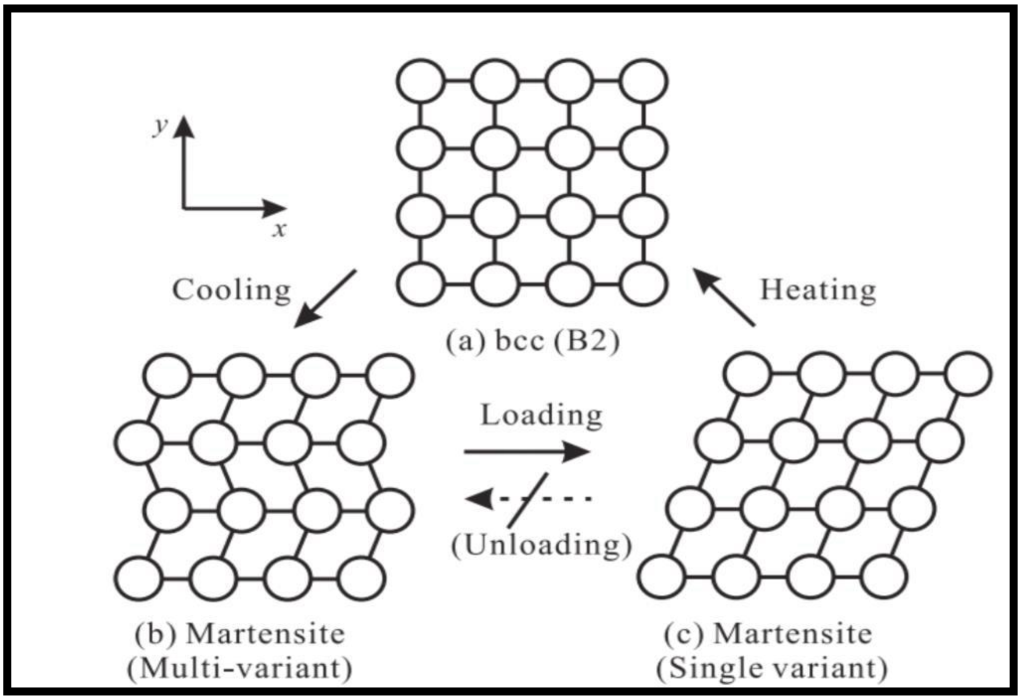

Figure (2.2) Schematic illustration of deformation and shape recovery of a SMA[10].

2.4. Properties of SMA:

2. 4.1 Shape memory effect:

During martensitic phase transformation the molecular structure is twinned. On a macroscopic scale the size and shape of undeformed martensite phase is same as the cubic austenitic phase. The temperature at which starting and finishing of both parent austenitic phase and daughter martensitic phase has characterized by the following variables Ms, Mf, As, Af . Ms is the martensite start temperature upon cooling and Mf is the martensite finish temperature upon cooling, during heating AS and Af are the temperatures of the austenite starts and finishes. The loading quantity of SMA increases with the four variables (Ms, Mf, As& Af), shape memory effect (SME) is noticed when SMA temperature is below Mf , when the alloy is in deformed martensite, SMA will be recovered the original shape by heating the specimen above Af as shown figure (2 .3) and (2.4).

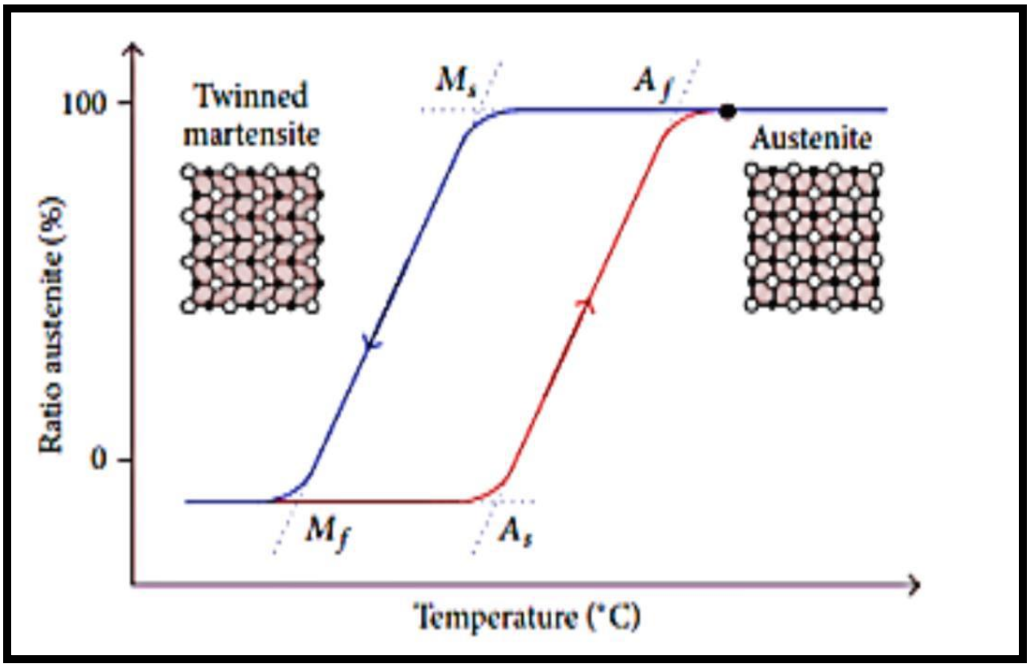

Figure (2.3); Temperature Hysteresis in SMA [60].

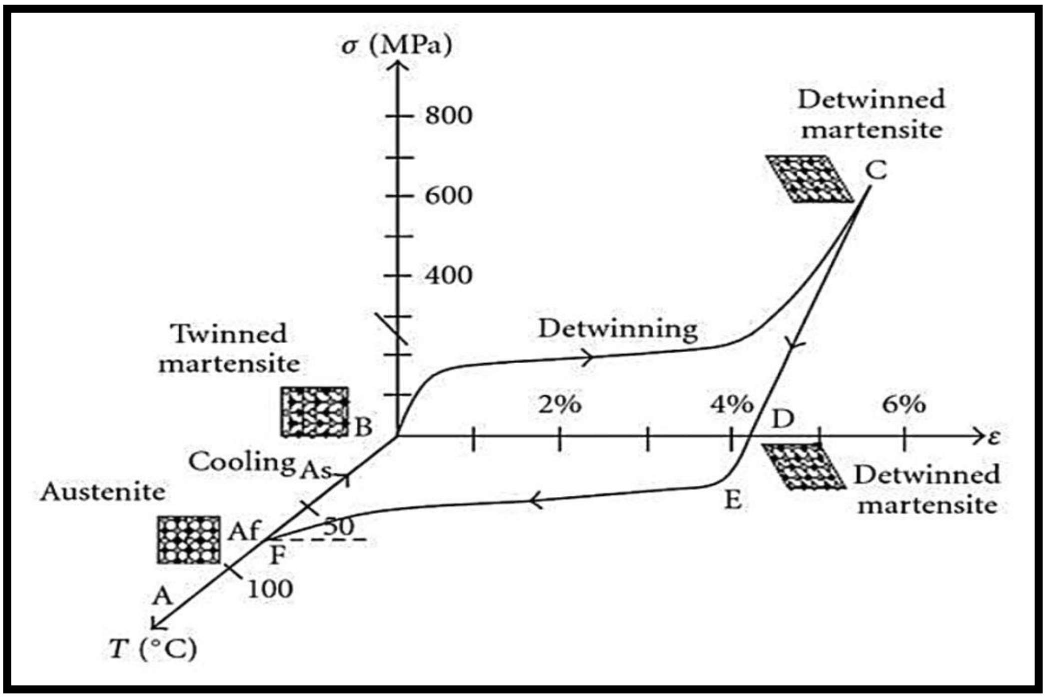

Figure (2.4); Stress-strain temperature of NiTi SMA [61].

Normally SME refers to the one-way SME in which external load makes to include de-twinning brings the SMA in to a current distorted structure that can be regain on heating above Af. In this type there is no transformation strains are induced during cooling, it resumes its original shape and rigidity when heated to its higher temperature form (austenite). This is called the one-way shape memory effect. The ability of shape memory alloys to recover a original shape upon heating above the transformation temperatures and to return to a certain alternate Shape upon cooling is known as the two-way shape memory effect. Two-way SME is the one in which transformation strains are persuaded during heating or cooling of SMA Two-way SME is not an essential, but a developed characteristic [62]. Two-way memory is exceptional. There is also an all-round shape memory effect, which is a special case of the two-way shape memory effect [63].

2.4.2 Pseudo elasticity:

Super elasticity or pseudo elasticity of SMA involves stress induced strain recovery upon unloading at a temperature above Af . In general super elastic thermo mechanical loading path starts at zero stress state where de-twinned martensite is stable examples of this characteristic are isothermal (constant temperature) and isobaric (constant pressure) loading paths indicated in Figures (2.5) & (2.6). For achieving the required constant stress by austenite is not shown in the constant pressure path. The point which we remember is the constant temperature conditions carry out only by quasi-static loading which we can treat as small strain increments. During phase transformation, there is a dissipation of latent heat which was generated during quasi-static process. For easy understanding this review paper concentrates most pressure and constant temperature loading paths will be considered [64].

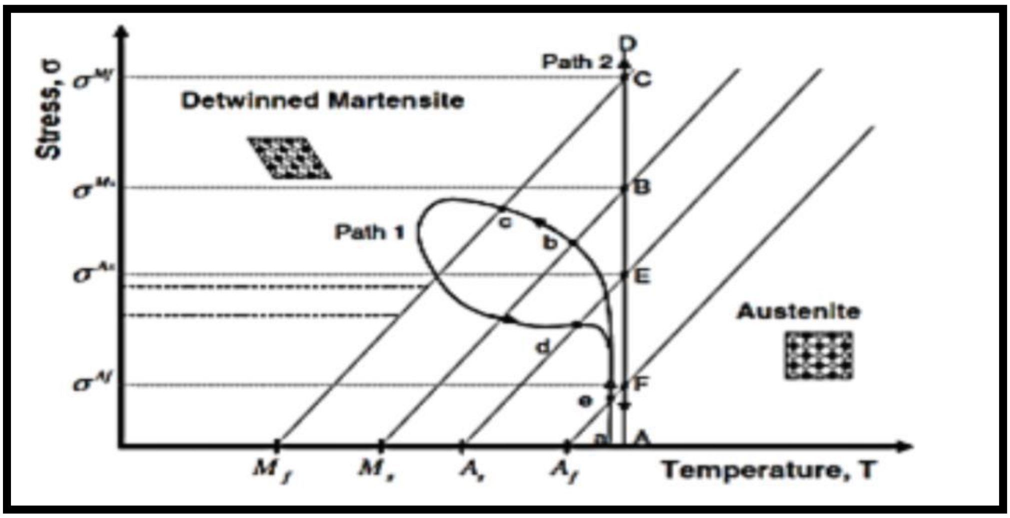

Figure (2.5); phase diagram and two possible [64].

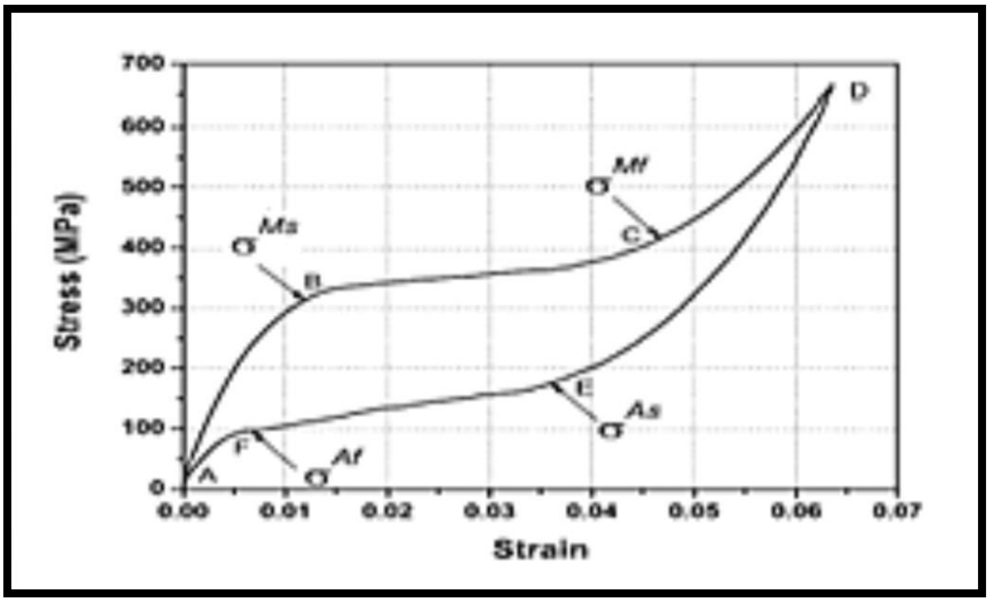

Figure (2-6);SMA pseudoelastic loading cycle pseudoelastic loading paths [64].

During loading at a temperature above Mf the transformation occurred at critical stress levels from austenite to martensite that stress is called as Transformation stress (a-b). This phase transformation usually occurs during (b-c) path. During thermo elastic critical stress level large in elastic strains are going to be developed. If the load increased further de twinned martensite region (c-d) does not produce any more phase transformation, during multi-axial loading there may be re-orientation of martensite twins will occur. At point (d) there will be Reverse transformation (RT) from martensite to austenite which will leads to recovery of in elastic strains. At point (e) there will be a complete transformation from martensite to austenite and the final element of the loading path (e-a) is identified by regaining of thermo elastic strains which leads to zero macroscopic strains upon completion of the path. This transformation process concludes in a hysteresis which returns the energy dissipated in the cycle.

2-5 Titanium

Titanium alloys have become increasingly popular as biomaterials throughout the previous two decades. Some time ago, pure titanium α-phase Cp-Ti and the first generation titanium alloys α+β phase Ti-6Al-4V were introduced. However, second generation titanium alloys, also known as β -phase titanium alloys, have received a lot of interest recently. This section will provide a summary of titanium's general properties, crystals structure of titanium, titanium Alloys, and alloying elements biocompatibility. [65].

2.5.1. Advantages of Ti-alloys Compares to Other Metallic Alloys.

After Al, Fe, and Mg, Ti is the fourth 18th most abundant metal and it is the ninth most plentiful element on earth. It has a metallic silver appearance. Titanium has a density of 0.6 that of iron and close to 0.5 that of cobalt. However, it is distinguished with a modulus of elasticity about 0.5 that of molybdenum-cobalt alloys and stainless steels [66]. Titanium outperforms cobalt-chromium and stainless steel alloys in terms of (specific strength), but falls short in terms of tribological properties. Because titanium's properties are intermediate between those of steel and aluminum [67]. Because of its low density, exceptional corrosion resistance, and good biocompatibility, titanium is frequently utilized in medical applications. Titanium and its alloys, on the other hand, have several disadvantages, such as high cost, fabrication problems, embrittlement (at high temperatures, oxygen transport occurs in the surface oxide layer), high reactivity or strong sensitivity to temperatures over 480°C , and high energy content in producti on[68].

2.5.2. Crystals Structure of Titanium

At low point temperatures, pure titanium metal has a hexagonal close packed (hcp) structure (α-type phase), whereas heating the -transus temperature leads the alloy to β transition to the body centered cubic (BCC) β-type phase [69]. It is at 882°C and is determined by the titanium composition. Its microstructure can be manipulated through thermomechanical and thermal processes. Furthermore, crystallographic texture may be evolving; thus, the microstructure can be controlled [66].

2.5.3 Titanium alloy

Titanium and its alloys are getting much attention for biomedical applications in both medical and dental fields because of excellent biocompatibility, light weight, ideal balance of mechanical properties, excellent corrosion resistance. etc. They are mainly used for implant for example, artificial hip joints, ،devices replacing failed hard tissue plates, dental implants, etc. [70]. The demand artificial knee joints, bone for Titanium and its alloys has grown considerably.

Commercially pure (CP) titanium material and a number of its significant alloys in use during the biomedical device domain, along with their mechanical properties, are exhibited in table (2.5). .

Table (2.5): Mechanical Properties of Biomedical Titanium Alloys [71].

Alloy	Alloy Young modulus (GPa)	Yield stress) (MPa	Ultimate tensile strength (MPa)	Elongation%	Stress fatigue (107)
Ti-6A1-4 V	110	860	930	10-15	610-625
Ti-6Al-7Nb	105	795	860	10	500-600
Ti-5Al-2.5Fe	110	820	900	6	580
Ti-12M0-6Zr-2Fe (TMZF)	74-85	1000 - 1060	1060-1100	18-22	525
Ti-15Mo	85	544	1440		
Ti-15M0-2.8Nb-0.2Si-0.26 (SRx٢١)	83	945-987	980-1000	16-18	490
Ti-35.5Nb-7.3Zr-5.7Ta (TNZT)	55-66	793	827	20	265
Ti-13Nb-13Zr	179-84	863-908	973-1037	10-16	500

Over 1000 tones or 2.2 million pounds of appliances made from Titanium were used for patients worldwide each year. The elastic modulus of Titanium and its alloys is closer to that of the bone and much lower than the stainless steel and cobalt-chromium alloys. Therefore, Titanium and its alloys are favored in continuing requests [72] The modulus of elasticity of various biomedical alloys is compared with bone and shown in figure (2.7).

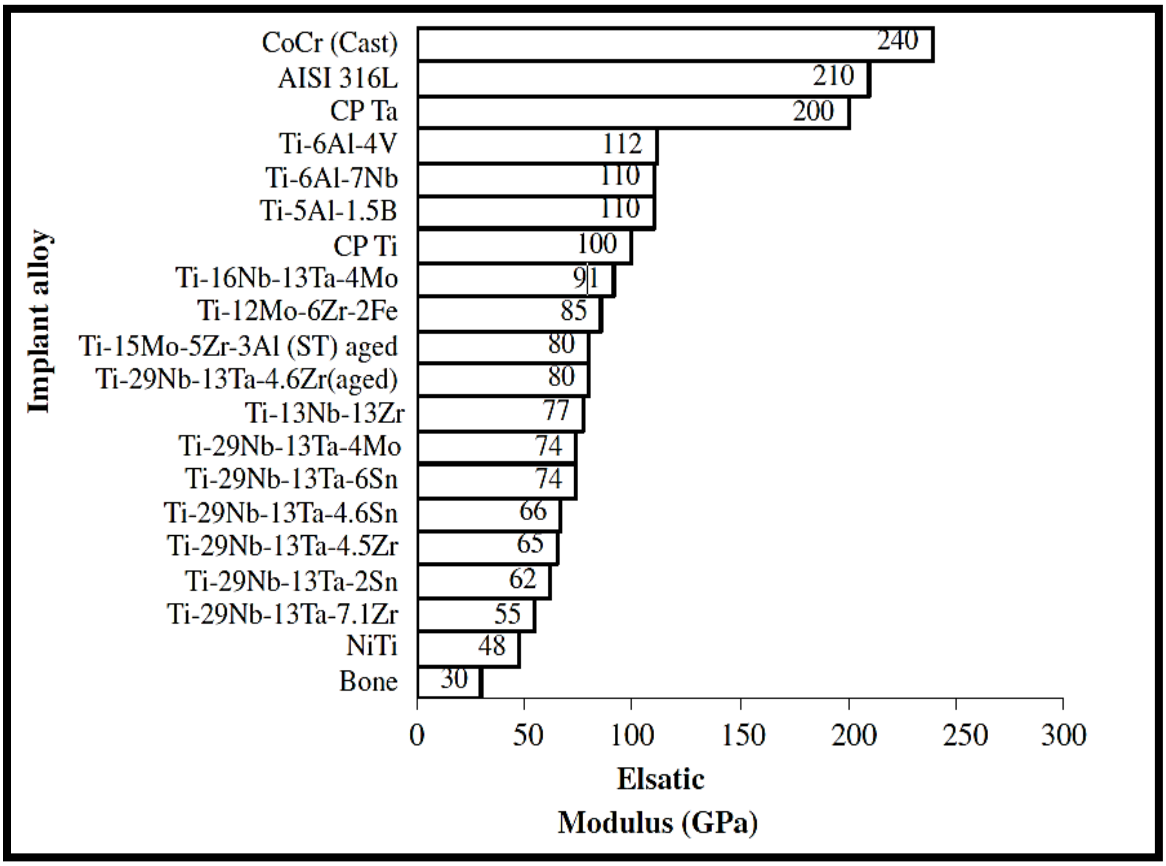

Figure (2.7): Elastic modulus of Biomedical Alloys [72].

2.5.4 . Classification of Ti alloys.

Ti presents two allotropic forms in thermodynamic equilibrium; at low temperatures, it has a compact hexagonal crystalline structure (HC) constituting the matrix phase called α, while above 883ºC it has a cubic body-centred structure (BCC), called β, as shown in figure (2.8); the temperature of transformation from α to β of pure titanium increases or decreases depending on the nature of the alloying elements [73].

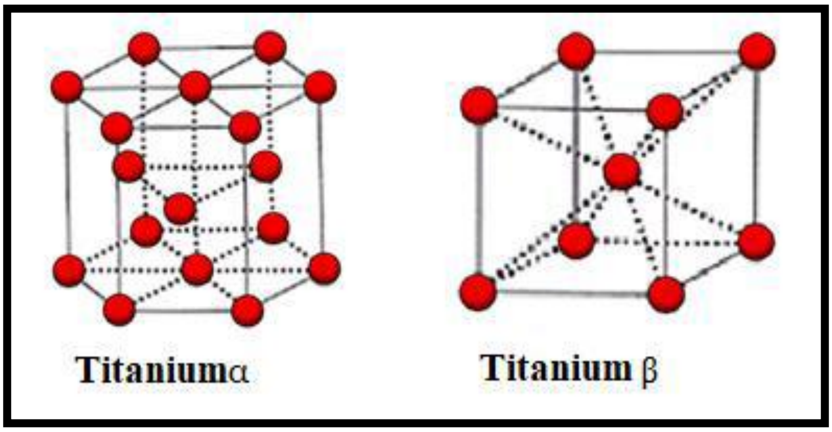

Figure (2.8): Crystallographic Cell and Allotropic Transformation of Pure Titanium.

Figure (2.8) crystalline structure and phase transformations of pure Ti. Adding most other components stabilizes one phase or the next. A-Stabilizers include Al, O, N, and C, while two types of β-stabilizers are β-isomorphous and β-eutectoid with the main element of (Mo, V, Nb, and Ta) and (Fe, W, Cr, Si, Ni, Co, Mn, and H), respectively [71] The small elastic modules that are feasible with these alloys have lately. drawn interest in applying the implants β-Isomorphous Ti alloys if adequately processed. The Zr and Sn components found in some Ti alloys are deemed' neutral' elements with no essential effects on stability in α-or β-phase [71].

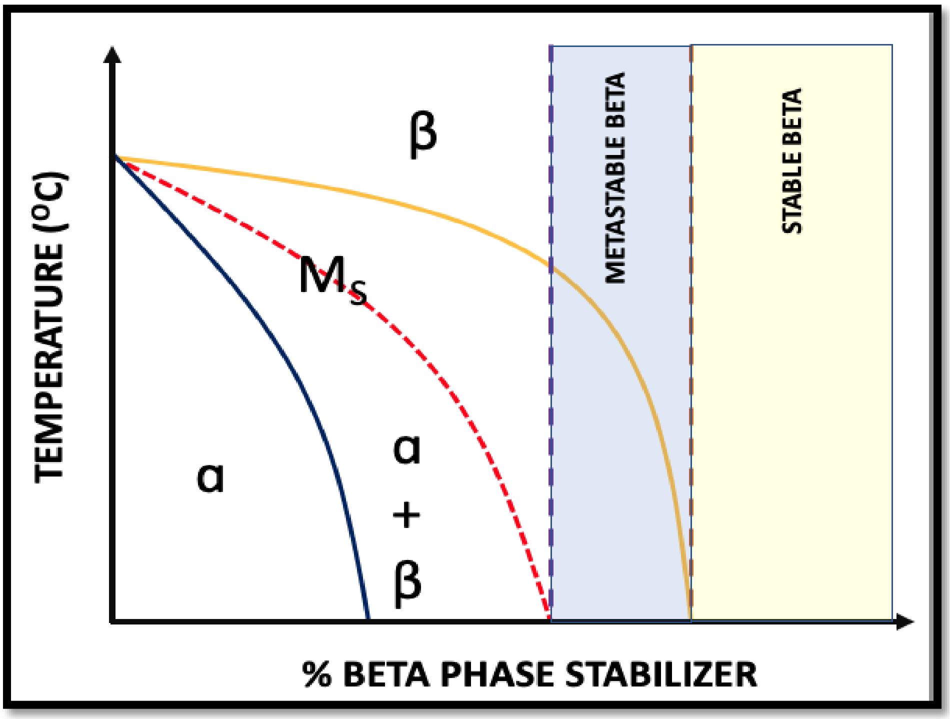

Figure (2.9). Ti alloy equilibrium pseudo binary phase diagram [71].

Titanium alloy can be classified as either α, β, and α- β phase

2.5.4.1 Commercial Purity Ti (α type).

Small numbers of interstitial elements, including O, N, and H, may include unalloyed Ti (commercial purity or CP Ti). Although the amounts are low, as indicated in Table (2-2), mechanical characteristics are affected by reinforcement of interstitial solid solution [74].

. CP-Ti is available in four grades with the lowest O content, the highest flexibility, Grade IV with the highest O content, and the most insufficient ductility. Grade I for the manufacture of implants for use in osteosynthesis (repair of fractures and spinal fusion), Grades III and IV type, while mechanical strength (particularly low fatigue strength) prevents their use with joint substitution prostheses. However, CP Ti is used for dental endosseous implants where it is particularly appealing for its trait of encouraging fast Osseo integration. The resulting hydroxylase area with components ($Ca2+$ and $(PO4)3$ is supposed to be due to OH - Ions' addition bone mineral phase within the passiveTiO_2 layer. The strengthening of the CP Ti is responsible

for the strain hardening during mechanical forming and the size of the fin grain and interstitial solid solutions [71].

Table (2.6). Interstitial element limits and mechanical properties for CP Ti (Grades 1-4) [74]

Grade	N(max)	H (max)	O (max)	Yield stress (MPa)	Ultimate tensile Strength (MPa)	elongation %
1	0.18	0.03	0.015	170	240	24
2	0.25	0.03	0.015	275	345	20
3	0.35	0.05	0.015	380	450	18
4	0.40	0.05	0.015	483	550	15

2.5.4.2 Ti Alloys with ($\alpha + \beta$) structure

Ti alloy is used to form a two-phase alloy with a strength (an $\alpha + \beta$) more significant than that of CP Ti, retaining an outstanding resistance to Corrosion and osseointegration, again due to a quick-forming surface movie TiO_2/OH. The Ti (α+β) alloy with the most extended history of application for significant load-bearing applications is Ti6Al4V, with more latest solutions with comparable characteristics, Ti6Al7Nb and Ti5Al2.5Fe. In clinical applications, all three alloys are equally good. The bar inventory of such alloys is created by thermal processing miller (inforcement) which results in elevated fatigue strength mattresses [75]. Compared to other metal biomaterials, implants made of these alloy have superior corrosion-fatigue characteristics combined with their outstanding corrosion resistance. The Ti alloys (α + β), in specific fatigue strength, are heavily dependent upon size and β phase distribution [75].

2.5.4.3.β-Titanium Alloys

The β-stabilizing components in these alloys show Mo one of the greatest impacts. Table (2-1) includes several β-Ti alloys for use in orthopaedic implants. The Mo equal of these alloys > 10. For the elements added as a Ti alloy, i.e., Mo equivalent to 1.0 wt.% Mo, 0.67 wt.% V , 0.38 wt.% W, 1.6 wt.% Cr, 1.6 wt.% W , 0.22 wt.% Ta, 2.2 wt.% Fe, 1.6wt.% Cr, 1.7 wt.% Cr. This is calculated using separate weighting variables. Although the Ti and Ti (α+ β) moduli are considerably lower than the Co- Cr-Mo or alloys of stainless steel, they are 5–10 times greater than the cortical bone module (10–20 GPa). Concerning the use of long-term implants (albeit less than the higher module co-based stainless-steel alloys), a problem of the bones' stress shielding next to the well-set CP Ti or (α+ β) Ti alloy implants is concerned. If properly processed, the β alloys and so-called near-β Ti alloys show considerably reduced elastic modules value as small as 44-51 GPa for Ti-13Nb-13Zr, a near-β alloy [76] . These alloys show good formability, elevated hardness, great corrosion resistance, improved noise sensitivity (α + β) than the Ti alloys if properly processed [77].

2.6. Effects of Alloying Elements for Titanium Alloys

Titanium alloying element falls into three classes α- Stabilizers, β Stabilizers, and neutral. The alloying elements (Al, O, N, etc.) that tend to stabilize α phase are called α Stabilizers. The addition of their elements leads to an increase in the allotropic transformation temperature (ATT However, elements that stabilize the β phase are known as β Stabilizers (Nb, Ta, Mo, Mg, V, W, Fe, Ni, Cr, Co, Mn, Cu, etc.). The addition of these elements decrease the β transit temperature; when a eutectoid -transformation happens, this β stabilizer is described as a eutectoid β stabilizer; otherwise, its called an isomorphous β- stabilizer. Suppose no significant change in the ATT is observed. In that case, the alloying elements are defined as neutral elements (Zr and Sn), the addition of α andβ stabilizers to Ti gives rise to a field in the corresponding phase diagram where both α and β phases may coexist [78]. Figure (2.10) shows a schematic representation of the phase diagram types between Titanium and its alloys elements.

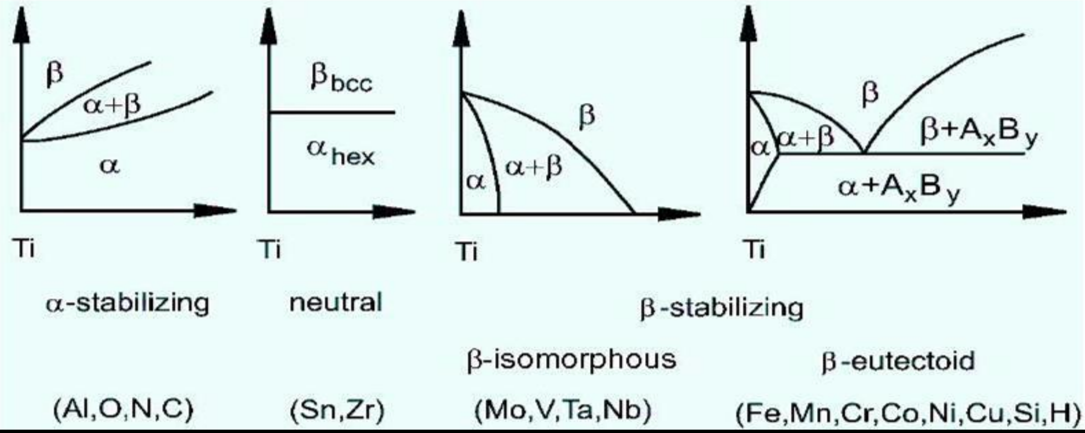

Figure (2.10): Shows Schematic representation of Kinds of Phase Titanium and its Alloying Elements [78].

Zirconium (Zr)

Zirconium is a neutral element when dissolved in Ti. Zirconium belongs to Group 4 (according to the new IUPAC name) in the Periodic Table, which is the same as Titanium and hafnium, have similar chemical structure and properties. Thus, they have been recognized as non-toxic and non-allergic. Zirconium is a transition metal with an atomic number of 40 and an atomic weight of 91.22 . As a greyish-white lustrous metal, Zirconium has exceptionally high melting (1857 °C) and boiling (4409 °C) points. Zirconium has excellent resistance to Corrosion, similar to Titanium and is highly biocompatible [79]. Since both metal surfaces form a stable oxide layer on their surface within nanoseconds when exposing to oxygen. Thus، the oxidation passivates the materials. However, Zirconium could not be used in dentistry in its pure for An extensive review article [80] suggested that Zirconium implants had a lesser degree of osseointegration than titanium analogue using removal torque tests. Some surface modifications could restructure the implant that could remove torque test values comparable with the titanium implants. Although the removal torque test values highly depend solely on the surface structure (in terms of mechanical retention and biological interaction) than on the implant material itself [81], the atomic structural arrangement allows the torque performance in metal alloys better than in ceramics. The reason for using a zirconia implant is merely due to improvement in esthetic qualities in dental restorations. Thus, the development of Ti-alloys is still viable and active [81]. Recently titanium alloys have been developed by adding different properties of Zirconium as Beta stabilizer which obtaining a low modulus of elasticity close to the bone (6-30GPa). the changes of Young's modulus with respect to Ti%, Nb% and Zr% in an increasing order. As it is evident from the 18 histogram distribution graphs in Figure (2.11) and (2.12) , Figure 4 and Figure 5, it is difficult to establish a trend on the effect of the alloying elements on the modulus of Ti-Nb-Zr alloys.

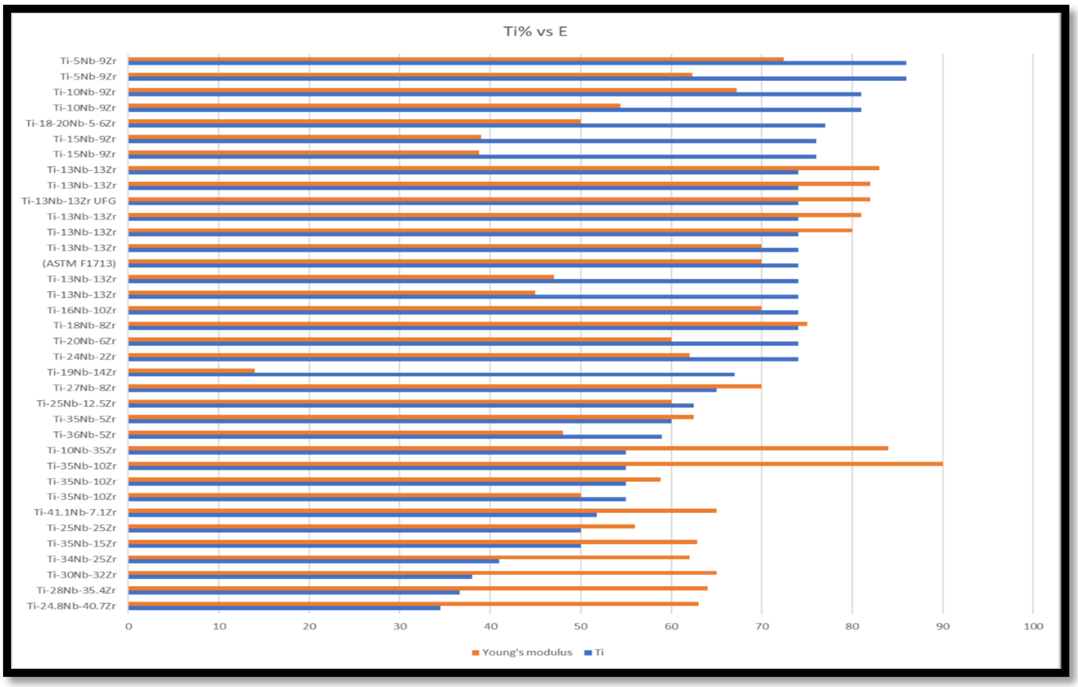

Figure (2.11) : Plot of Ti-Nb-Zr alloy vs Young's modulus with respect to Ti% in an increasing order.

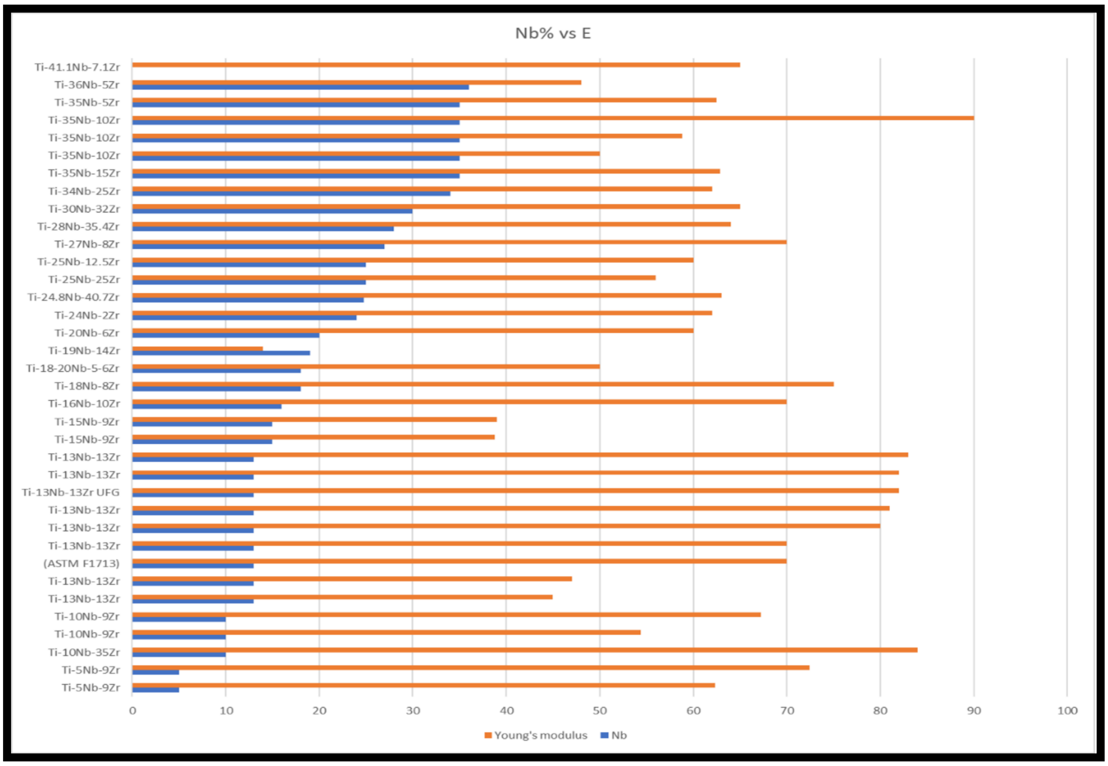

Figure (2.12) Plot of Ti-Nb-Zr alloy vs Young's modulus with respect to Nb% in an increasing order.

Silicon.

Silicon (Si) has been found to be an essential trace element for the growth and development of normal bone and cartilage. In 1970s, Carlisle [82] performed an initial Si deficiency study, which demonstrated the significant dependence of healthy skeletal development on Si. Furthermore, he reported that chicks deprived of dietary Si contained lower level of collagen in the cartilage and they were more apt to suffer from the deformation to the ends of tibia, femur and metatarsus [83]. Following dietary Si supplement studies on ovariectomized mice conducted by Nielsen and Poellot showed that Si had stimulatory effects on cartilage synthesis and might inhibit the physiological resorption process [84]. A recent clinical report [85] Indicated that the increase of dietary Si intake in men and premenopausal women could lead to a higher bone mineral density (BMD). In addition, aqueous Si has been shown to improve osteoblast proliferation, differentiation and collagen production [86,87]. All these findings revealed that Si plays an important role in the bone and cartilage system, especially in the growth and development of skeletal system.

2.7. Heat Treatment and Strengthening Effects.

Heat treatment and strengthening work are two potential methods that could be utilized to enhance the mechanical properties of the β-type Ti alloy .It is one common method used to improve the mechanical strength of titanium alloys. Solution treatment is utilized to enhance the uniform distribution and microstructure across the element [88]. The cooling rate needs to be fast enough to prevent solid – state diffusion and precipitation of the phase. The rapid quenching creates a saturated solution and allows for increased hardness and improved mechanical properties of the material. In addition, studies have shown that the highest degrees of corrosion resistance have been obtained through the maximum rates of quenching. In general terms, liquid quenching is performed in water, oil and more recently, in aqueous polymer solutions. Water and oil quenching cover the extremes in terms of cooling rates, with water being the fastest and oil being the slowest [89].

2.8. Beta type with nontoxic element (Ti-Nb) alloys.

Niobium In the human body, it has a poorly understood biological role. This is related to the toxicity of certain niobium compounds, such as niobates and niobium chloride [90,91]. According to one study, niobium is one of most poisonous metal ions, causing immune cell death and encouraging DNA damage [91]. As a result, until further information is known, niobium should be handled with caution, particularly when combined with other alloying elements [92]. Ti-Nb-based alloys are expectable to be used to biomedical parts due to their low elastic modulus, superior biocompatibility [93,94], superelasticity and good shape memory behavior [95]. Being able to use powder metallurgy is vital due to the ability to produce near-net-shape components without requiring any deformation and machining operations [96,97]. Ti−Nb can be fabricated by powder metallurgy through several methods including conventional sintering, metal-injection moulding [98,99], self-propagating high-temperature synthesis [100], hot-isostatic pressing [101], spark-plasma sintering [102,103,104] and microwave sintering. The microwave sintering technique is a relatively new method to prepare Ti−Nb alloys, and it is considered a new sintering method for metals, composites, ceramics and semiconductors [105,106].

Overall, microwave sintering has several advantages such as enhanced diffusion process, reduced energy and sintering-process time, rapid heating rates, and improved mechanical and physical properties [105,107]. The presence of pores that reduce the elastic modulus of porous-titanium alloys [108,109] also allows the implant cells to grow into the pores and integrate with the host tissue [108−110]. This reduced elastic modulus diminishes the effect of “stress shielding”, which is generated due to the large mismatch of elastic moduli between the implant materials (>100 GPa) and hard tissue (<20 GPa). The “stress shielding” may cause resorption of these hard tissues, loosen the implants and finally lead to implantation failure [111,112].

2.9.Phase diagram of Ti-Nb Shape Memory alloys

Titanium alloys can be classified into three main categories α, α+β and β-type, depending on alloy solute content and heat treatment applied [113]. As shown in figure (2.13) Beta-Ti alloys form one of the most versatile groups of materials with respect to processing, microstructure and mechanical properties [113,114]. Titanium alloys microstructure is a result of a number of solid/solid transformations. Firstly, the solidification process results in β-phase precipitation [115]. Beta grains develop during the cooling stage along the solidification temperature range and the β transformation temperature.

As a consequence, large sections, which cool slower, have larger beta grains. The α phase, typically plate-like shaped, is formed along the β grain boundaries when the sample is cooled through the (α+β) phase field. Alpha plate colonies are the transformation products of the β phase when cooled below the β transformation temperature [115]. A number of studies have shown that the resulting microstructure influences the final mechanical properties [116–117]. In the case of Ti alloys, modifications of microstructure by using several processes such as casting, solution-treating, aging [118], quenching [113,119], roll bonding [115], cold or hot working followed by heat treatment and forging [1 15] have provided considerable changes in tensile strength, fracture toughness, fatigue crack propagation, wear, corrosion and oxidation resistances and modulus of elasticity .An increase on Nb content tends to decrease the modulus of elasticity and stabilizes the β phase. Alloys with lower modulus of elasticity are nowadays desired in the search of similarity to that of bone. Some studies have shown that Ti–Nb alloys ranging from 20 to 50 wt%Nb exhibit a modulus of elasticity of about 60 GPa [120,121,121], which is closer to that of bone when compared to those of other conventional Ti alloys, stainless steel and Co–Cr alloys [114–115]. Afonso et al. [114] have recently analyzed the microstructures, phases and mechanical properties of Ti–20Nb alloy samples as a function cooling rate. They have concluded that high cooling rates increase the Vickers hardness and decrease the Young modulus (which is about 74 GPa for a cooling rate of 160 K/s) [114]. They have also found a high volume of martensite within the β grains.

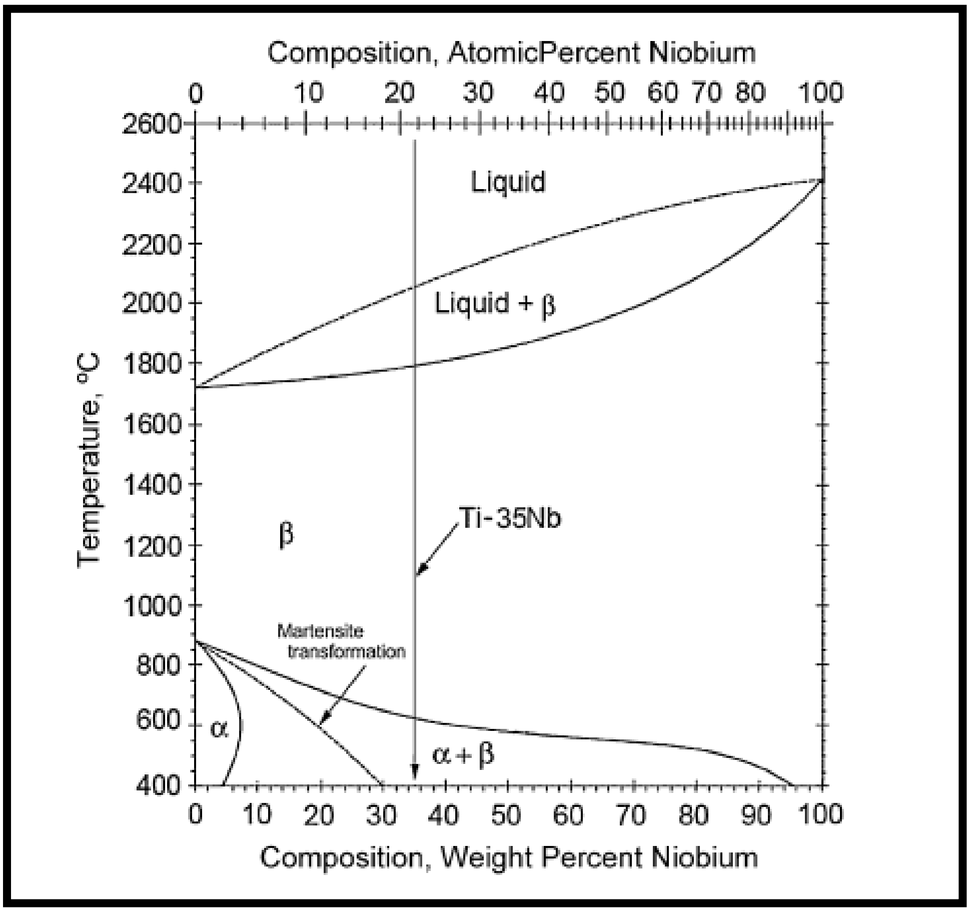

Figure.(2.13). The phase diagram of the Ti–Nb system.

2.10. Titanium Alloys Processing

The properties of titanium alloys are affected obviously by the manufacturing operation. Fabrication techniques can be classified as casting and powder metallurgy.

٢,١٠,١ Casting

Processes of casting are among the oldest methods for industrialization metal goods. In more early casting processes (much of which are still used today), the mould or form must be destroyed to remove the product after solidification. The need for a permanent mould, which could produce components in endless quantities, was the apparent alternative [122].

Casting techniques are employed when: 1. the finished shape is so large or complicated than any other method would be impractical, 2. A particular alloy is so low in ductility that forming by either hot or cold working would be difficult, and 3. in Compared with other manufacturing processes, the final step in the refining of even ductile metals may [123]. The casting process involved the following steps 1-It was melting 2- pouring it into a previously made mould 3- allowing the molten metal to cool and solidify in the mould. 4-. Remove the solidified component from the mould and cle aning it [123].

2.10.2 Powder Metallurgy

Powder Metallurgy (PM) is a celebrated technology to produce parts of small size and sophisticated shapes. This might be one of the most important niches of applications for this technology, More recently, where the vast majority of manufacturing of industrial parts is based on the PM. Manufacturing methods, where an easy manufacturing route is produced by compressing the powder .

This manufacturing path might be called the mass production PM method. Cost is the main parameter to consider , and properties, always under the engineering requirements, are in the .The main steps to manufacture parts by powder metallurgy processare shown in Figure (2-11).The measure include blending and mixing ofpowders, cold compaction, and sintering [124]. Powder metallurgy is an essential commercial technology, and this level [125] s because of the following request's second considerations:

i. PM parts can be accumulated and produced to net shape or near-net eliminating or decreasing the subsequent machining requirement ،shape [125].

ii. PM process is low in wasting materials - about 97% of the starting powders are converted to product. This compares satisfactorily to methods of casting in which sprues, runners, and risers [126].

iii. In PM parts, porous metal parts such as filters, gears, and oil-impregnated bearings can be made with a particular level of porosity [127]

iv. Some metals that are hard to manufacture by other methods can be shaped by powder metallurgy, such as Tungsten filaments for incandescent lamp bulbs [126] .

v. PM distinguishes how producing such as certain alloy combinations and cermets made by PM cannot be shaped in other methods [126].

vi. PM is the most favourable casting process in dimensional control tolerances of + 0.13 mm are regularly held [126].

PM production methods can be mechanical for economical production [127]

There are Limitations associated with PM processing [128]:

i. Owing to the reasonably high compacting pressures required to press the powder, the dies' wear is increased.

ii. Due to the high rate of wear of dies, increased costs for dies and the method is rendered uneconomical, particularly for small runs،presses.

iii. Since the compacted parts must be ejected from the die without therefore, the shapes that may be made by this method are ،fracture limited

iv. The equipment required is very costly.

v. An utterly dense product is not possible without heating the product after pressing operation.

vi. In the low melting powders such as zinc, tin, and cadmium, some thermal difficulties appear ،occasionally.

vii. The physical properties obtained by this process are lower than those obtained by other methods

viii. Many metal powders are explosive at room temperature.

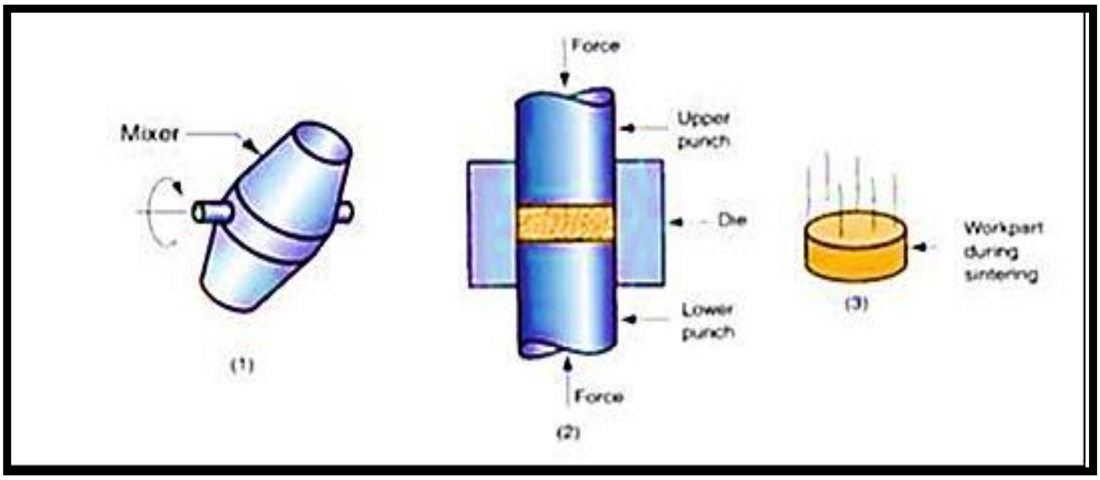

Figure (2.14): Basic Steps of Powder Metallurgy Technique: (1) Mixing of Powders, (2) Pressing of Powders, (3) Sintering [129].

2.10.2.1 Mixing and Blending of the Powders

To achieve good results in compaction and sintering, the metallic powders must be thoroughly homogenized. Blending is an operation of inter mingling powders of the same composition or substance but possibly different in particle sizes. Different particle sizes are often blended to reduce porosity, while mixing is defined as using powders of several or more different materials [126].

The mixing process is used to produce a homogeneous distribution of powders in the least possible time. The mixing time can be differed from a few minutes to 24 hours or even some days, depending on the results desired. Long mixing time leads to work hardening of particles; thus, it must be avoided. Mixing may be either dry or wet. Wet mixing is used to produce a uniform mixture of powder particles. It may be obtained by adding alcohol, benzene, or acetone as a liquid medium inadequate amount to bring the powder to a thin paste's consistency. After completing the mixing process, benzene or acetone is removed by mixing in the air or. controlled oven up to 50 ºC [130].

2.10.2.2 Compacting of the Powders

The compaction process is the shaping step in which the very complex geometries can be achieved with sufficient strength to withstand ejection from the tools and subsequent handling up to the completion of sintering without breakage or damage. The pressure used for producing a green compact of the component depends on the material and the powder's characteristics. The compacting process must be designed so as the pressure will be uniformly distributed on the affected area [131]. The part after compacting is called a green compact with a density called the green density; figure (2-15) illustrates the compaction pressure effect [132].

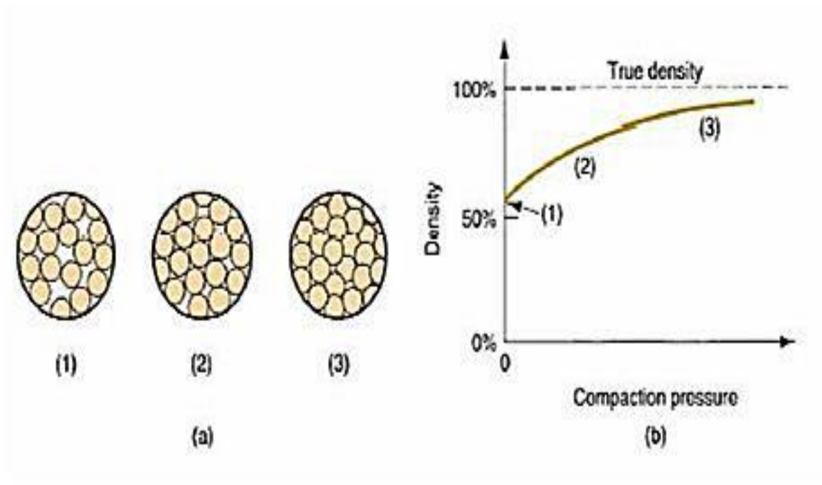

Figure (2.15): (A) Effect of Pressure on Particles Arrangement during Compaction; (B) Density of the Powders as a Function of Pressure [132].

2.10.2.3. Sintering

The sintering process is a heat treatment operation performed on the green compact to bond its metallic particles to increase hardness, strength. The treatment is usually done at temperatures between 0.7 and 0.9 of the melting point of the metal. Sintering processes can be divided into two types: solid-state sintering and liquid-phase sintering. This solid-state sintering is termed when the metal remains un-melted at the treatment temperatures. The liquid-state sintering termed when a minor constituent becomes molten at the treatment temperature; the amount of liquid phase must be limited so that the part retains in shape [133]. Figure (2.16) shows a microscopic scale, the changes that occur during the sintering of metallic powders [131].

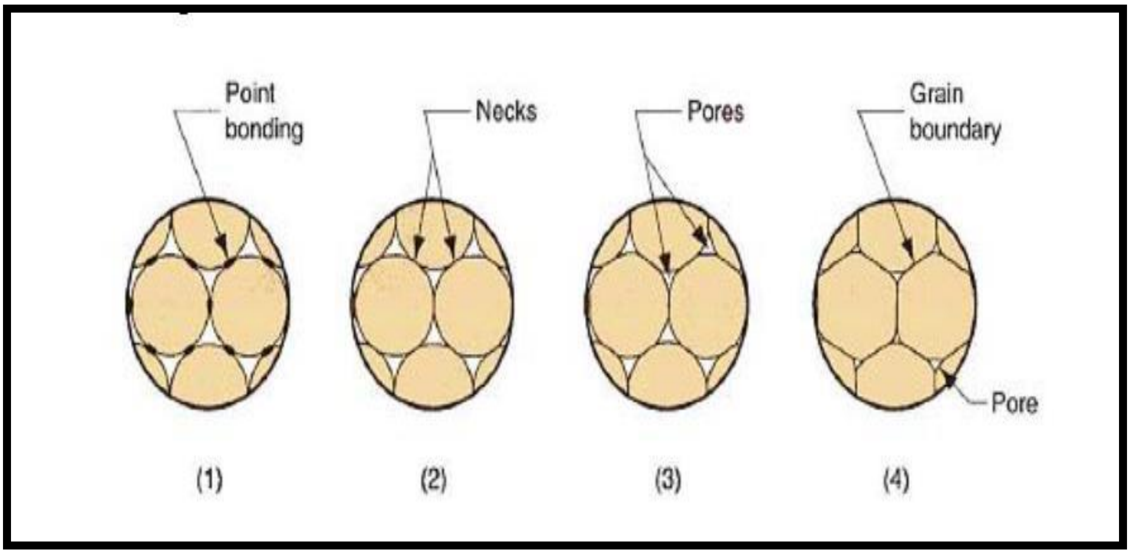

Figure (2.16): Change during Sintering of Metallic Powders: (1) Particles Bonding is started at Contact Region; (2) Contact Region Grow into Necks (3) The Pores between Particles are Reduced in Size, and (4) Grain Boundaries Develop between Particles in Place of Necked Regions [131] .

The driving force of solid-state sintering is the difference in free energy or chemical potential between the particles' free surface and contact points of linked particles [134].

The rate of particle bonding during sintering depends on temperature materials, particle size. Small particles are more energetic, so they sinter faster. Parameters such as particle size and surface area, time temperature, green density, pressure, and atmosphere are functional parameters during sintering [135].

Literature Review

A shape memory alloys (SMA) is an important functional material for biomedical implants applications. Such biomedical SMAs should exhibit good corrosion resistance and biocompatibility as well as shape memory effect (SME) and/or superelasticity (SE). In this study a systematic attempt has been made to develop new Ni-free SMAs composed of Ti and non-toxic element.

In 2009 B. L. Wang, et al .[136] investigated the effects of Zr addition and potentiodynamic polarization on the microstructure and corrosion resistance of Ti–22Nb and Ti–22Nb–6Zr alloy samples, results of XRD and optical microscopy indicated that the addition of Zr stabilized the β phase, which plays a crucial role in the corrosion resistance improvement of the Ti–22Nb–6Zr alloy. From the polarization curves, it can be seen that the alloys exhibited a wide passive region without the breakdown of the passive films and also low corrosion current densities. In addition, the values of the corrosion current densities and passive current densities decreased with the addition of 6 at% Zr into the Ti–22Nb alloy.

In 2011L.W.Ma,et al. [137] investigated fabrication and characterization of porous Ti-22Nb-6Zr (at.%) shape memory alloys produced using elemental powders by means of mechanical alloying and hot isostatic pressing. It is found that the porous Ti-22Nb-6Zr alloys prepared by the HIP process exhibit a homogenous pore distribution with spherical pores, while the pores have irregular shape in the specimen prepared by conventional sintering. X-ray diffraction analysis showed that the solid solution-treated Ti-22Nb-6Zr alloy consists of both β phase and ᾰ martensite phase. Morphologies of martensite were observed. Finally, the good porous Ti-22Nb-6Zr SMAs produced by both MA and HIP exhibit mechanical properties, such as superior superelasticity, with maximum recoverable strain of 3%.and high compressive strength.

In 2012 E. N Camargo et al [138] produced a new nickel-free titanium alloy Ti-22Nb-6Zr (%at) in order to expand the application field of SMA. Samples were produced by mixing of initial metallic powders followed by uniaxial and cold isostatic pressing with subsequent densification by sintering between 800-1600 °C, in vacuum. Sintered samples were characterized for phase composition, microstructure and microhardness by X-ray diffraction, scanning electron microscopy and Vickers indentation, respectively. Density was measured by Archimedes method. It was shown that the samples were sintered to high densities and presented homogeneous microstructure with complete dissolution of alloying elements in the titanium matrix.

In 2013, A.LRoselino Ribeiro, et al [139] studied the behavior of new Ti35Nb5Zr andTi35Nb10Zr alloys in artificial saliva at 37 ◦C to verify if they are indicated to be used as biomaterials in dentistry as alternatives to Ti6Al4V alloys in terms of corrosion protection efficiency of the material. Electrochemical impedance spectroscopy (EIS) experiments were carried out for different periods of time (0.5–216 h) in a three-electrode cell, where the working electrode (Ti alloys) was exposed to artificial saliva at 37 ◦C. the result show that ,the new TiNbZr alloys showed similar behavior to that observed for theTi6Al4V. XPS results suggest, in the case of the TiNbZr alloys, the presence of a thicker passive layer containing a lower fraction of TiO_2 phase than that of Ti6Al4V. After long-term immersion, all alloys develop a calcium phosphate phase on the surface. The new TiNbZr alloys appear as potential candidates to be used as a substitute to Ti6Al4V in the manufacturing of dental implant-abutment sets.

In 2013, A. Terayamaa ,et al [140] investigated The effects of ternary alloying additions of Ta, Al and Sn and cold working on the shape memory characteristics of the Ti–Nb based alloys fabricated by powder metallurgy (PM) process.. The mixed elemental powders at compositions of Ti–22at%Nb and Ti–22 at%Nb–4at%X (X=Ta ,Al and Sn) sintered by a pulse-current sintering equipment .The solution treatment was carried out to obtain homogeneous microstructure .As a result, the solution-treated Ti–22 at%Nb alloy consisted of (ά+β) phases at a temperature 300K. The martensitic transformation start temperature of the Ti-22%Nb alloy was lower than that of the wrought alloy of the same composition The Ti–22at%Nb–4at%Al alloy indicated a super elastic-like behavior in the stress–strain curve, but the super elastic behavior could not be observed in the solution-treated alloys of other compositions.

In 2014 M, Y Gaoet al. [141], studied Nickel-free Ti–22Nb–6Zr alloys were fabricated by conventional powder metallurgy sintering method. X-ray diffractometer (XRD) investigation showed that the as-sintered alloys mainly consisted of β phase with a few needle-like α phase precipitates Differential scanning calorimetry (DSC) measurement in the temperature ranging from −70 °C to 400 °C and constant stress thermal cycling test by dynamic mechanical analysis (DMA) were unable to reveal the martensitic start temperature of sintered Ti–22Nb–6Zr alloys There was an obvious drop of both Young's modulus and recoverable strain at −85 °C ~ −80 °C in the Young's modulus-temperature and recoverable strain–temperature curves of sintered Ti–22Nb–6Zr alloys respectively, which was attributed to the occurrence of thermal elastic martensitic transformation at this temperature. The result had revealed that sintered nickel free Ti–22Nb–6Zr alloys are thus thought to be potentially competitive biomaterials for biomedical applications.

In 2014, B. Y, , Zheng et al [142], studied a Ti–45Nb alloy with low Young's modulus and high strength was developed, and microstructure, mechanical properties, corrosion behaviors, cytocompatibility and *in vivo* osteo-compatibility of the alloy were systematically investigated for the first time. The results of mechanical tests showed that Young's modulus of the Ti–Nb alloy was reduced to about 64.3 GPa (close to human cortical bone) accompanied with higher tensile strength and hardness compared with those of pure Ti. Importantly, the Ti–Nb alloy exhibited superior corrosion resistance to Ti in different solutions including SBF, MAS and FAAS (MAS containing NaF) media.

In 2015 , A.M.. Tavares. et al, [143], studied the microstructures and properties of Ti-35Nb-xSi alloys wt. %) which were thermally treated and (,0.13 , 0.55 , conditions: furnace cooling cooled under the following (FC), air cooling (AC), and water quenching (WQ). The results showed that Si addition is effective to reduce the density of omega precipitates making beta more stable, and to produce grain refinement. In all cooling conditions, the hardness values increased with the increasing of Si content, as a result from the strong Si solid solution strengthening effect while the elastic modulus underwent a continuous reduction due to the reduction of omega, precipitates in beta matrix. Lower elastic moduli were observed in water-quenched alloys, also the increase in Si concentration also produced an increase in the alloys' mechanical strength of Ti-35Nb-0.55Si alloys.

In 2016, M.Yahaya.et al [144] investigated effect of addition Nb Niobium powder to the elemental titanium (Ti) powder by wt %, cold-compacted and sintered at 1200°C. The samples were characterized in microstructures ،term of shape and sizes of the particle, phases present and compressive strength. XRD pattern showed that increasing Nb content resulted in increased beta-phases which also evidenced by a greater fraction of light gray-scale image in back-scattered SEM analysis. lowest The alpha phase region almost eliminated in the 35 wt% Nb. The compressive strength was observed in 45 wt% Nb is due to partly crystallized region in the microstructure observed. The alloy containing 35 wt% Nb exhibited better beta-phase structures in the matrix. All sintered samples are potential candidates for implant applications

In 2017 J. W. et al.[145] founded that the alloy Ti-13Nb-(0-6) Zr alloys. were fabricated by conventional powder metallurgy sintering method Their microstructure, phase transformation temperature and mechanical properties were investigated by optical microscopy, scanning electron microscope, X-ray diffraction, differential scanning calorimetry and compression test. It was found that with more Zr addition, the content of β phase increased while the content of precipitated α phase reduced. With 1 at.% Zr increase, the Ms ofTi-13Nb-(0~6) Zr alloys decreased linearly their Ms temperature by around 10 °C.

In 2018 E. Yilmaz et al [146] investigated the effects of Sn content (2 and 4 wt%) on microstructure and mechanical properties of Ti16NbXSn sintered alloys. The results indicated that Ti16Nb (0–4)Sn alloys were composed of α+ β phases. Hardness and Young's modulus E of the alloys measured using Nano indentation technique. These results show that there is a relationship between the mechanical properties and Nb–Sn content. It is concluded that addition of Nb to the cp-Ti resulted to a decrease in Young's modulus.

In 2018 Mustafa K. IBRAHIM1 et al [147] The effects of microwave-sintering on the microstructure, phase composition, phase-transformation temperature, mechanical properties and shape- memory effect were investigated. The results show that the density and size of porosity vary based on the sintering time and temperature, in which the smallest size and the most uniform pore shape are exhibited with Ti−23%Nb SMA after being sintered at 900 °C for 30 min. The microstructure of porous Ti−Nb SMA consists of predominant α'', α, and β phases in needle-like and plate-like morphologies, and their volume fractions vary based on the sintering time and temperature. The β phase represents the largest phase due to the higher content of β stabilizer element with little intensities of α and α'' phases. The highest ultimate strength and its strain are indicated for the sample sintered at 900 °C for 30 min, while the best superelasticity is for the sample sintered at 1200 °C f or 30 min. The low-elastic modulus enables these alloys to avoid the problem of "stress shielding". Therefore, microwave heating can be employed to sinter Ti-alloys for biomedical applications and improve the mechanical properties of these alloys.

In 2019 Yuqing Zhang et al [148] study the influence of low Nb content (0–25 wt%) on the comprehensive parameters of tensile stress–strain relationships (ultimate strength (rUTS), yield strength (r0.2) and elastic modulus (E)), surfaces properties (Vickers microhardness, surface roughness (Ra), water contact angle (WCA), X-ray diffraction (XRD) and scanning electron microscopy (SEM)), corrosion resistance (in artificial saliva and lactic acid) and biological properties XRD results shown that b Ti alloy phases, such that the β phase all the Ti–xNb alloys comprised a increased correspondingly with the increased amount of Nb in the alloy, as well as the reduction of E (69–87 GPa). Except Ti–5Nb, all other Ti–xNb alloys showed a significantly higher hardness, increased rUTS and r0.2, and decreased WCA compared with cp-Ti. No corrosion was detected on Ti–xNb alloys and cp-Ti in artificial saliva The cytotoxicity of Ti–xNb alloys was comparable to that of cp-Ti in MC3T3-E1 pre-osteoblasts without interference from differentiation behaviour, but the proliferation rate of the Ti–5Nb alloy was lower than other groups. and lactic acid solutions.

In 2020 Elena O. Nasakina et al ,[149] Using the methods of electric arc melting, intermediate heat treatments, and consecutive intensive plastic deformation, a Ti–Nb–Zr alloy wire with a diameter of1200 _m was obtained with a homogeneous chemical and phase (β_-Ti body-centered crystal lattice) composition corresponding to the presence of superelasticity and shape memory effect, corrosion resistance and biocompatibility. Perhaps the wire structure is represented by grains with a nanoscale diameter. For the wire obtained after stabilizing annealing, the proof strength Rp0.2 is 635 MPa, tensile strength is 840 MPa and Young's modulus is 22 GPa, relative elongation is 6.76%. No toxicity was detected. The resulting wire is considered to be promising for medical use.

In 2020 ,Kyong Min Kim et al ,[150] investigate the effects of the Nb and Zr contents on phase constitution, transformation temperature, deformation behavior, and Young's modulus were investigated. Ti–Nb and Ti–Nb–Zr alloys over a wide composition range, i.e., Ti–(18–40)Nb, Ti–(15–40)Nb–4Zr,Ti–(16–40)Nb–8Zr,Ti–(15–40)Nb–12Zr,Ti–12-17)Nb –18Zr were fabricated and their properties were characterized. The phase boundary between the α phase and the β martensite phase was clarified The Ti–25Nb, Ti–22Nb–4Zr Ti–19Nb–8Zr, Ti–17Nb–12Zr and Ti–14Nb–18Zr alloys exhibit the lowest Young's modulus among Ti–Nb–Zr alloys with Zr content of 0, 4, 8, 12, and 18 at.%, respectively. Particularly, the Ti–14Nb–18Zr alloy exhibits a very low Young's modulus less than 40 GPa. Correlation among alloy composition, phase stability, and Young's modulus was discussed.

In 2020 Yuya Ishiguro ,et al [151], show that the addition of low amounts of oxygen remarkably enhances the β-phase spinodal decomposition at high temperatures. The β phase in Ti-23Nb-XO (at.%) alloys (X =2, 3, 4, and 5) separates into the β1 phase, i.e., (Ti)(O, Va)3, and the β2 phase, i.e., (Ti, Nb)(Va), at 1073 K. Moreover, nanoscale concentration modulation is introduced. In Ti-23Nb-1O (at.%) alloy, the β-phase spinodal decomposition occurs at a temperature below 1000 K. The volume fraction and composition of the β1 and β2 phases depend on the heat treatment condition and alloy composition, in particular, the oxygen content. The spinodal decomposition of Ti–Nb–O alloys take about 10−2–10−3 s at 1073 and 900 K, which is significantly faster than that in Ti-40Nb (at.%) alloy at 600–700 K. Hence, the spinodal decomposition in Ti–Nb–O alloys is presumed to progress even during water quenching. The results suggest that the control of the microstructure of Ti–Nb–O alloys requires careful control of both the alloy composition and heat treatment conditions, including the cooling rate.

Table (2.7) Comparison between some researches and this study

Reference	Alloy composition	Addition alloying	Fabricated Method	Results
١٣٦	Ti-22Nb	٦ Zr	Arc melting	the addition of Zr stabilized the β phase, which plays a crucial role in the corrosion resistance improvement
١٣٧	Ti-22Nb		Powder metallurgy HIP	The solid solution-treated Ti-22Nb-6Zr alloy has both martensitic ᾰ phase and β phase, according to X-ray diffraction investigation .
١٣٨	Ti-22Nb	6Z r	Powder metallurgy	It was shown that the samples were sintered to high densities and presented homogeneous microstructure with complete dissolution of alloying elements in the titanium matrix .
١٣٩	TiNbZr	(5,10) Zr	Arc melting	The existence of a thicker passive layer in the case of TiNbZr alloys with a lower TiO2 phase percentage than Ti6Al4V.
١٤٠	Ti– 22 %Nb	٤ Al 4Ta 4 Sn	Powder metallurgy HIP	The Ti-22%Nb alloy has a lower martensitic transformation start temperature than the wrought alloy of the same composition. The alloy Ti-22at%Nb-4at%Al .
١٤١	Ti-22Nb	6Zr	Powder metallurgy	sintered alloys mainly consisted of β phase with a few needle-like α phase.
١٤٢	Ti-45Nb			mechanical tests showed that Young's modulus of the Ti–Nb alloy was reduced to about 64.3 GPa accompanied with higher tensile strength and hardness compared with those of pure Ti. Importantly, the Ti–Nb alloy exhibited superior corrosion resistance.

١٤٣	Ti-35Nb	0.13and 0.5 si	Arc melting	. As the Si concentration rose, the hardness values climbed but the young modulus decreased
١٤٤	Ti	35 Nb	Powder metallurgy	The alloy containing 35 wt% Nb exhibited better beta-phase structures in the matrix.
١٤٥	Ti-13Nb	(0-6) Zr	Powder metallurgy	It was found that with more Zr addition, the content of β phase increased while the content of precipitated α phase reduced.
١٤٦	Ti-16Nb	(0-4)Sn	Arc melting	It is concluded that addition of Nb to the cp-Ti resulted to a decrease in Young's modulus .
١٤٧	Ti-32 Nb		Powder metallurgy	The microstructure of porous Ti−Nb SMA consists of predominant α'', α, and β phases The highest ultimate strength and its strain are indicated for the sample sintered at 900 °C for 30min .
١٤٨	Ti -(0-25) Nb		Powder metallurgy	results shown that all the Ti–β Ti xNb alloys comprised a alloy phases, such that the β phase increased correspondingly with the increased amount of Nb in the alloy
١٤٩	Ti-Nb-Zr		Electric arc melting	tensile strength is 840 MPa and Young's modulus is 22 GPa,. relative elongation is 6.76%
١٥٠	Ti-Nb-Zr Ti-Nb		arc melting	alloys exhibit the lowest Young's modulus among Ti–Nb–Zr alloys with Zr content of 0, 4, 8, 12, and 18 at.%, respectively .
١٥١	Ti-23Nb	O (2,3,4,5)	Powder metallrgy	In Ti-23Nb-1O (at.%) alloy, the β-phase spinodal decomposition occurs at a temperature below 1000k

Most of the research is titanium niobium but manufactured by casting method. And the other thing is that the study of corrosion of titanium niobium alloys with the addition of different proportions of silicon was not addressed in previous studies and also the heat treatment of alloys manufactured by the method of powder metallurgy and conducting a thermal treatment on them.

3.1. General View

The materials and equipment utilized in this study are discussed in this chapter. Powder mixing was utilized in the experiment to prepare specimens from elemental powders, compaction and sintering, based on traditional powder metallurgy techniques, have also been discussed in depth. Several tests are also explained, including microstructure, phase identification by X-ray diffraction, Differential Scanning Calorimeter corrosion resistance, wear resistance.

3.2. Materials Used

The materials used to prepare (Ti-Nb) alloys in this research are detailed in table (3.1) with average particle size, purity and the original ingredients from HWNANO-company in china.

Table (3.1) Powders Used in Alloys

Powder	Purity%	Average particle size ((µm)
Titanum	99.6	25.42
Niboum	99.95	5.16
Zirconium	99.9	20.48
Silicon	99.8	4.742

3.3. Particles Size Analyzer

Particle size distribution of elemental powder (Ti, Nb, Si, and Zr) was carried out in College of Materials Eng. /Ceramics and Building Materials Labs./University of Babylon" by Laser particle size analyzer of type: Better size 2000,China,as shown in Figure (3.1).

Figure (3.1): Laser Particle Size Analyzer

3.4. Design and Steps of the Experimental Procedures

Figure (3.2) depicts the experimental procedure utilized in this investigation.

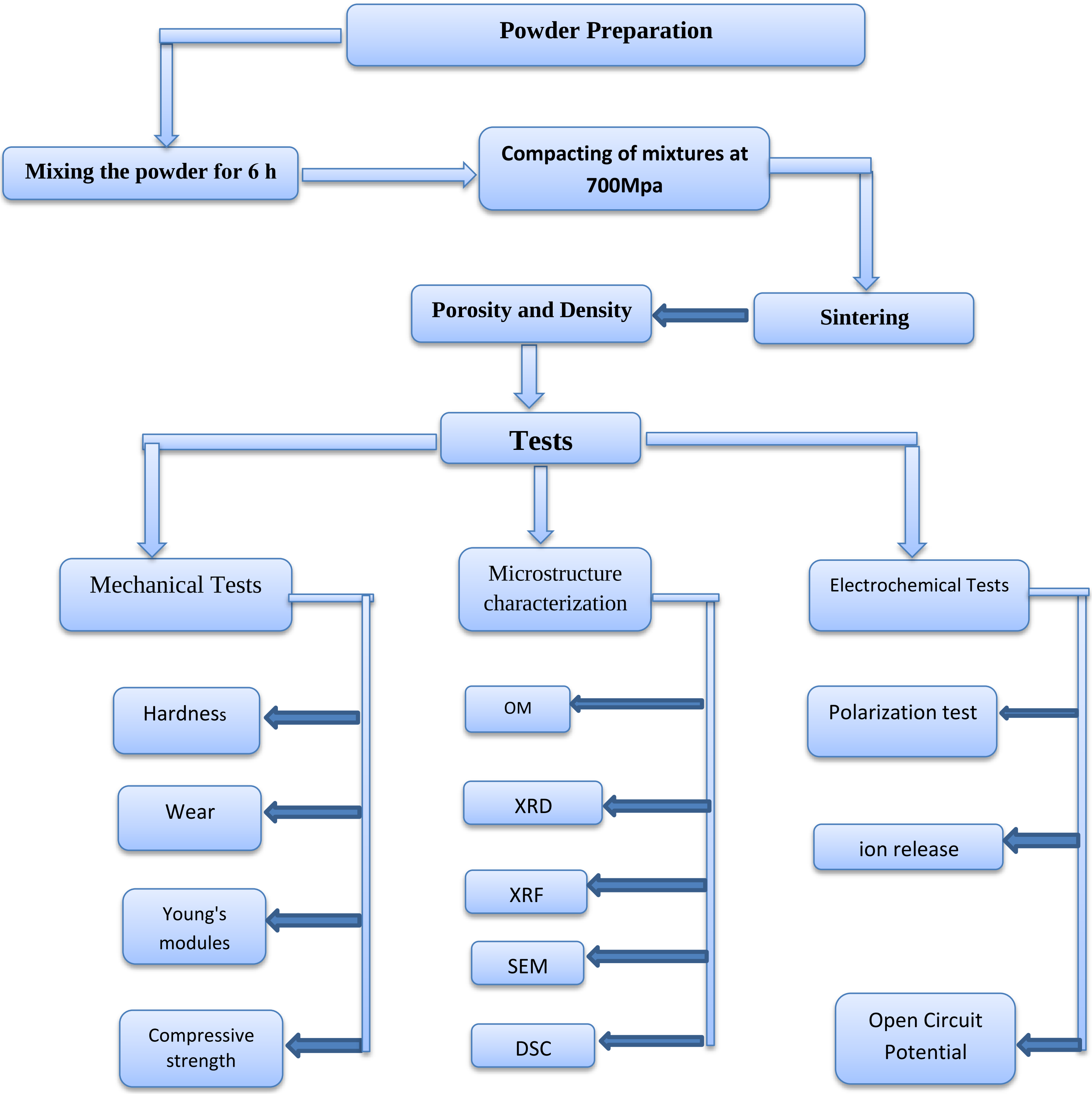

Figure (3.2): Program of the Present Study

3.5 .Preparation of Specimens.

Powder metallurgy technique was used to prepare the specimens. The procedure involves four steps:

3. 5.1. Preparation of mixing powders

Mixing mixtures from elemental powder given in table (3. 1) with different weight percent have been prepared in this stage. The base mixture of (Ti-Nb) contain of (Ti-35Nbwt%) have been prepared. Furthermore; additives from Si and Zr each alone added to the base mixture to explain the effects of alloying element on the corrosion resistances, wear resistances and hardness. Chemical Compositions of prepared alloys from elemental powders used in this study have been shown in table (3.2).

Table (3.2) The code and composition of the alloys which are used in this work

Alloys	Specimens Coding	Alloy Compositions%(wt)			
		Nb	Zr	Si	Ti
A	Alloy A	35	---	---	bal
B	Alloy B	35	---	---	bal
C	Alloys C1	35	3.9	---	bal
	Alloys C2	35	5.4	---	bal
	AlloysC3	35	6.9	---	bal
D	AlloysD1	35	---	0.2	bal
	Alloy D2	35	---	0.4	bal
	Alloy D3	35	---	0.6	bal

3.5.2. Mixing Procedure

The mixing of an elemental powders has been done by using a ball mill shown in the figure (3.3a). Stainless steel balls with different diameters as shown in figure (3.3 b) has been used to mix and refine metal powders for about 6 hours. The increment in the number of contact areas between the elemental powder particles enhance the mixing process. wet mixing is done by using 0.5 cc of Ethyl alcohol to every 25 g of powder mixture. The wet mixing is used to minimize the temperature generated by friction between the balls with walls and powder.

a b

Figure (3.3) a: The Electrical Rolling Mixer , b: Stainless Steel Balls

3.5.3. Compaction of Mixed Powders.

In this stage electric uniaxial hydraulic press as shown in figure (3.4) is used to compact the mixed powder to green specimens with dimensions (D=13.4mm and t≈ 6 mm) that used for the tests .The die used was single action die made from stainless steel shown in figure (3.5) Graphite has been used as lubricant in order to minimize the friction between the punch and the die wall as well as the friction between the green compact and the die wall and to avoid the cracks initiated from the ejecting of green compact . Various compression stresses from (500 , 600, 700 , 750 , 800) Mpa with loading rate (2 ton/ min) and period of applied pressure time is (4 min) has been used in order to determine the optimum compression stress that give higher density and low green porosity.

Figure (3.4) Electric hydraulic press one channel, CT430-CT440

Figure (3.5) : Compaction die

3.5.4 Sintering of Green Compacts

The green compacted specimens have been sintered in a tube furnace. The sintering process was performed in an argon atmosphere to inhibit the specimens oxidation.

The sintering process include the following steps:

1. Heating green compact from room temperature to 500 °C.
2. Soaking for (2) hours at 500 °C.
3. Heating from temperature 500 °C to 1100 °C
4. Soaking for (6) hours at 1100 °C.
5. Slow cooling in the furnace with continues argon circumstances to the room temperature. This procedure is agreeing with **[152]**.

Figure (3.6): Tube furnace with a continued stream of argon.

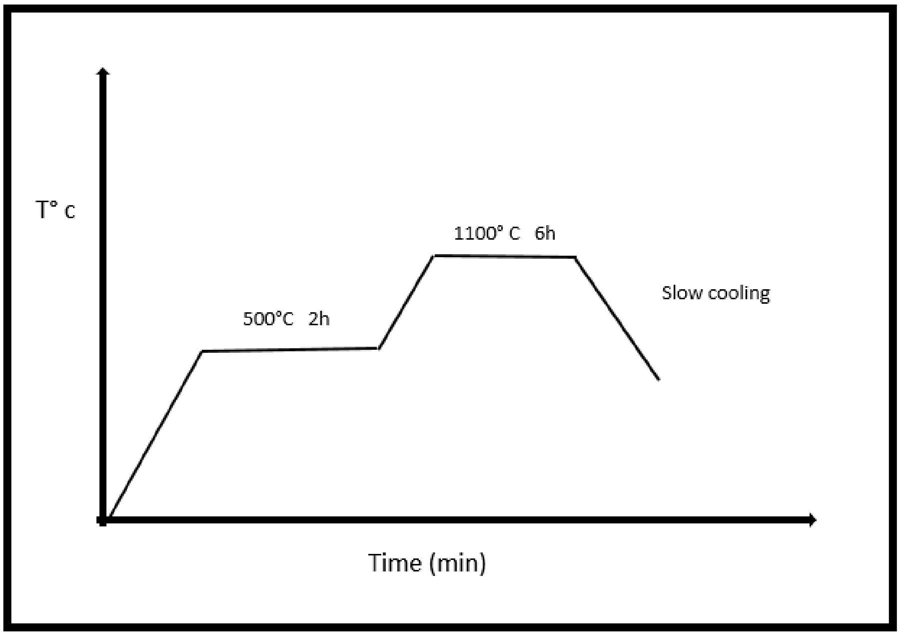

Fig (3.7): Heating cycle in sintering.

3.6 . Heat Treatment

The heat treatment process involved heating the sintered specimens to 900 ºC and holding it at this temperature for 30 minute then rapidly cooling in iced water, Fig (3.8) shows the schematic for this process.

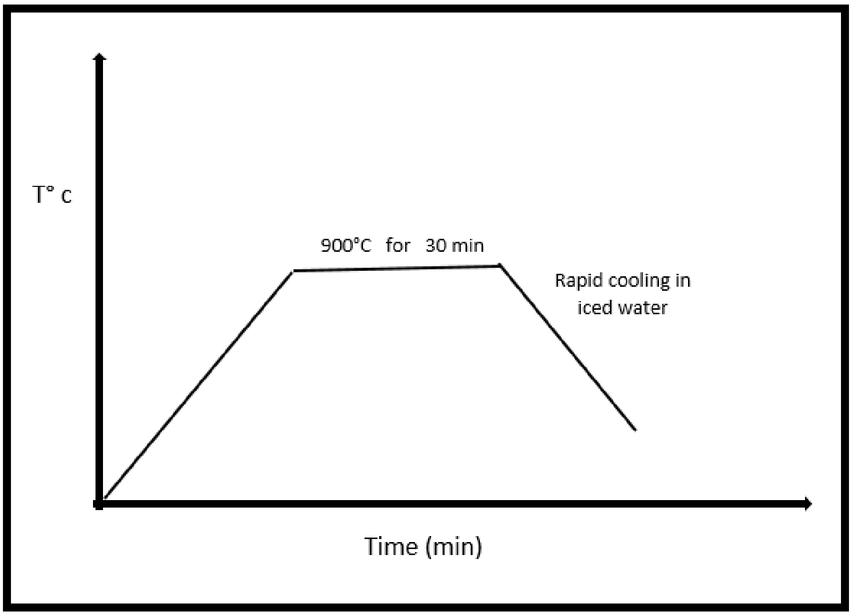

Figure (3.8). The procedure of heat treatment used in this study.

3.7. Preparation of specimens for the Testing

After sintering the surfaces of specimens were grounded with 180, 350, 400,600, 1000,1500 , 2000 and 2500 grit silicon carbide, then polished with 3µm diamond paste to get mirror finish. Then being washed with acetone in Ultra Sonic Cleaning Device in (figure 3.9), ethanol and distilled water respectively. Etching of specimens was achieved in solution with ingredients as the following [153]:

i- HF 3 ml

ii- HNO_3 6ml

iii- H2O 91ml

Preparation specimens were spent 7 seconds submerged in the etching solution, then dried after being cleaned with distilled water.The specimens are now prepared for microstructure analysis.

.

Figure (3.9): UltraSonic Cleaning Device.

3.8. Porosity and Density of Sintered Specimens

The porosity of sintered specimens are calculated according to ASTM B-328 **[154]**:

1- The specimen is dried up to 100 C° for 5h under vacuum for (10^{-4}) tor then cooled to room temperature by using vacuum drying furnace figure (3.10). The weight of dry spacemen is measured as mass A.

2-At room temperature, using a suitable evacuating pump which was manufactured for this purpose. The pressure was reduced over the immersed specimen in oil for 30 minutes.

3-The fully immersed specimen was weighted in the air as mass B.

4-Weighing the specimens in water as mass F

5-Finally, the porosity is calculated as:

P=[B−A(B−F)D°∗100] Dw .... (3.1)

ρF=[AB−F] Dw ……………………………………….. (3.2)

where :

Dw = density of water (0.9956 g/cm3)
D° = density of oil (0.4 g/cm3)

Figure (3.10) Vacuum drying furnace

3.9. Testing and characterization

3. 9.1.X- Ray Diffraction Analysis XRD

Using an XRD apparatus type (XRD- 7000, X- ray) in Babylon university, Department of Ceramics - Faculty of Materials Engineering. and part of specimen tested at Tehran University, apparatus model PW1730 made in USE. The alloys were subjected to X-ray diffraction techniques. The specimen after the sintering procedure were X-ray diffraction tested. The Cu target was employed with a 40 KV and 30 mA XRD generator with a scanning rate of 5°/min. (10–80) was the scanning rate.

Fig (3.11) X- Ray diffraction analysis type (XRD-6000).

3.9.2 Optical Microscope Observation

Grain boundaries have several features, including the identification and measurement of the phases, form, and grain size. These all have unique qualities that make them each stand out. The test done at the University of Babylon ,department of metallurgical engineering in materials engineering college.

croscope with (100x, 400x

Fig (3.12): Light optical microscope.

3.9.3. Scanning Electron Microscopy (SEM)

The microstructure of etched specimens is revealed using a scanning electron microscope. Various magnifications were employed. SEM examination was performed in Tahran university, apparatus Models Mira3 as shown in figure (3.13).

Figure (3.13): Scanning Electron Microscop.

٣.٩.٤. Energy Dispersive X-ray Spectroscopy (EDX) .

Energy dispersive analysis have been done for all specimens in order to estimate the chemical composition and to see the distribution of alloying elements in the specimens, two areas has been taken for each specimens. The test has been done in Tahran University's.

3.9.5. X ray Fluorescent Analysis (XRF).

(XRF) analyzer, model (XEPOS) type (76004814), is used to explain the chemical composition for alloys. The test has been done in Tahran university.

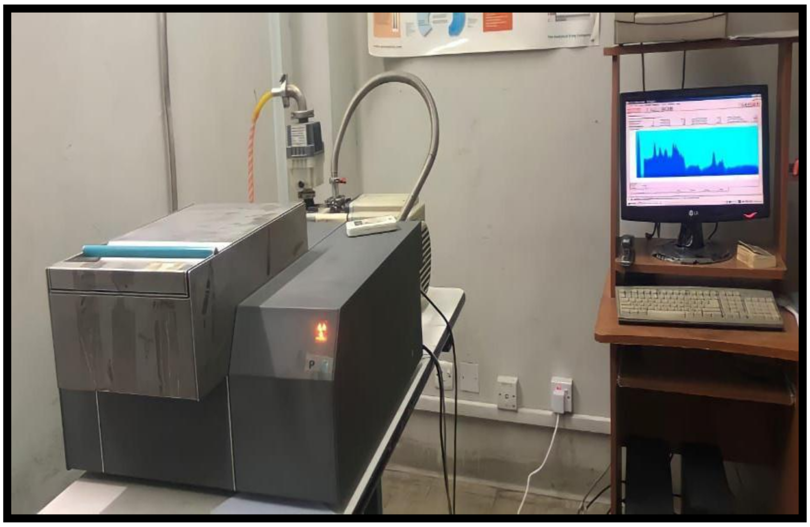

Fig (3.14) X-Ray Fluorescent (XRF).

3.9.6. Shape memory properties.

3.9.6.1 Differential Scanning Calorimeter (DSC) Test.

Differential Scanning Calorimeter (DSC) analysis has been done in order to estimate the transformation temperatures for specimens for the forward transformations to determine the A**s** (austenite start temp.), A**f** (austenite finish temp.), Ms (Martensite start temp.), and Mf (Martensite finish temp.) and use these temperatures for shape memory effect test. DSC tests are carried out in Tahran university laboratories with devices models Q600 made in USA while one test done in Faculty of Materials Engineering, department polymer as shown in Figure (3.15).

Figure (3.15) Differential Scanning Calorimeter (DSC) Type I Series.

3.9.6.2 Shape Memory Effect

Shape memory effect can be determined from the brinell impression by using Brinell macrohardness test with load of 36.5kg and holding time of 10 sec. The heat treatment temperature was done depending the results from DSC test. After the heat treatment completed, carried out the cooling process for specimens inside the furnace under control argon gas carried out.The diameter of the ball impression before and after the heat treatment has been measured using light optical microscope with X100 as magnification then the shape memory effect can be calculated from the equation below [155].

$$SMA=\frac{db-da}{db}*100\% \qquad (3.3)$$

Where: db= diameter of impression in μm before heat treatment.

da= diameter of impression in μm after heat treatment.

3.10. Mechanical Test.

3.10.1. Measuring Macrohardness.

The macrohardness Brinlle test includes use of load (36.5kg/mm²) on the specimen to measure its hardness by a carbide ball diameter of (3.9 mm) for (10 sec) as shown in Figure (3.16) located in the metals laboratory in the Laboratories of the Department of Metallurgical Engineering -University of Babylon. The average value used was taken for three readings for each specimen to analysis the behavior of the alloys.

Fig (3.16) Wilson hardness machine type (UH-250).

3.10.2. Compression Test.

The Compression test was performed according to ASTM (E9-200) at room temperature. By using computer control electronic universal testing machine, Model (wdw 200, No.W1124).The dimensions of specimens are (13.4mm diameter and 20-21mm in height) the specimens were placed vertically between the jaws for measuring the compression strength is shown in figure (3.17). The test was run at a constant loading speed of 0.5 mm/ min. The compressive strength is calculated by using the following equations [156] .

Compressive force **(MPa)=**$\frac{\boldsymbol{Max\ force}\ (\boldsymbol{N})}{\boldsymbol{Cross\ sectional\ \ area}\ (\boldsymbol{mm2})}$

Figure (3.17): Compressive test.

3.10.3. Dry Sliding Wear Test

The wear testing was down at the University of Babylon/Materials Eng. College-Metallurgical Eng. Labs, using wear tester device type (MT-4003, version 10) according to ASTM (G99). A pin on a disc device was used. Figure (3. 18) shows a schematic of pin-on-disk wear test system. The test was performed at room temperature, utilizing loads (10 and 15) N.A rotating speed of 400 rpm, a constant radius of 6.5mm with different sliding distances. Before starting the test, the specimen was weighed using a sensitive balance model M254 A with (±0.0001) accuracy. The specimen was weighed after 5, 10, 15, 20 ,25 and 30 min, the rate of wear calculated according to the following equation (3.4) [157]

.

$$\mathbf{W.R} = \Delta \mathbf{w} / \boldsymbol{\pi} \mathbf{rnt} \qquad (3.4)$$

.

Where: -

R.W:-wear rate (g/N.m.t)

ΔW:-weight lost (gm) which is the difference in weight of the specimens before and after the test

t:-Sliding time (min.).

r:-The radius of the specimens to the center of the disc (6.5mm).

n:-Disk rotational speed (400 rpm).

Fig (3.18) pin on disk wear instrument.

3.10.4. Ultrasonic wave Test .

To investigate the longitudinal and transverse velocities, an ultrasonic wave device type (cct-4) was employed, located in Department of polymer laboratories, material Engineering, University of Babylon with a digital display that shows the time of transfer of the ultrasonic wave and can calculate them by applying the elastic modulus and the Poisson ratio in the equations below [158] . the values for longitudinal and transverse velocities are given.

$$\nu = (1 - 2(VT/VL)2\,)/(2 - 2(VT/VL)2)$$

$$E=\frac{VL2\ \ \rho\,(1+\sigma)(1-2\sigma)}{(1-\sigma)} \qquad (5.4)$$

Where:

VL: Longitudinal velocity (m/sec).

VT: Shear (Transverse) velocity (m/sec)

ρ: Density (Kg/m3).

ν: Poisson’s ratio,

E: Elastic modulus (GPa)

3.11. Electrochemical Tests .

Because of the importance of the Ti alloys and their use as an implants within the human body, corrosion tests should be done on specimens to determine the behavior of corrosion of specimens in the human body. This test was done in Corrosion Laboratory in the Laboratories of the Department of Metallurgical Engineering -University of Babylon. In this test were used two different body solutions. Hanks and Simulated body fluid solutions have chemical compositions as illustrated in Table (3.3) and (3.4) respectively [159] [160].

Table (3.3) chemical composition of Hanks solution's [159]

NO.	Constituent	(g/Ml)
1	NaHCO3	0.35
2	NaH2PO4H2O	0.06
3	NaCl	8
4	CaCl2	0.14
5	MgCl2.6H2O	0.1
6	Glucose	1
7	KH2PO4	0.06
8	MgSo4.7H2O	0.06

Table (3.4) chemical composition of simulated body fluid(SBF) solution's [160].

.NO	Constituent	Amount (g)
1	KCl	0.373
2	Na_2HPO_4.2H2O	0.178
3	$NaHCO_3$	2.268
4	NaCl	6.547
5	$(CH_2OH)_3CNH_2$	6.057
6	Na_2SO_4	0.071
7	$MgCl_2$.6H2O	0.305
8	$CaCl_2.2H_2O$	0.368

3. 11.1. Open Circuit Potential (OCP)

The experimental arrangement for the measurement of open circuit potential is shown in figure (3.19) a schematic drawing describes the experimental situation. A 500 ml capacity glass electrolytic cell is used. The tests were carried out with the specimens immersed in a Hanks and simulated body fluid solutions. The potential of the working electrode is measured with respect to a Saturated Calomel electrode (SCE). A voltmeter is connected between the working electrode and the saturated reference electrode. For each specimen three hours' open circuit potential measurement was performed.

The first record was taken immediately after immersion then the voltage was monitored for the intired period of test at an interval of (5min).

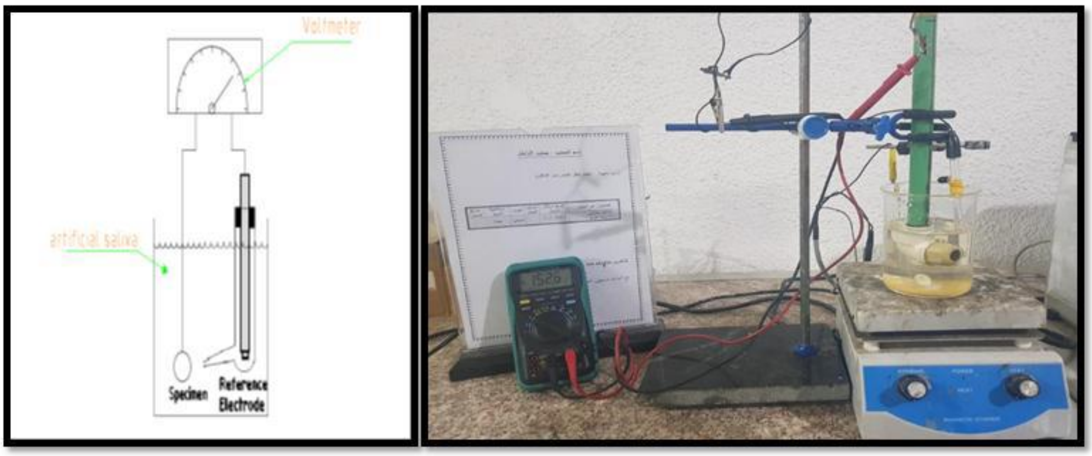

Fig (3.19): Schematic drawing and experimental arrangement for the open circuit potential measurement

.

3. 11.2 Potentiodynamic Polarization

Electrochemical experiments were performed in three electrode cell containing and electrolytes Hanks and simulated body fluid solution. The counter electrode was Pt electrode and the reference electrode was SCE and working electrode (specimen) according to the American society for testing and materials ASTM (GS-87). The potentiodynamic polarization curves were plotted and both corrosion current density (I corr.) and corrosion potential were estimated by Tafel plots by using anodic and cathodic branches. The electrochemical system used . The test was conducted by stepping the potential using a scanning rate 0.2 mV/s from initial potential of 350 mV below the open circuit potential and the scan continued up to 350 mV above the open circuit potential. Corrosion rate measurement is obtained by using the following equation **[161]:**

$$\textbf{corrosion rate=} \quad \frac{\mathbf{0.13}\ \boldsymbol{I\,corr}\ (\boldsymbol{Ew})}{\boldsymbol{\rho}} \qquad (3.6)$$

Where:

E.W= equivalent weight (g/eq.)

ρ= density (g/cm^3)

0.13 = metric and time conversion factor

icorr.= current density ($\mu A/cm^2$).

mpy = Corrosion rate (mils per year).

3.11.3. Metals Ions Release (Static Immersion Test) .

The test of static immersions is recognized in agreement with the currently specified JIS T-0304 standards for metallic biomaterial **[1٦٢]**. Specimens are immersed in plastic containers 50 mL of each solution for three week in the incubator (Specimens are immersed in small containers, where these containers are immersed in controlled water temperature) to keep the temperature at 37° C (2). Assessing the metals ions Ti,Nb,Zr and Si concentrations by Atomic Absorption flame as shown in Figure (3.20). The test has been done in university of Baghdad -Ibn Sina Factory.

Figure (3.20) Atomic absorption spectroscopy.

3.12. Contact Angle Test

To assess the impact of additives on the wettability of pure materials, a contact angle test was conducted. The tool employed was an SL 200KS dynamic optical KINO Industry Co., Ltd. sells a static interfacial torsiometer and contact angle meter. In the United States (0° to 180°). located in Department of Ceramics, material Engineering, Babylon University.This device computes contact angles and determines their average values, providing a real-time data graph that tracks changes in contact angles while video is being recorded Figure (3.21).

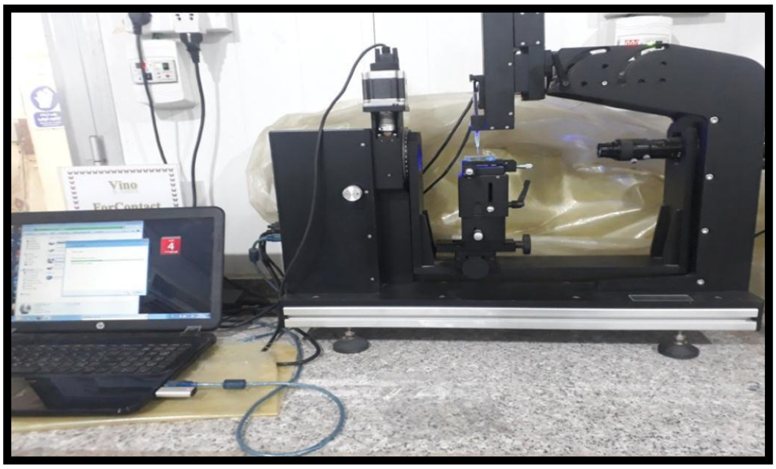

Figure (3.21): contact angle device.

٤,١ .Introduction

Experimental results have been demonstrated in this chapter, they consist of the features related to the specimen that manufactured using the method of powder metallurgy. The porosity and density of the sintered specimens, are clarified microstructure analysis results from light optical microscope and SEM, phases analysis results from XRD technique, Differential Scanning Calorimeter, hardness results, compression results, dry sliding wear and corrosion results have been cleared and discussed.

4.2. Particle Size Analysis

The particles sizes of (Ti, Nb, Si, and Zr) powders have been analyzed. The results are shown in figures (4.1) to (4.4). It is clear that powders had an average particle size of about. (5.100 to 25.420) The particle size of the powder plays an important role in the behavior of the metal powders during compacting and sintering operations where dissimilar particle size ranges are favorite for good compacts and else, for good properties of sintered products [163].

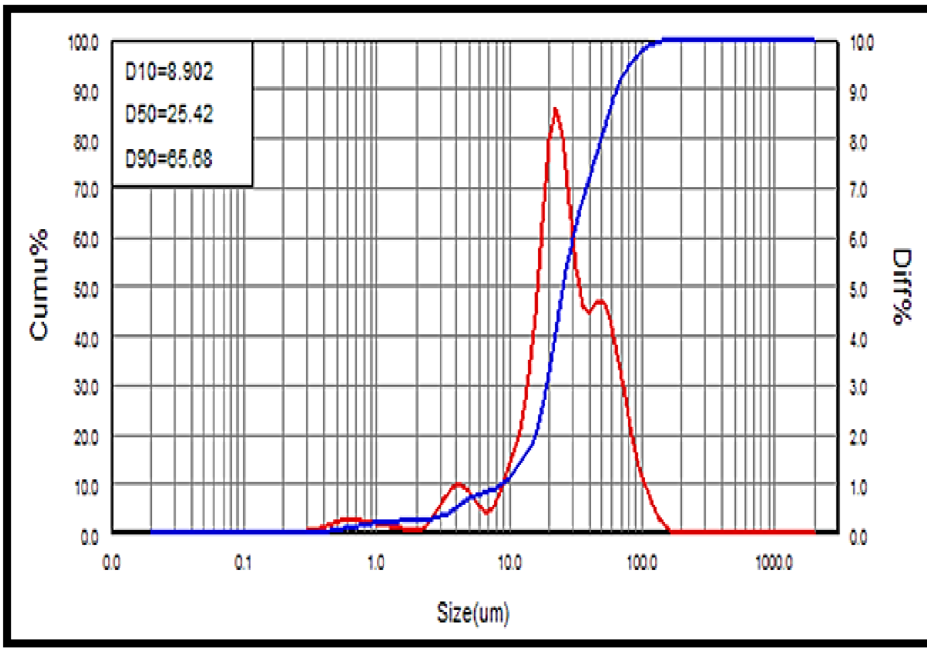

Diam um	Percent
0.500	0.53
1.000	1.90
2.000	2.56
5.000	7.07
10.000	11.11
20.000	33.35
45.000	76.07
75.000	93.50
100.000	97.99
200.000	100.00

Figure (4.1): Ti Powder Particle Size Distribution.

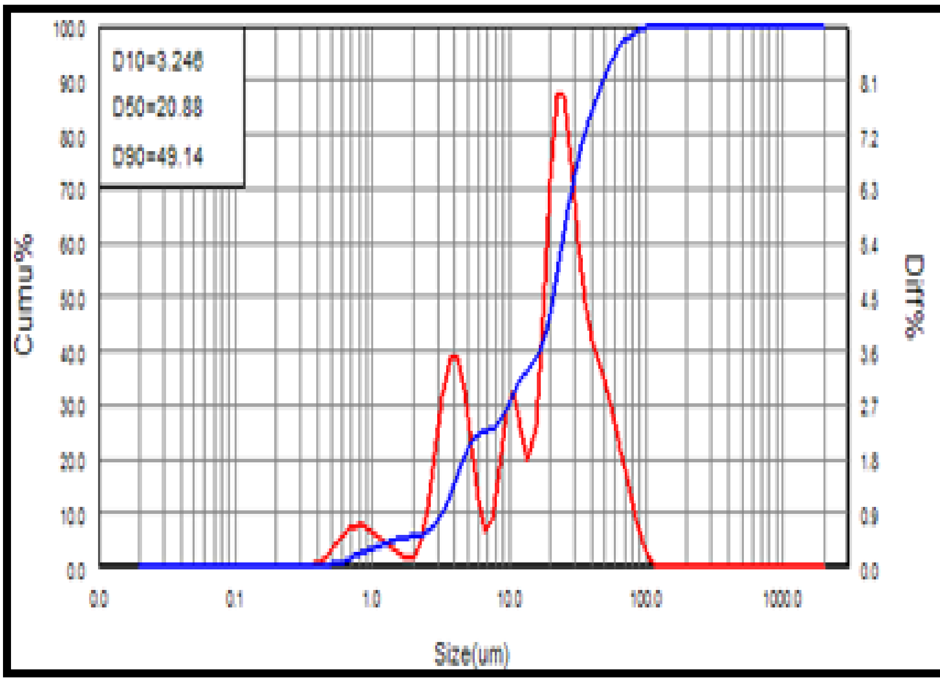

Diam um	Percent
0.500	0.32
1.000	3.54
2.000	5.45
5.000	21.63
10.000	29.86
20.000	47.59
45.000	87.50
75.000	98.09
100.000	99.87
200.000	100.00

Figure (4.2) Nb Powder Particle Size Distribution.

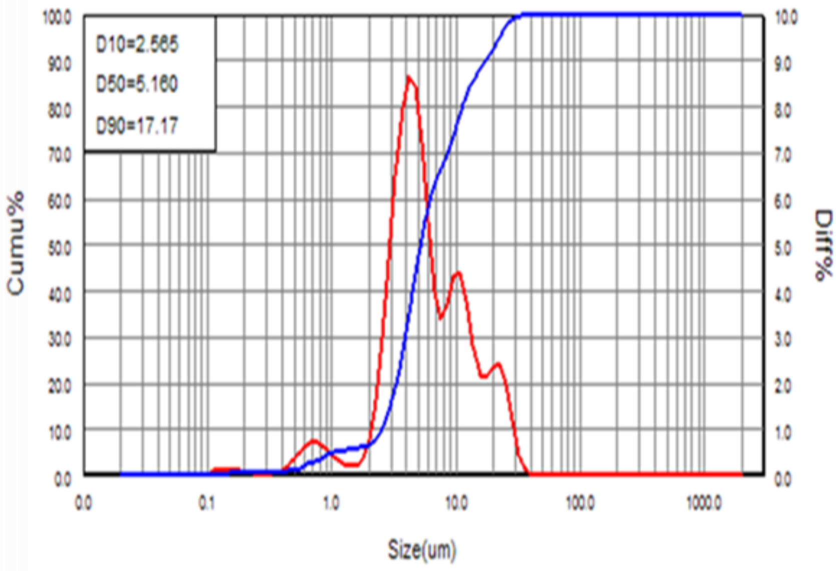

Diam um	Percent
0.100	0.00
0.200	0.50
0.500	1.14
1.000	4.66
2.000	6.54
5.000	48.16
10.000	75.23
20.000	92.80
45.000	100.00
75.000	100.00

Figure (4.3) Zr Powder Particle Size Distribution.

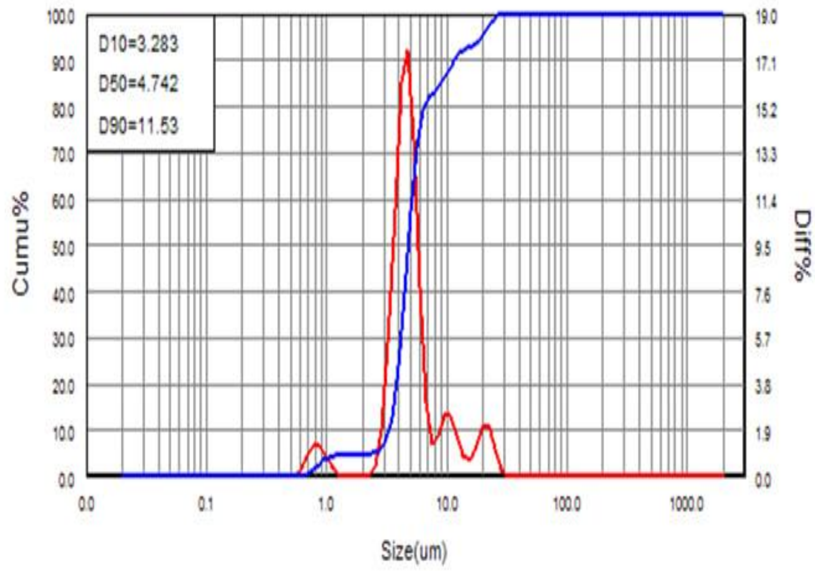

Diam um	Percent
0.100	0.00
0.200	0.00
0.500	0.00
1.000	3.90
2.000	4.83
5.000	57.78
10.000	86.97
20.000	95.59
45.000	100.00
75.000	100.00

Figure (4.4) Si Powder Particle Size Distribution.

4.3. Effect of Compacting Pressure on Green Density

Figure (4.5) shows that if the compacting pressure increases the green density increases too until it reaches a certain limit at which any further increase in the pressure has no or little effect on its value. So the preferred pressure was determined as 700 MPa for all the specimens prepared in the present study.

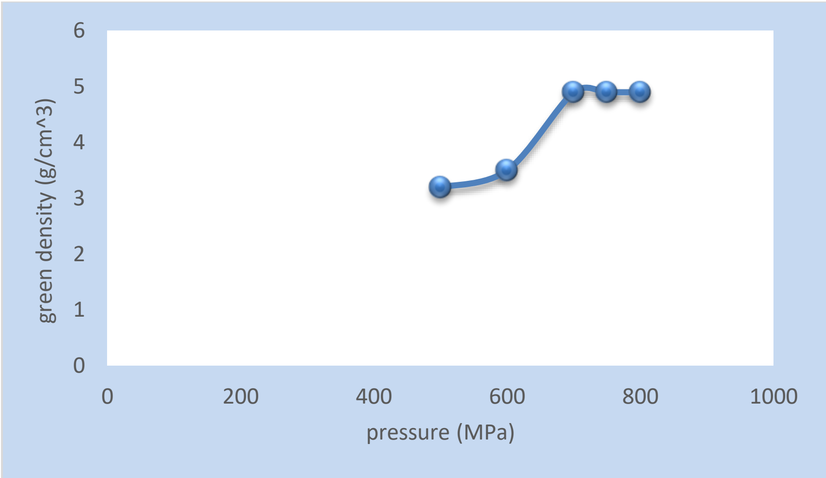

Figure (4.5): Green density vs. pressure before sintering.

4.4. Porosity of Sintered Specimens.

The porosity measured for all used alloys after the sintering process and the effect of Zr and Si on the porosity values has been cleared in Figures (4.6), and (4.7) respectively. It's clear from these figures that porosity values of the specimens decreased after sintering due to the distance among particles fills with small particles because of the difference with inside the granular size used for the powders, it found that the small sized particles take a seat down among the large sized particles.

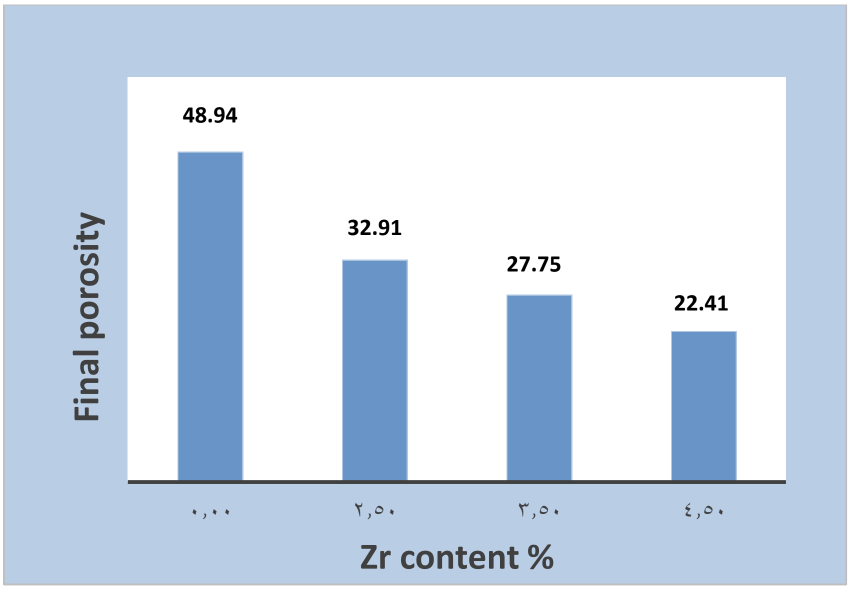

Figure (4.6): Final porosity for alloys A, C1, C2, and C3 and the effect of Zr content after sintering.

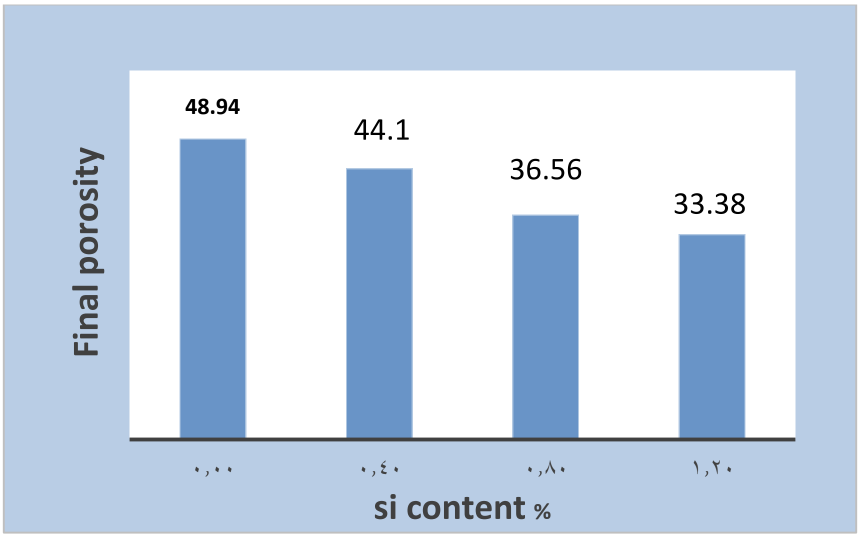

Figure (4.7): Final porosity for alloys A, D1, D2, and D3 and the effect of Si content after sintering.

Ti-35Nb alloy after heat treatment for 30 min at 900°C showed in figure (4.8) Where porosity decreases dramatically with compared to the base alloy before heat treatment where the base alloy before heat treatment is (48.94) while after heat treatment the porosity reach to (12.81).

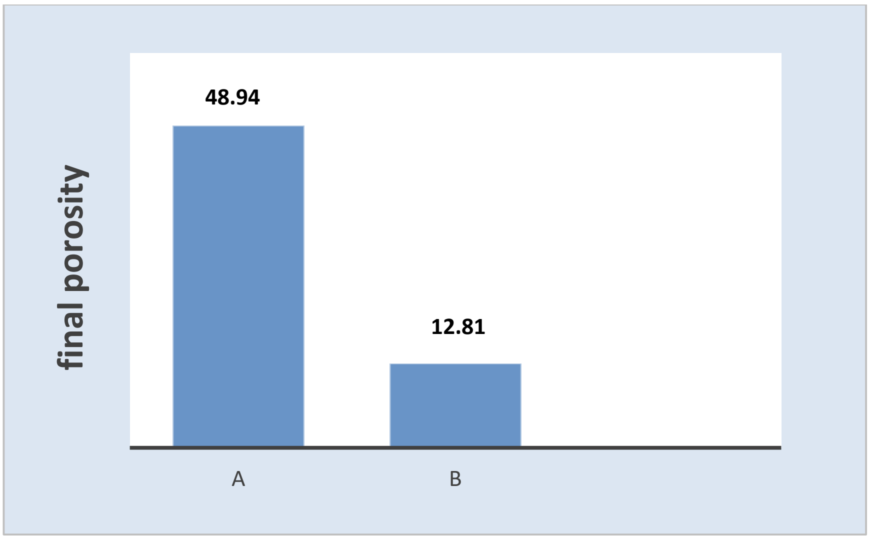

Figure (4.8): Effect of heat treatment on final porosity for A alloy after sintering.

Table (4.1): Show the Porosity After Sintering of All Alloys

Specimen code	Porosity after sintering	Improving%
A	48.94	
B	12.81	73.82
C1	32.91	32.75
C2	27.75	43.29
C3	22.41	54.20
D1	44.10	9.88
D2	36.56	25.29
D3	33.38	31.79

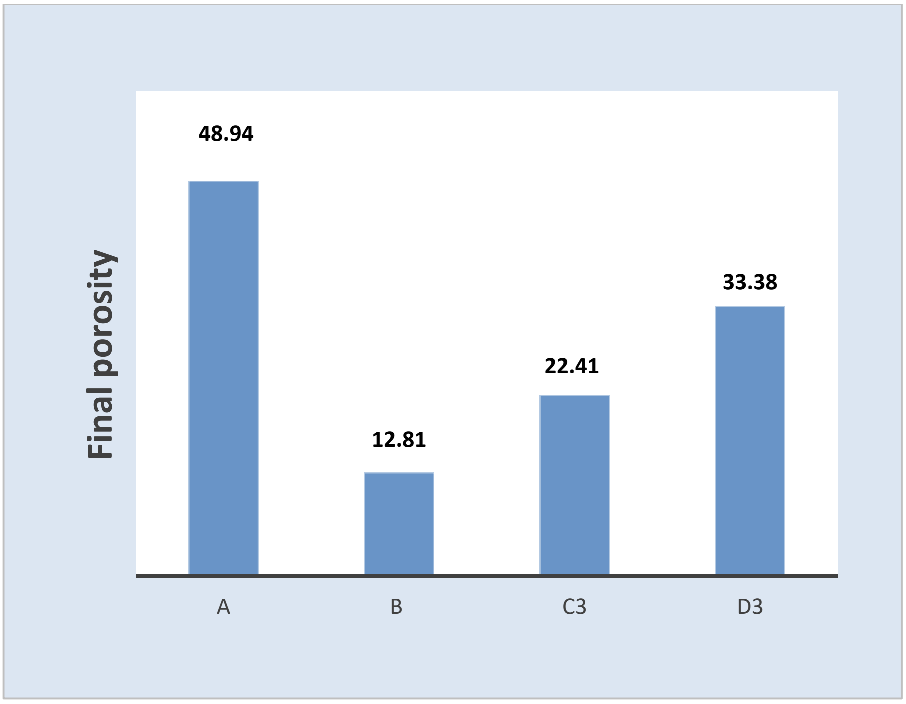

Figure (4.9): Comparison of porosity for all alloys.

4.5. Density of Sintered Specimens.

The final density after the sintering process and the effect of Zr and Si on the density values has been shown in Figures (4.10) and (4.11) respectively. The density is inversely proportional with porosity. From the results of the density values (after sintering), we notice an increase in the density value with an increase in the percentage of Zr and Si ratio because of the difference in particle size of elements where space between particles fills with small particles. Apparent density depends on factors such as particles size and distribution, surface area, particle shape, etc. [164].

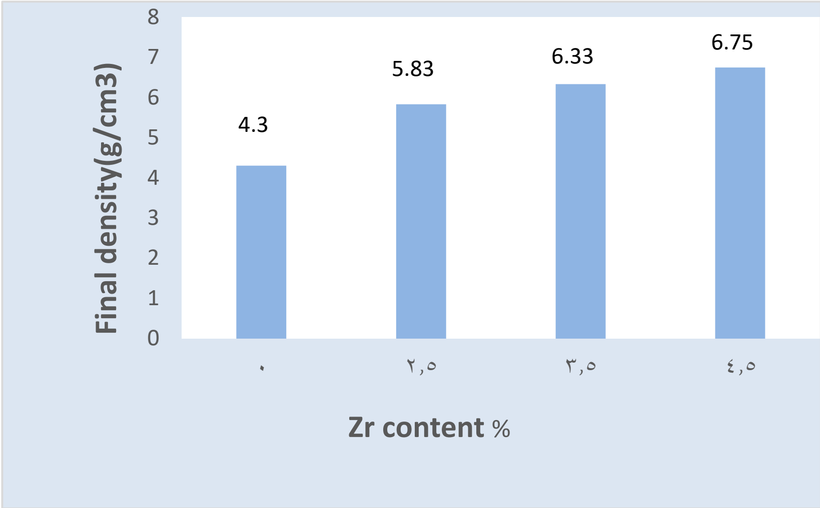

Figure (4.10) Effect of the zr concentration on the final densities of alloys A, C1, C2, and C3 after sintering.

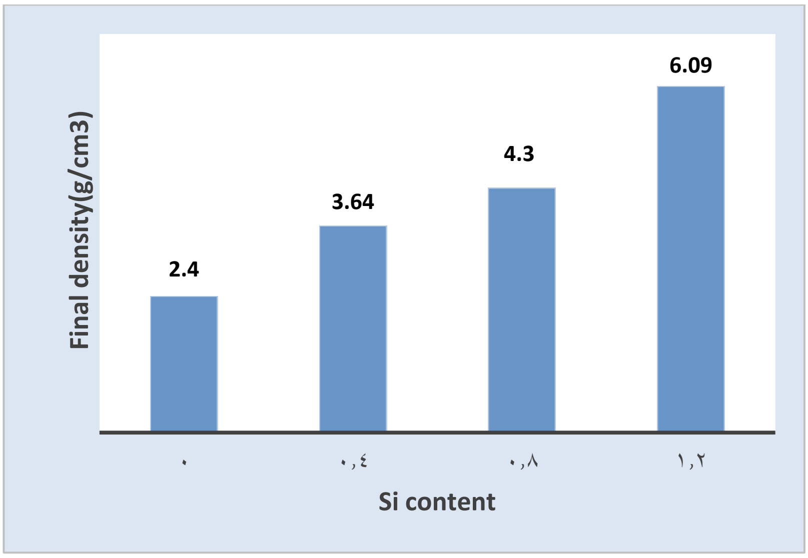

Figure (4.11): Effect of Si content on final density of A,D1,D2 and D3 alloys after sintering.

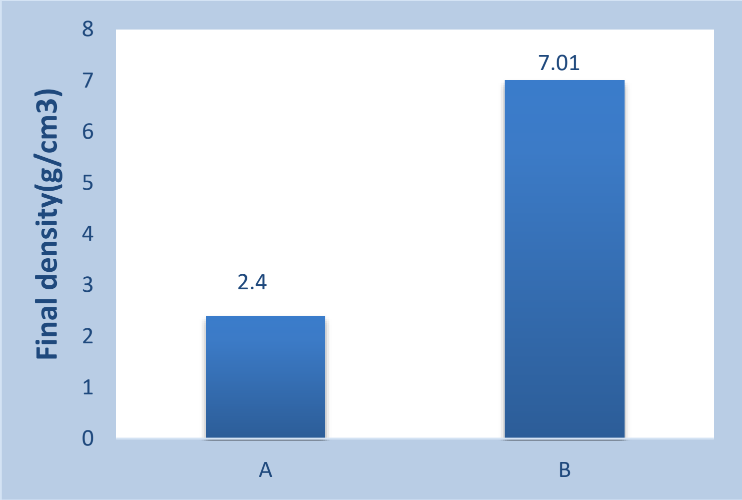

Figure (4.12): Heat treatment effect on A alloy after sintering.

As shown above figure (4.12) shows that the heat treatment effect on density of base alloy where the density was increased after heat treatment and improvement ratio is (65.76%). The increase in density after sintering regarded to reduction in porosity.

Table (4.2): Show the Density After Sintering of All Alloys.

Specimen code	**Density after sintering (g/cm3)**	**Improving%**
A	2.40	
B	7.01	65.76
C1	5.83	58.83
C2	6.33	62.08
C3	6.75	64.44
D1	3.64	51.66
D2	4.30	44.18
D3	6.09	60.59

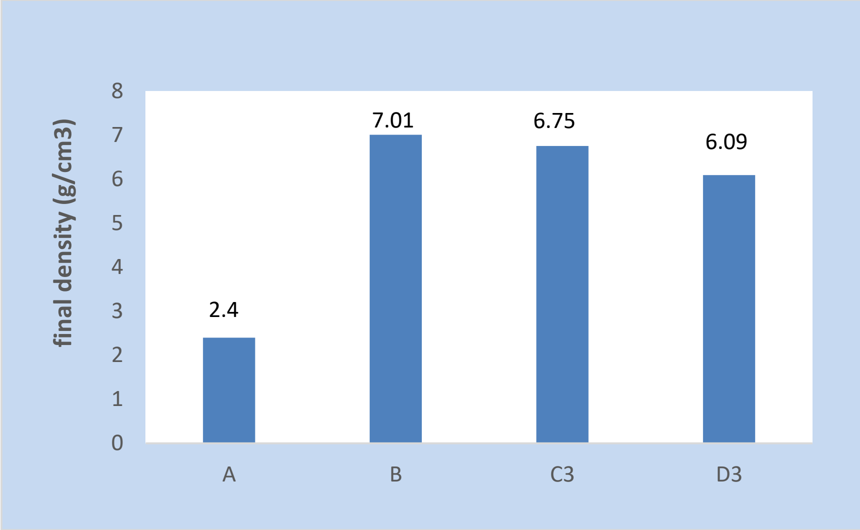

Figure (4.13): Comparison of final density of all alloys.

4.6. Chemical Compositions analysis

The chemical compositions for the prepared alloys, which were examined using (x-ray florescent test). According to the composition study, the principal alloying elements are present within the specified bounds. for the A, C3, and D3 specimens, as indicated in table (4,3).

Table (4.3) Chemical Composition of A, C3,D3

code	Ni	Cu	Cr	Mg	Ti	Fe	Zr	Nb	Hf	Si
A	0	0	0	0.02	65.42	0.208	0.371	31.8911	0	0
C3	0.037	0.04	0.088	0.054	55.778	0.242	6.504	33.217	0.196	0
D3	0.055	0	0	0.041	60.899	0.175	0.326	32.866	0	0. 7

4.7. Analysis of X-Ray Diffraction.

4.7.1. X-Ray Diffraction for green compacts.

Figures (4.14), (4.15), and (4.16) illustrated XRD for (Ti-35wt%Nb), (Ti-35Nb-6.9Zr) wt% and element silicon before sintering process.

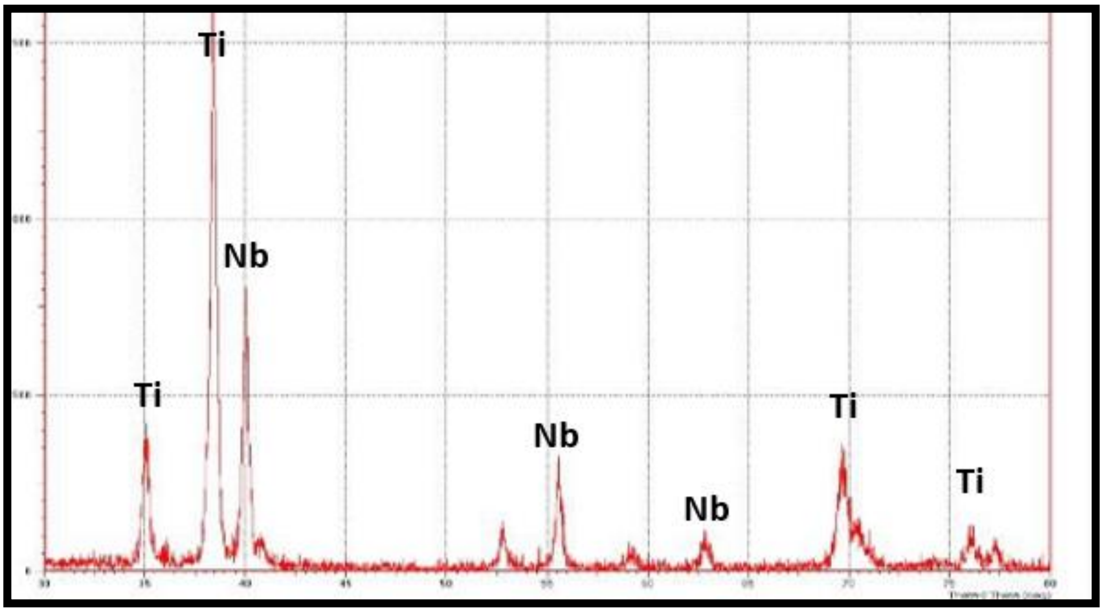

Figure (4.14) XRD for A alloy before sintering.

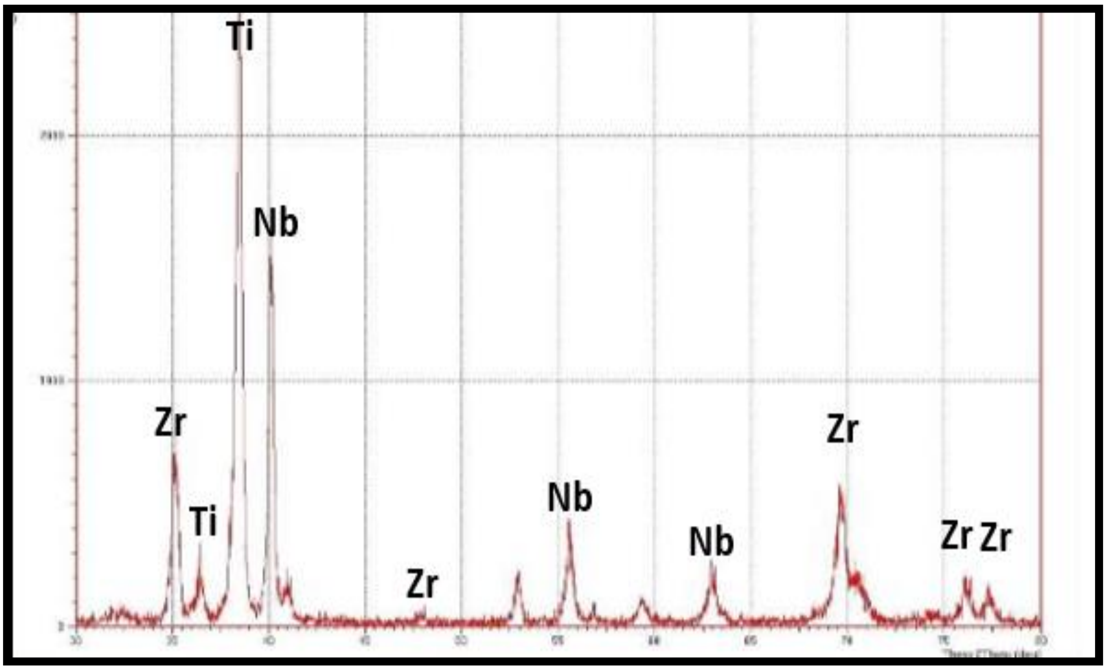

Figure (4.15)XRD for C3 alloy before sintering.

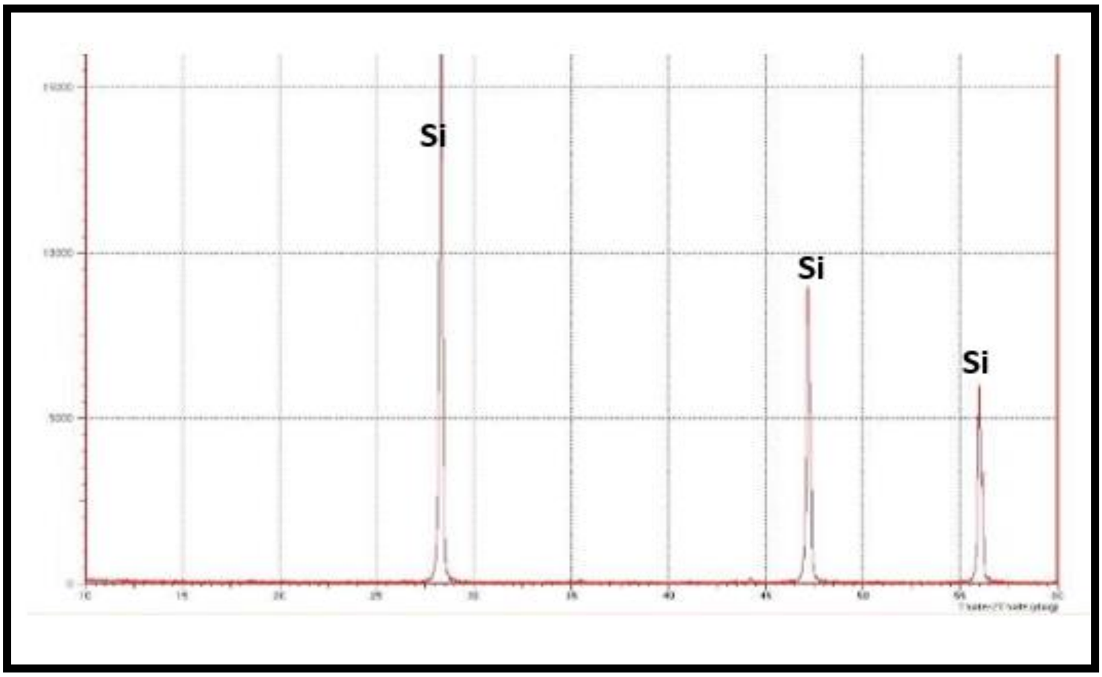

Figure (4.16) XRD for si element.

4.7.2. X-Ray Diffraction analysis after sintering.

Since the existence of phases change might affect the properties of the prepared alloy, the sintered (A, B, C2, C3, D2, and D3) alloys was examined using X-ray diffraction analysis. Diffusion processes like phase transition require a high temperature to take place, following 6 hours of sintering at 1100°C under argon gas, Figure (4.17) shows XRD pattern for the A alloy. All Ti, Nb were seen to convert into (α Ti) and (β Ti) phases respectively. In the Ti–35% wt Nb alloy, the α phase declined and the original β phase-dominated structure was transformed into a mixture of α and β phases.

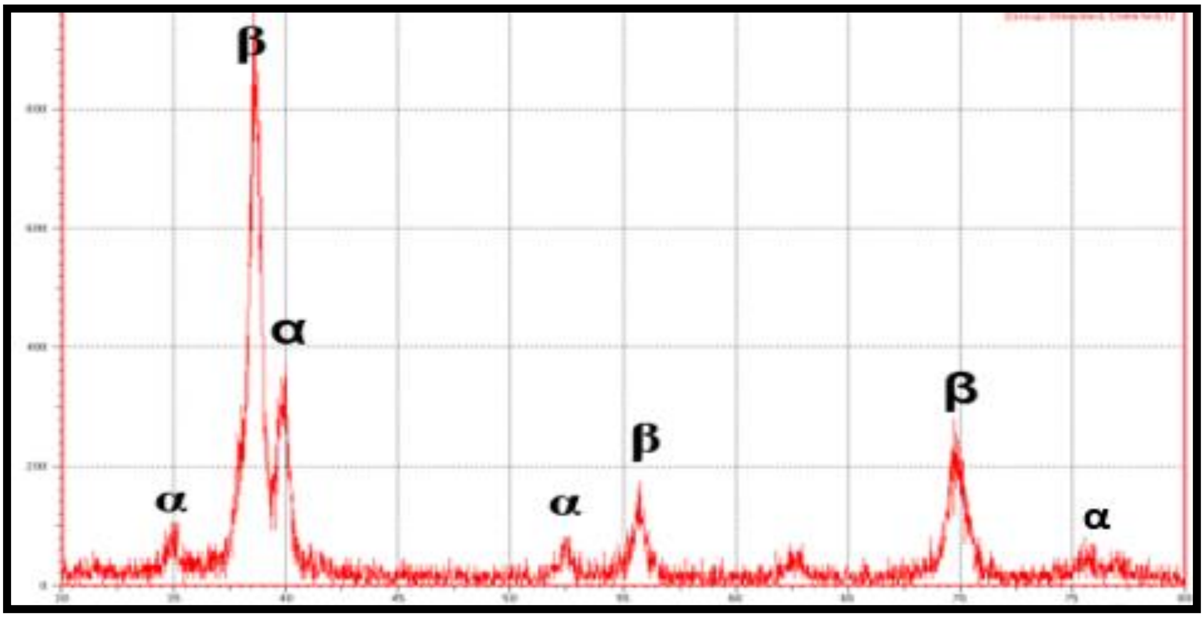

Figure (4.17): XRD patterns for A alloy.

Figure (4.18) illustrates the XRD pattern for B alloy (Ti-35Nb) sintered alloy after heat treatment at 900°C for 30 minute showed only α+β phases identified by XRD analysis [140]. It seems clear that the alpha phase was more pronounced than the alloys added to it zirconium and silicon in comparison with base alloy before heat treatment.

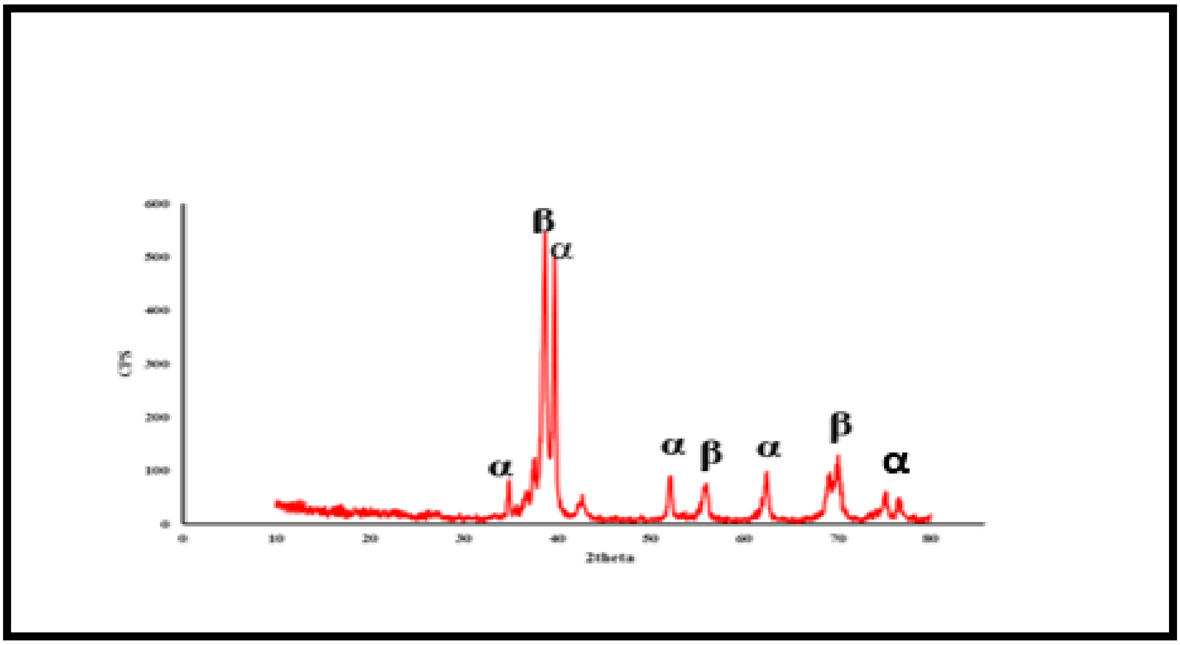

Figure (4.18): XRD patterns for B alloy.

The phases in the Ti-Nb-Zr alloys were analyzed in detail using X-ray diffraction (XRD). Figure (4.19) and (4.20) display the phases present in the Ti-Nb-Zr alloys are related to the Zr content. The presence of both α and β peaks is evident in an alloy with a 6.9 wt% Zr. The primary α peak diminishes gradually as the Zr content increases.

XRD pattern for C2 and C3 alloys illustrates after the sintering process that all amount of Ti, Nb, and Zr transformed to β Ti phase and small amount of α Ti because Zr β stabilizers depress the transition temperature by stabilizing the β phase. It was found that with more Zr addition, the amount of β phase increased while the amount of α phase reduced [145]. This means that 1100°C for 6 h under Argon gas was enough to complete the sintering process due to the enhancement of the interdiffusion between Ti, Nb, and Zr.

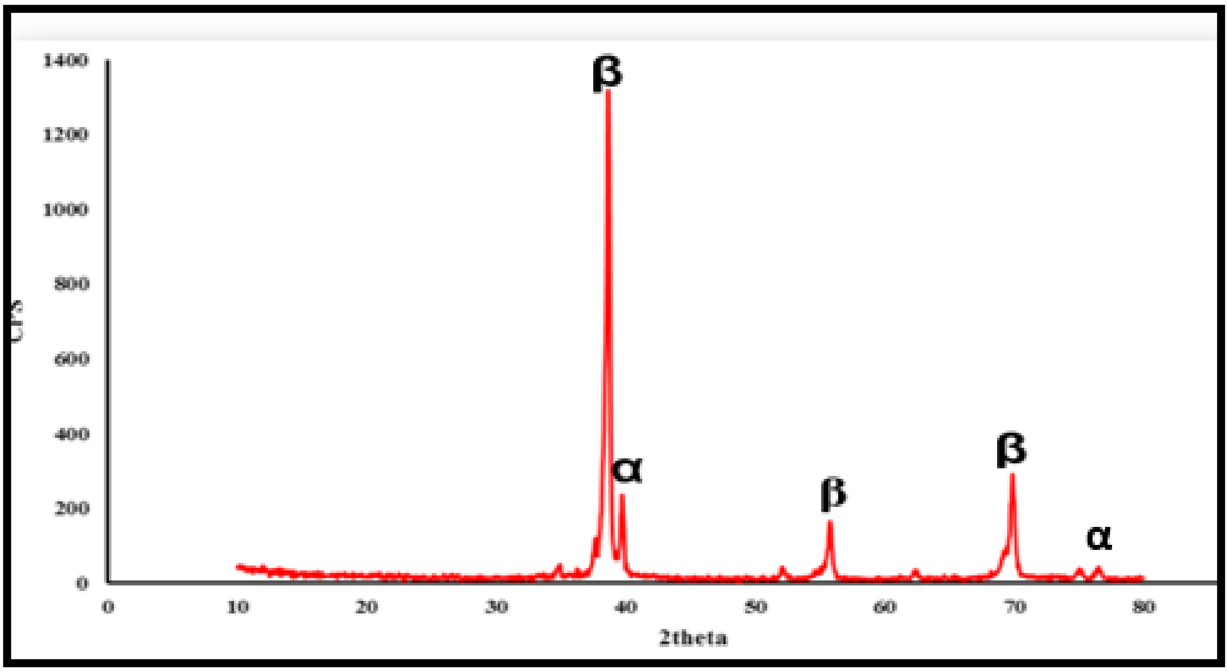

Figure (4.19): XRD patterns for C2 alloy.

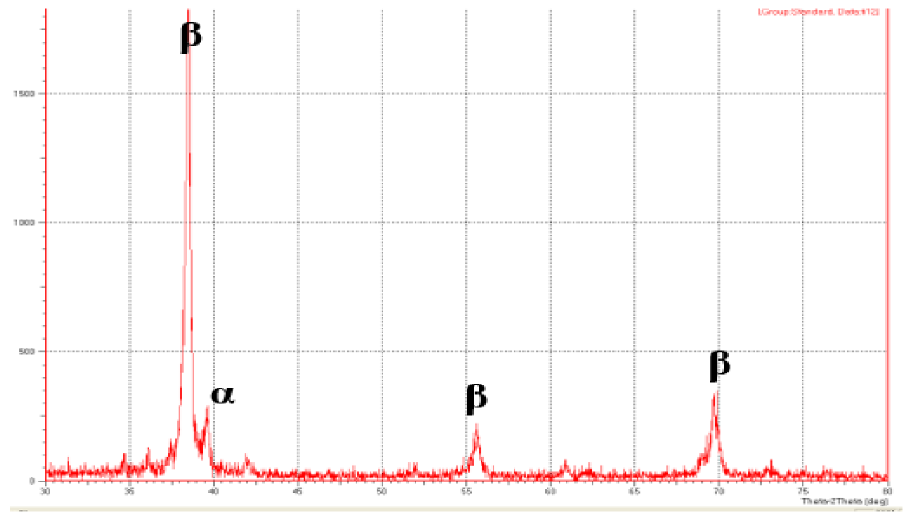

Figure (4.20) XRD patterns for C3 alloy.

Figure (4.21) and (4.22) illustrates XRD pattern for D2 and D3 alloy after the sintering process, all amount of Ti, Nb and Si transformed to β Ti phases, this means that 1100 C° and 6h under Argon gas was enough to complete sintering process due to the enhancement of the interdiffusion between Ti, Nb and Si. Higher Si concentration makes β-phase in the current alloy system more stable because Si plays a role in enhancing -β phase stability [143].

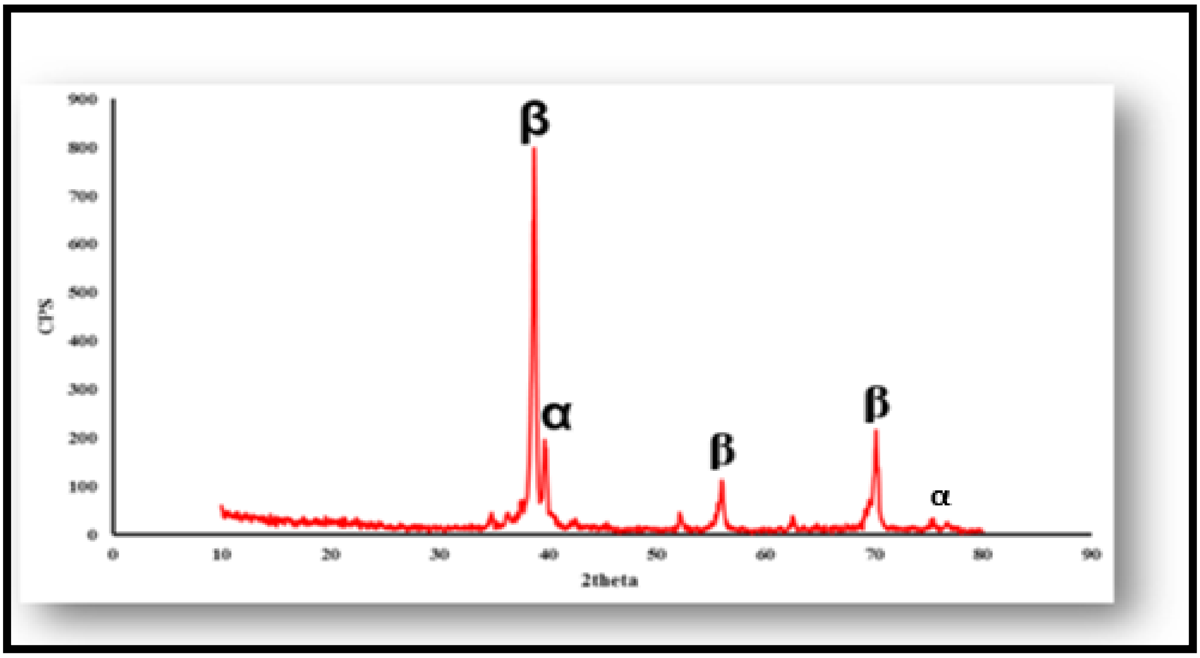

Figure (4.21): XRD patterns for D2 alloy.

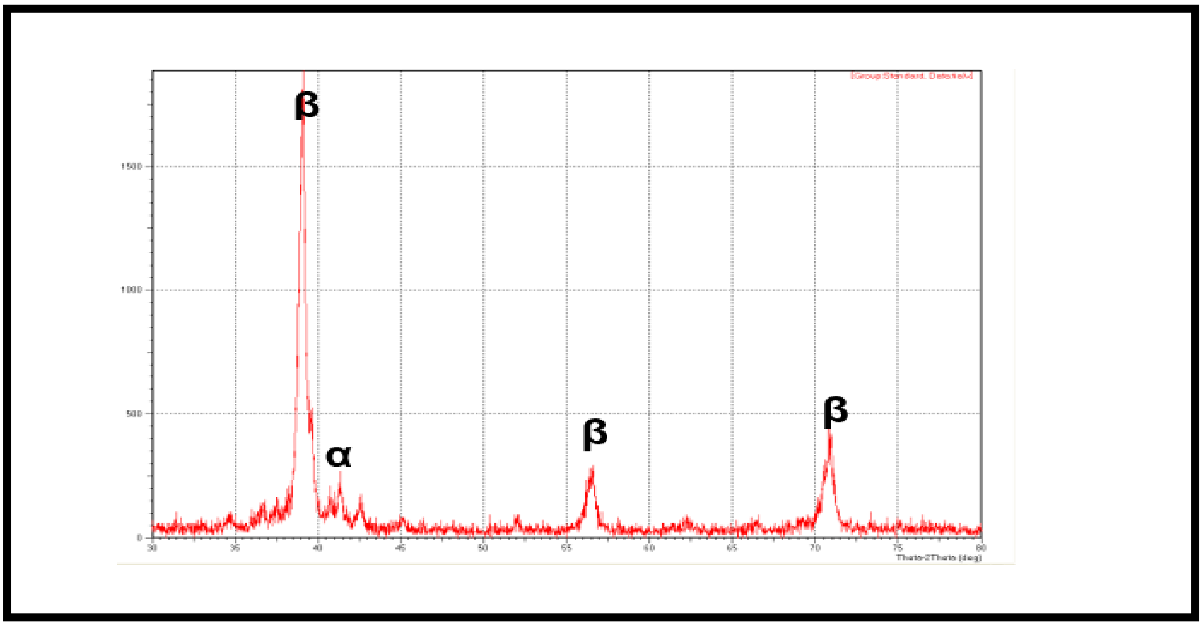

Figure (4.22): XRD patterns for D3 alloy.

4.8. Microstructure of the Sintered Specimens.

The microstructure of the etched specimens, were utilized by light optical microscopes (LOM) and scanning electron microscopes (SEM). Figure (4.23) shows the optical microstructures image of the base alloy, the microstructure demonstrates that at room temperature, all of the specimens alloys mostly have a two phase (α +β) structure. We notice from the figure (4.24) that the phases remained the same without any change in phases (α+β), but as we can see in the figure, there is a great refine softening of the microstructure compared to the alloy before the heat treatment, which has a clear role in improving the alloy's mechanical characteristics upon treatment. Figures (4.25) to (4.30) show that when the Zr and Si concentration rises, the proportion of the α phase drops. This is belong to the role of Zr and Si as beta stabilizers, and increasing the dark area (β-phase) when they are added. [165.166].

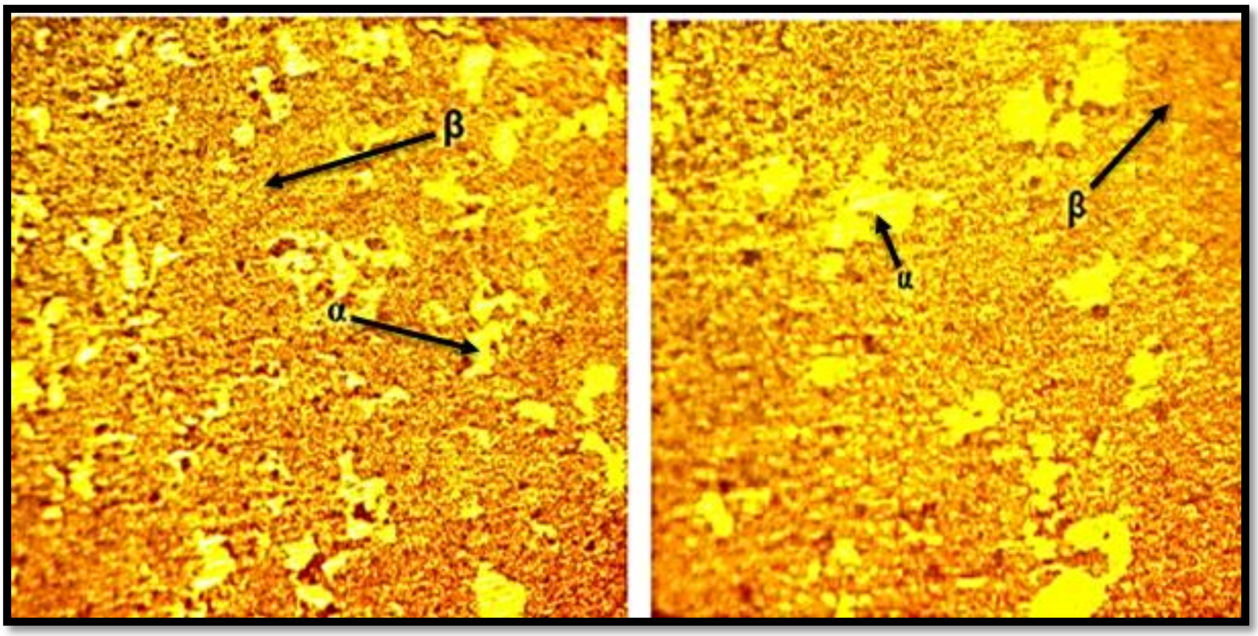

Figure (4.23): Microstructure for A alloy after sintering and etching with two magnifications (100x,200x).

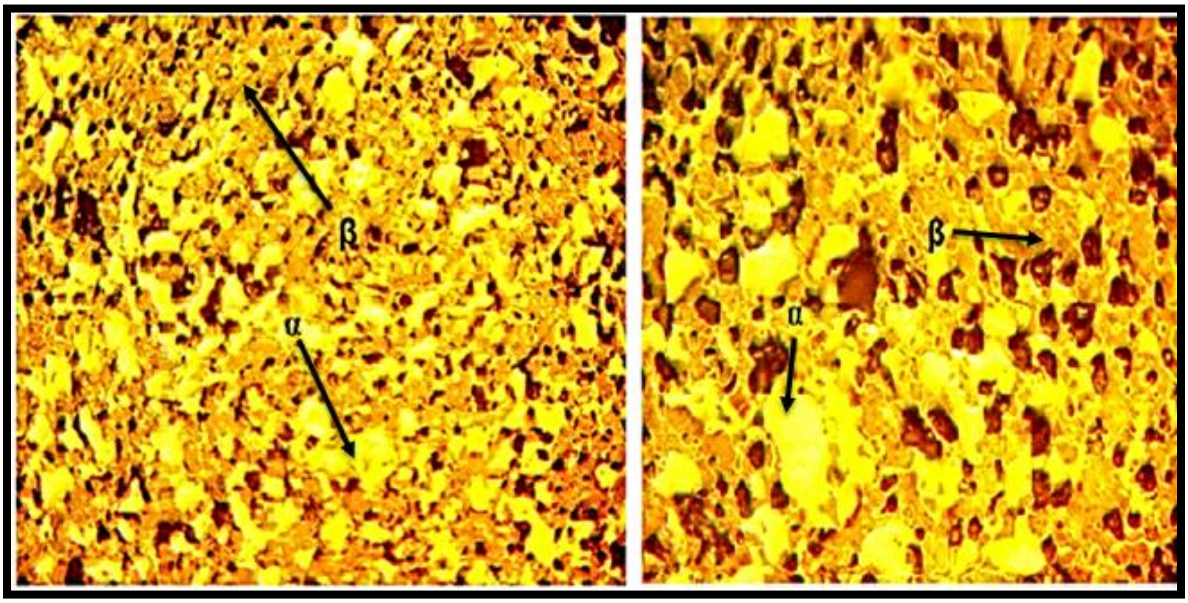

Figure (4.24): Microstructure for B Alloys after Sintering and Etching with two magnifications (100x,200x).

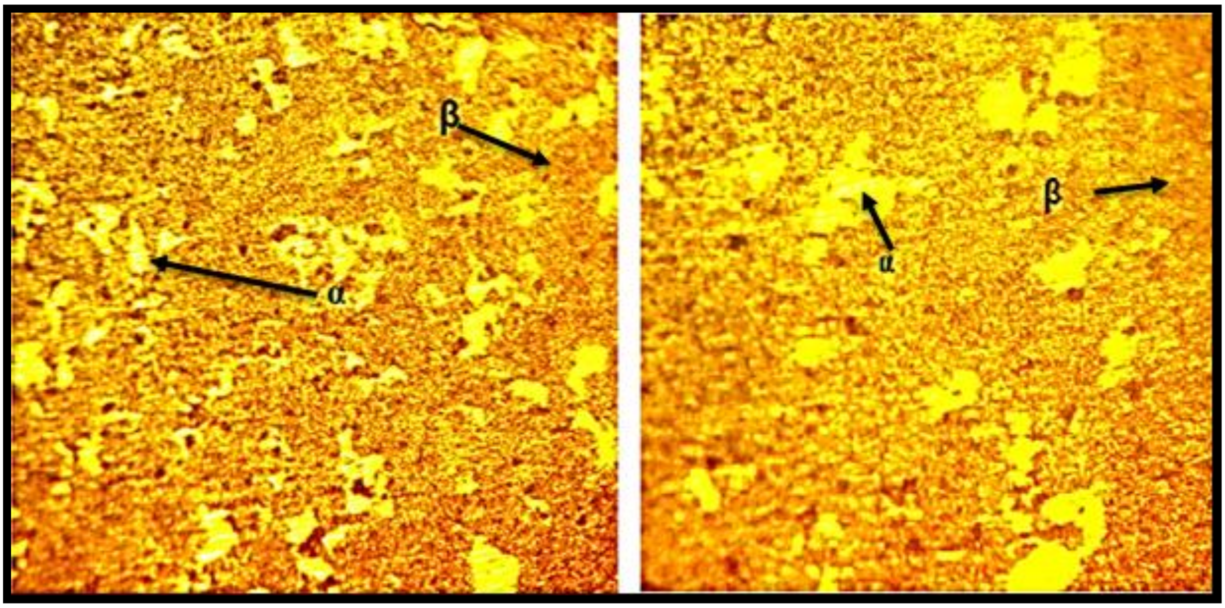

Figure (4.25): Microstructure for C1 Alloys after Sintering and Etching with two magnifications (100x,200x).

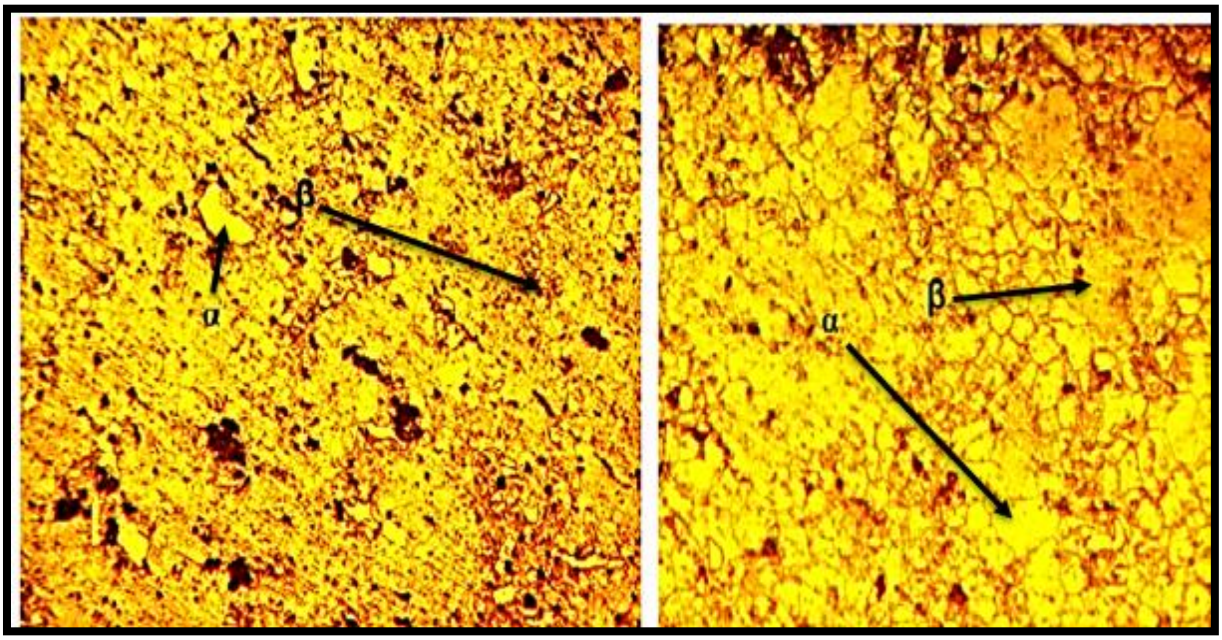

Figure (4.26): Microstructure for C2 Alloys after Sintering and Etching with two magnifications (100x,200x).

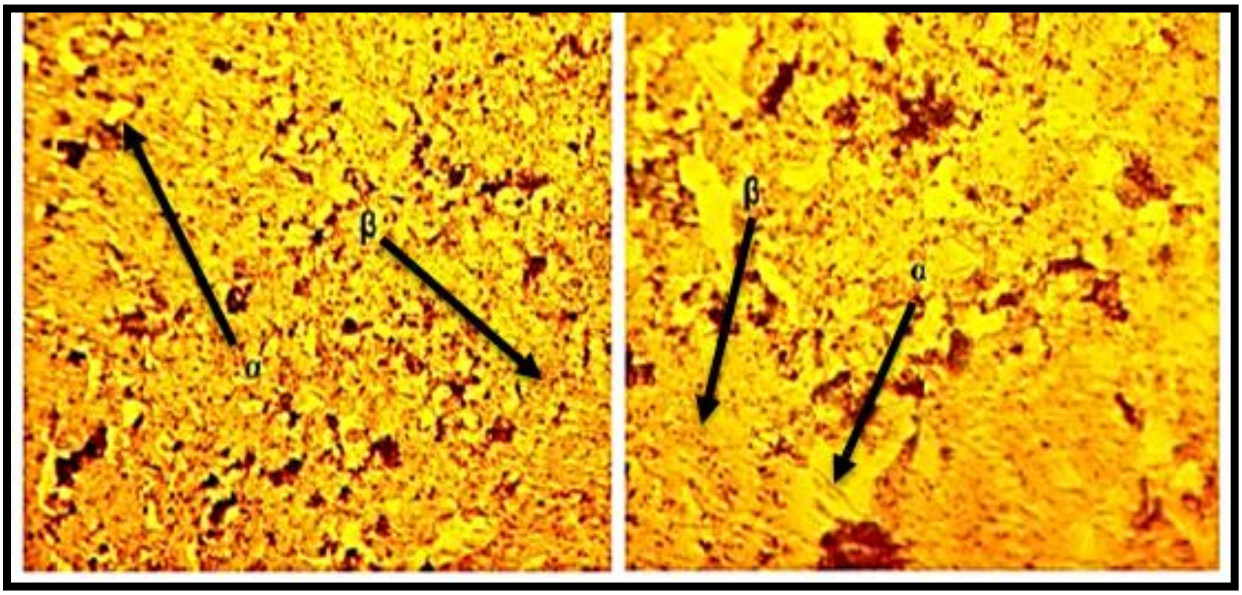

Figure (4.27): Microstructure for C3 Alloys after Sintering and Etching with two magnifications (100x,200x).

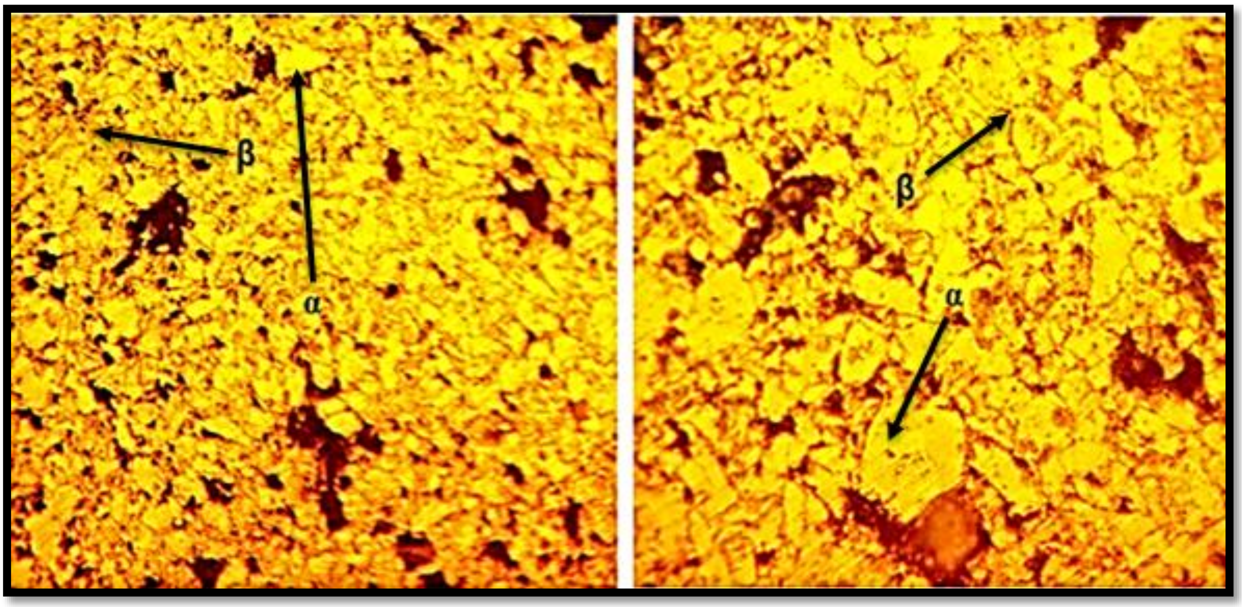

Figure (4.28): Microstructure for D1 Alloys after Sintering and Etching with two magnifications (100x,200x).

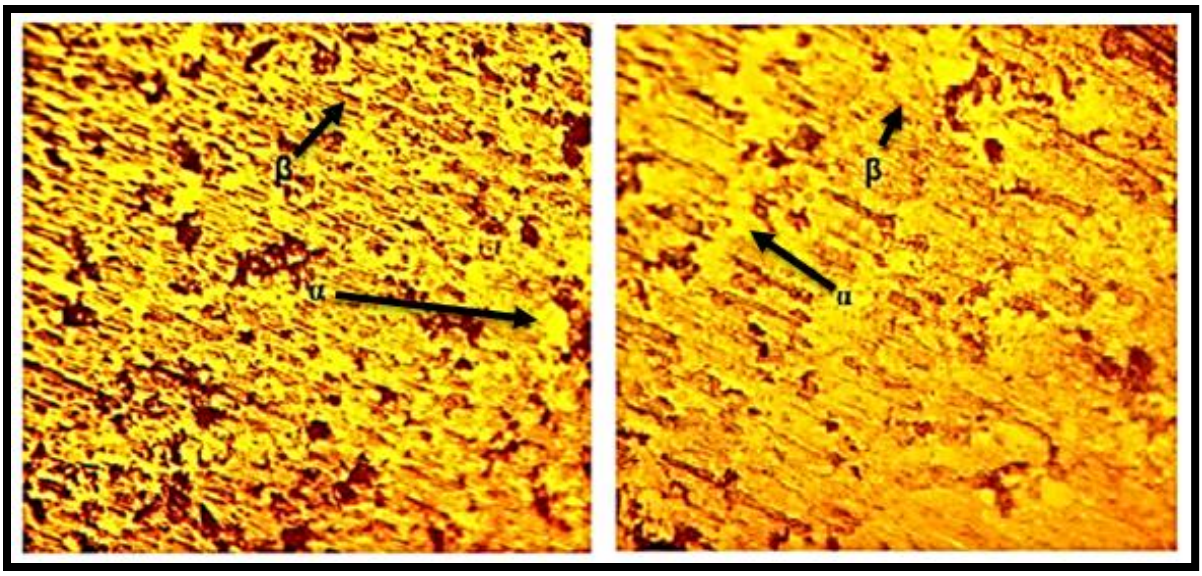

Figure (4.29): Microstructure for D2 Alloys after Sintering and Etching with two magnifications (100x,200x).

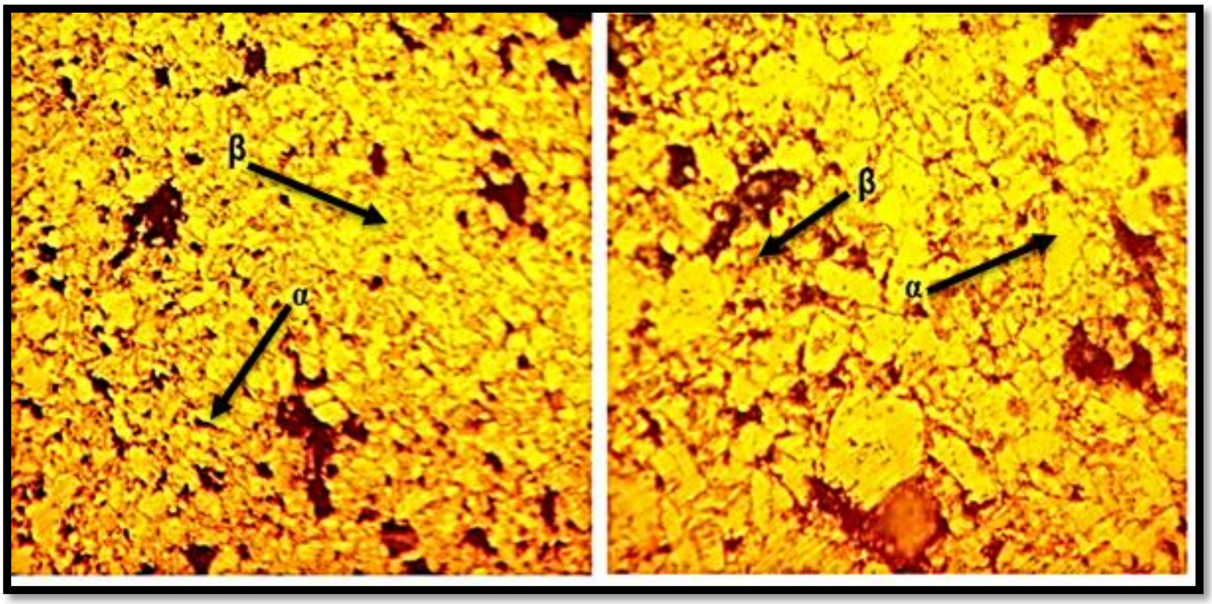

Figure (4.30): Microstructure for D3 Alloys after Sintering and Etching with two magnifications (100x,200x).

Due to the high sensitivity of SEM images to chemical composition, the sintered specimens' microstructure reveals a two phases (αTi and βTi) of a multiphase structure are supporting the XRD findings.

As shown in Figures (4.31 to 4.36), etching reveal phases ($\alpha+\beta$) and grain boundaries which are easily appear as thin gray or black lines. This means success of the manufacturing process by powder metallurgy and appearance multiphases of α alpha and beta β phases. The results of the SEM showed results similar to OM and XRD as the addition of Zr and Si elements in different proportions had a clear role in enhancing the beta phase and reducing the alpha phase, also the SEM images show that by increasing both silicon and zirconium ratios the beta phase increases**.**

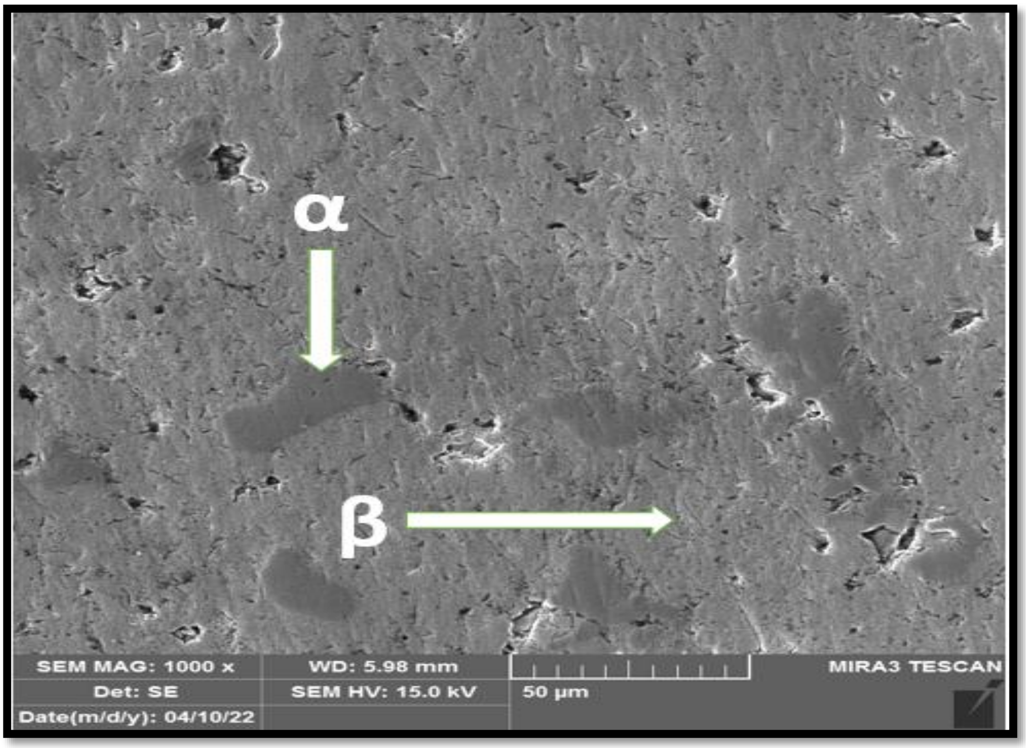

Figure (4.31): SEM for for A alloy after Sintering.

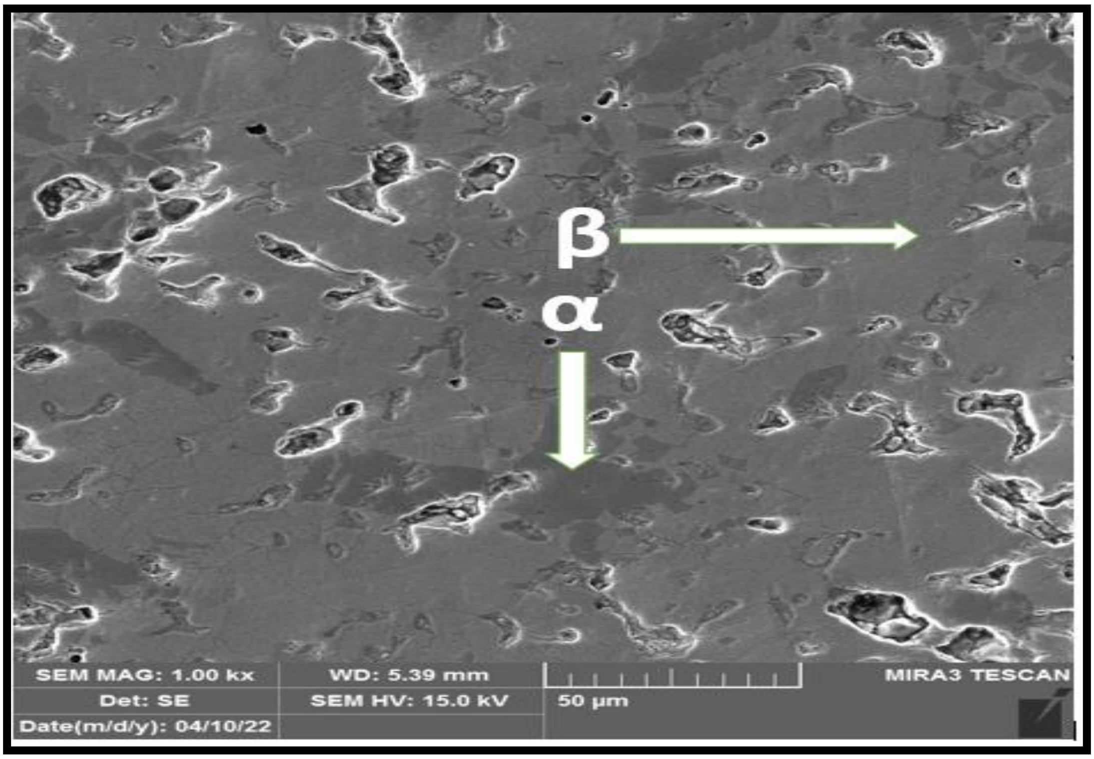

Figure (4.32): SEM for for B alloy after Sintering

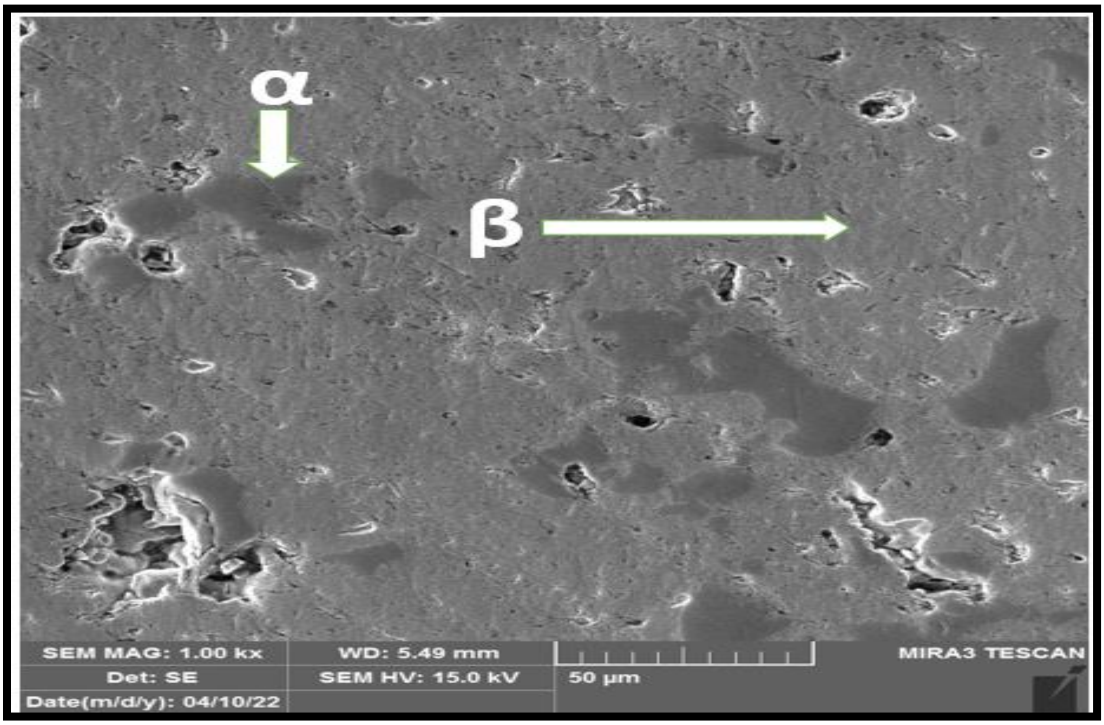

Figure (4.33): SEM for for C2 alloy after Sintering.

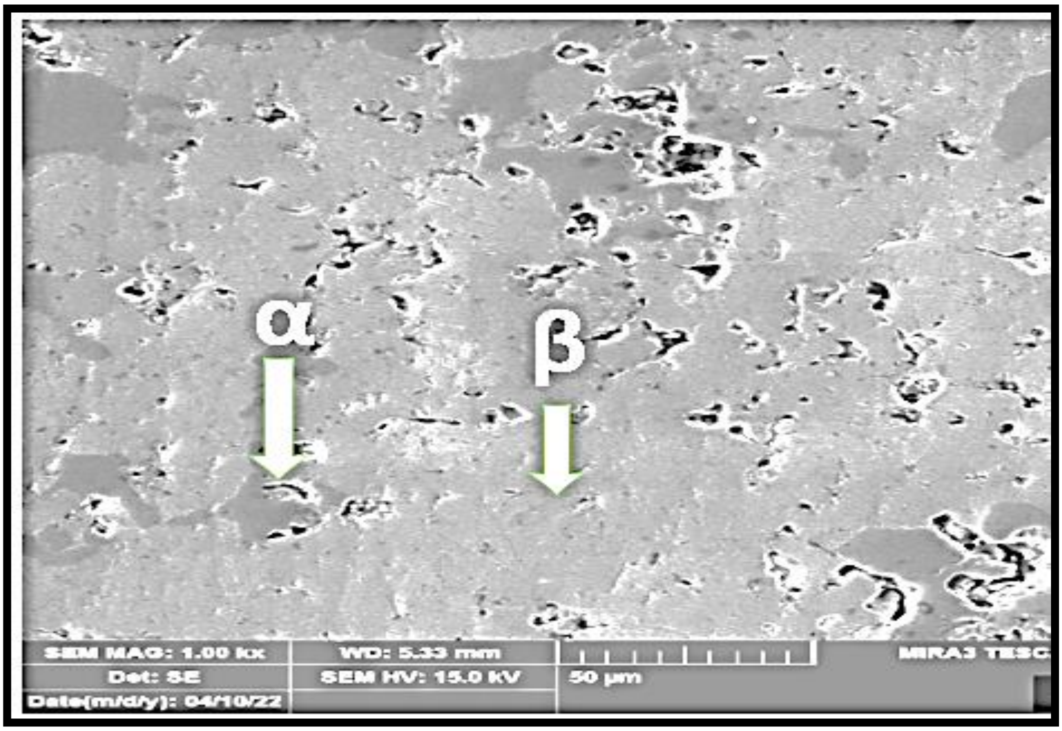

Figure (4.34): SEM for C3 alloy after Sintering.

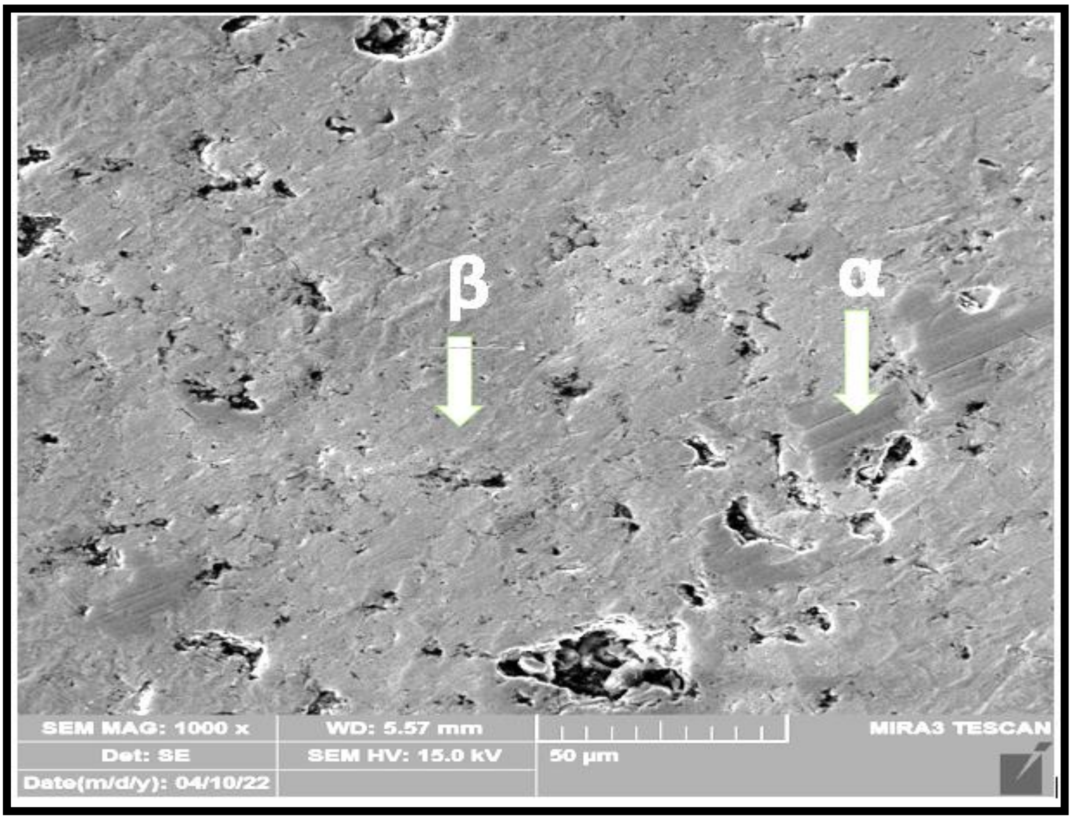

Figure (4.35): SEM for for D2 alloy after Sintering.

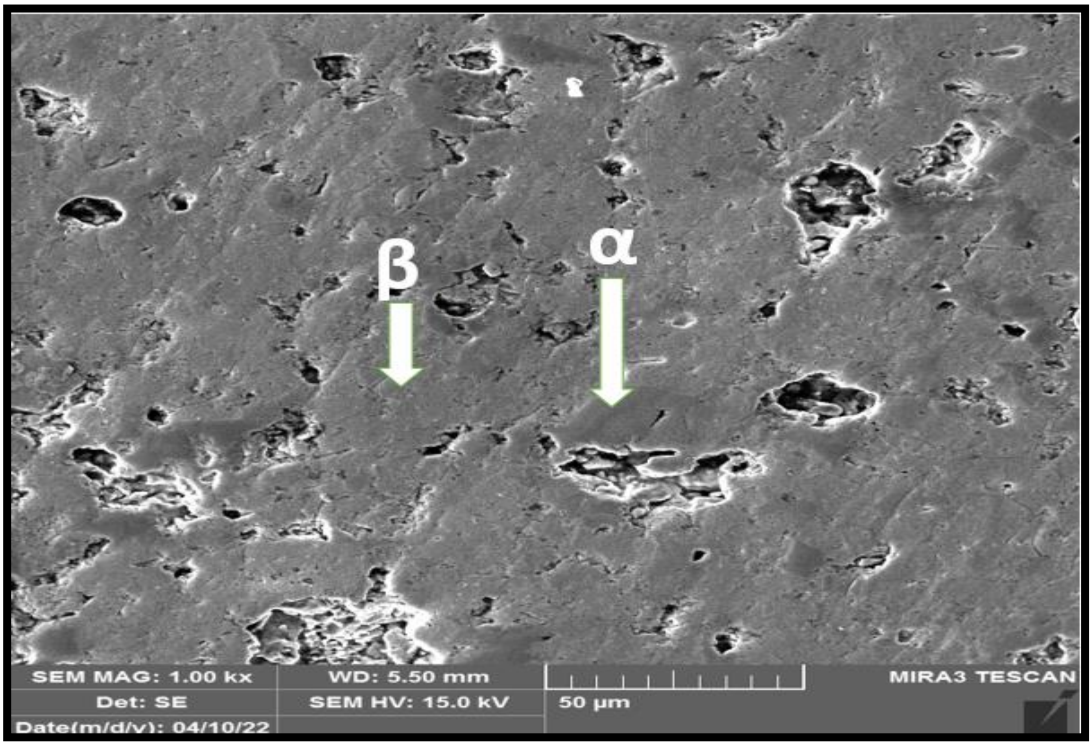

Figure (4.36): SEM for for D3 alloy after Sintering.

4.9. Energy Dispersive X-ray Spectroscopy (EDX)

Energy dispersive spectroscopy (EDS) utilized a high-energy focused electron beam to emit an X-ray spectrum of a solid specimen. EDS is able to identify the chemical composition that results from the contrast topography differences on an SEM image. Precision obtained from specimens is limited by statistical error. EDS was scanned on several different polished specimens. Figure (4.37) shows the EDS spectrum of elements found in base Ti-35%Nb alloys. The chemical analysis consists of Titanium, and Niobium where quantified because the basic components of the alloy consist of these elements with the presence of other elements present in very small percentages. On the other hand, the EDS analysis for the prepared specimens with (5.4wt% and 6.9wt%) addition of Zirconium, are shown in figures (4.39) and (4.40) respectively while EDS analysis for the prepared specimens with 0.4wt% and 0.6wt%)

addition of Silicon is shown in figure (4.41) and figure (4.42) respectively. It seems clear from the chemical analysis that Titanium, Niobium, Zirconium and Silicon material are present in the composition the chemist of prepared alloys. In addition to the main elements in the alloy (Titanium, Niobium, Zirconium and Silicon) with the presence of other elements present in very small percentages. As can be seen, the results of EDS analysis were relatively close from the percentage of addition, because the values gained from EDS analysis do not cover the total area, only the spot where the electron stroke [167].

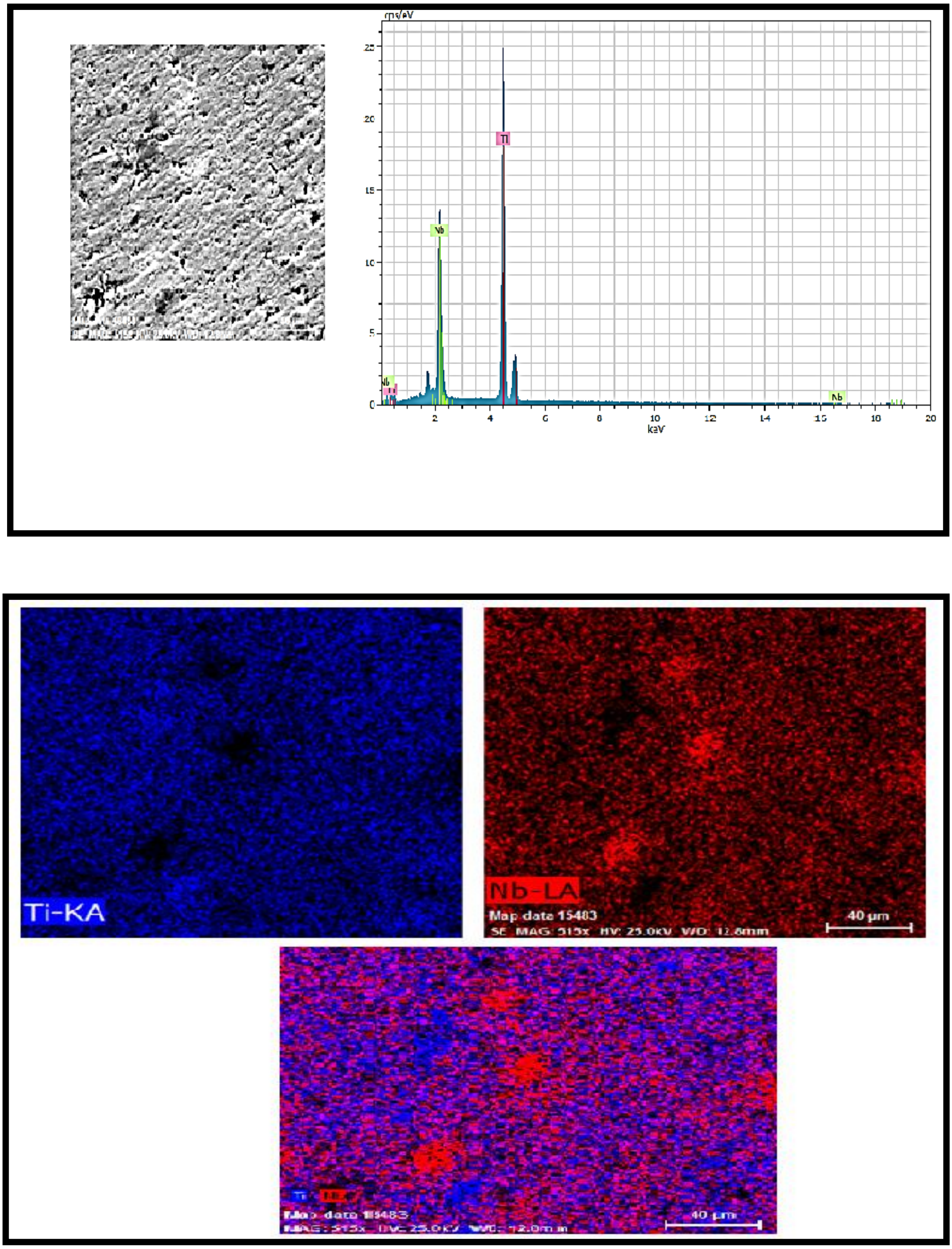

Figure (4.37) a :EDS for **A** alloy**,** b :mapping for A alloy.

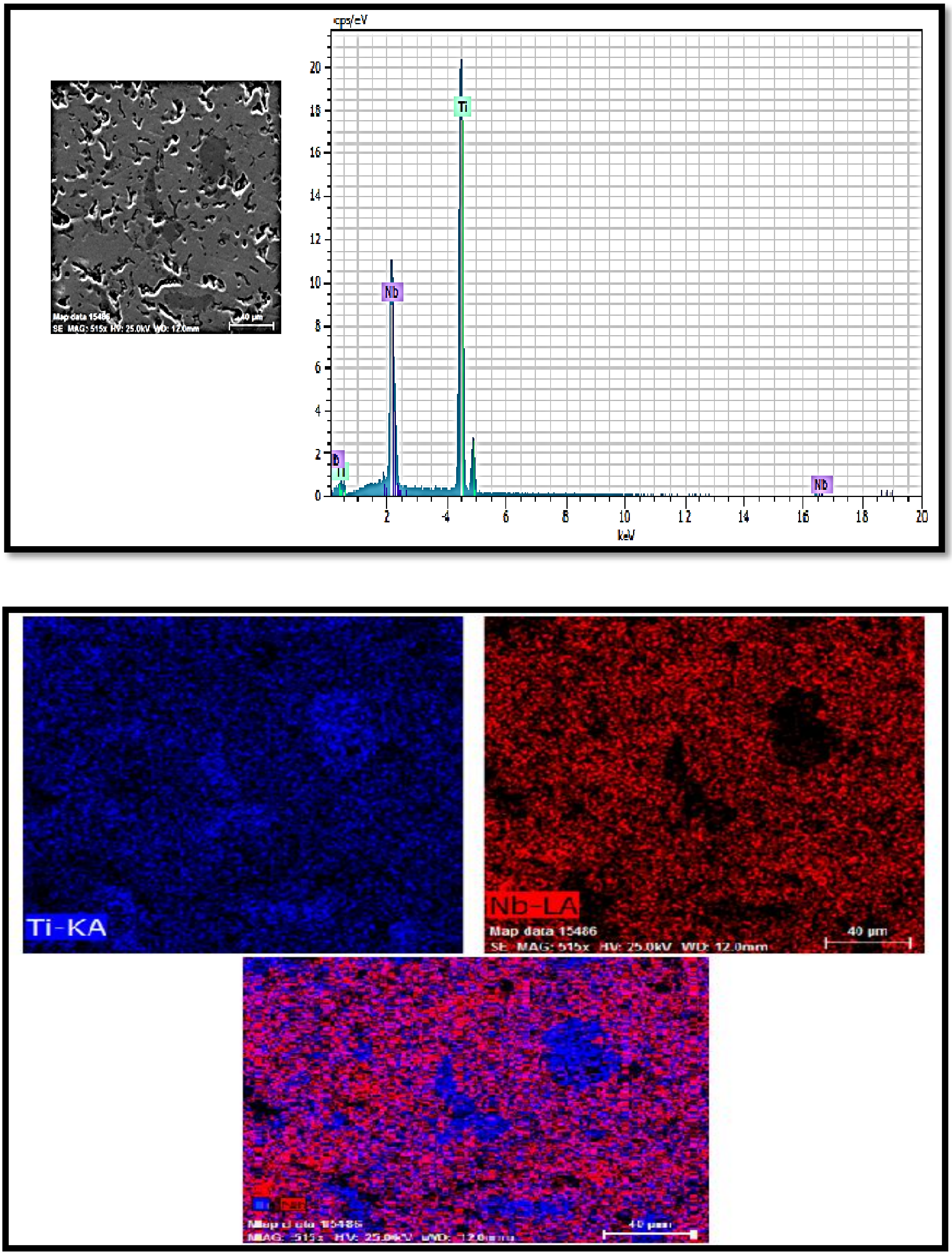

Figure (4.38) a :EDS for **B** alloy**,** b :mapping for B alloy .

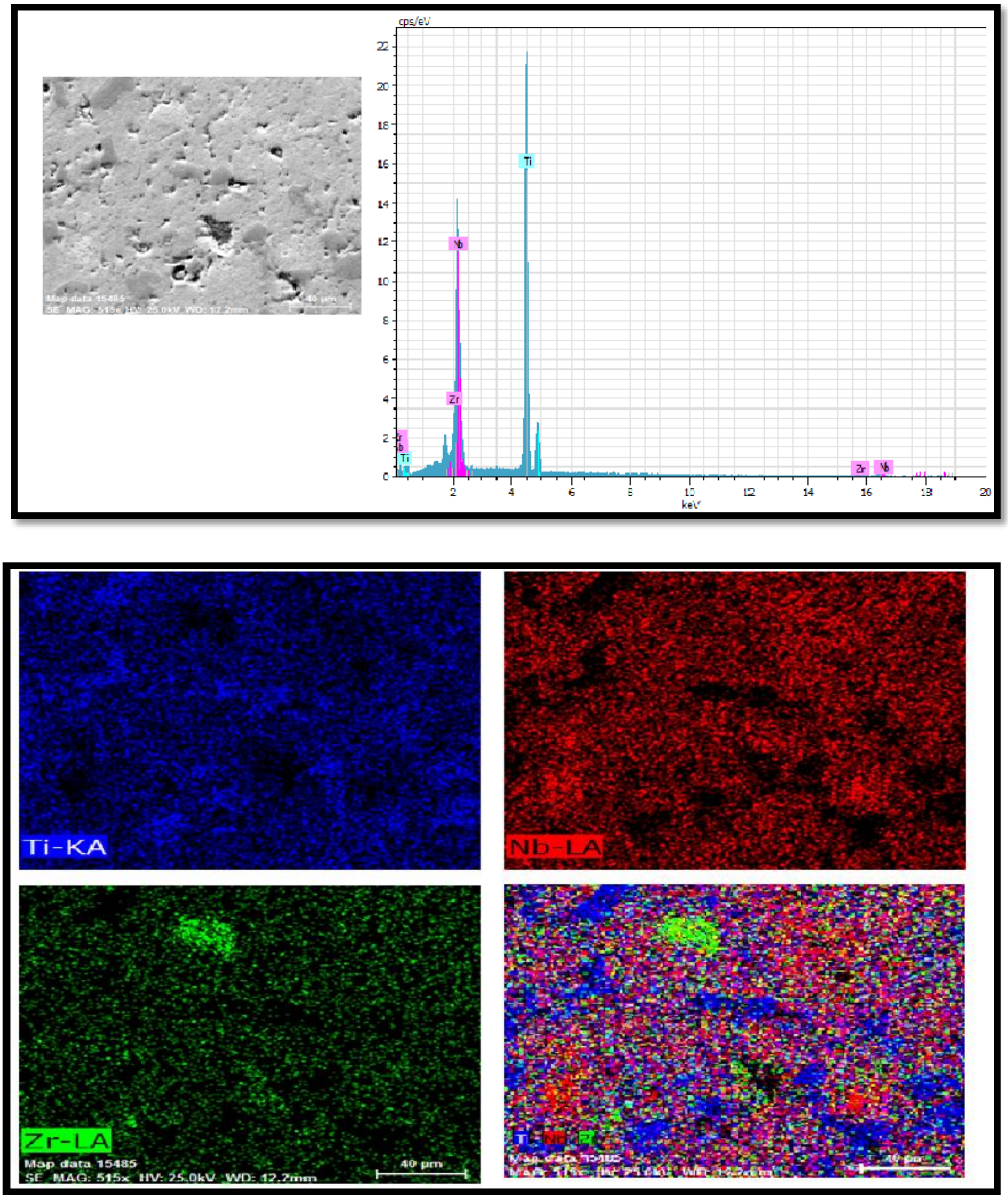

Figure (4.39) a :EDS for **C2** alloy**,** b :mapping for C2 alloy.

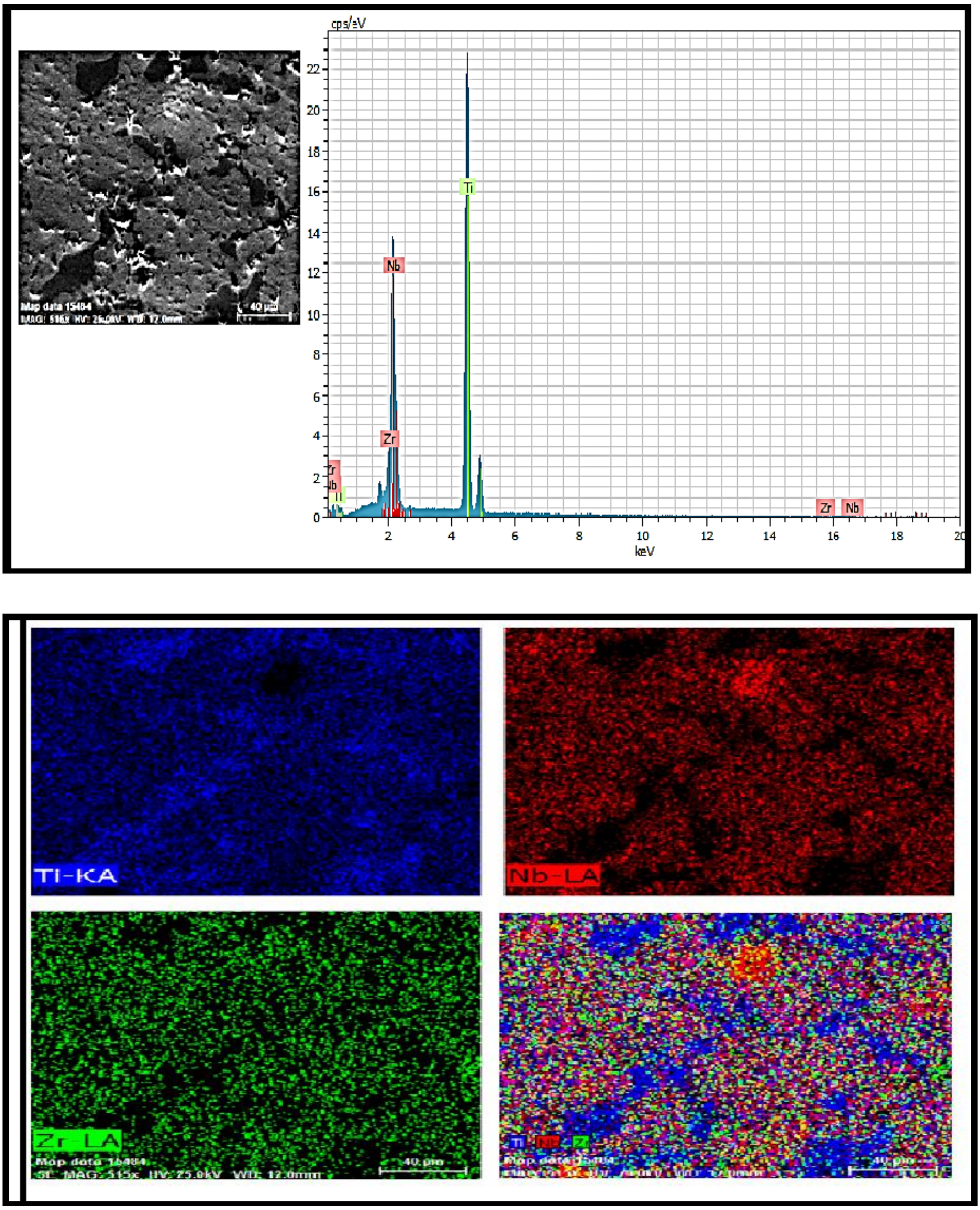

Figure (4.40) a :EDS for **C3** alloy**,** b :mapping for C3 alloy.

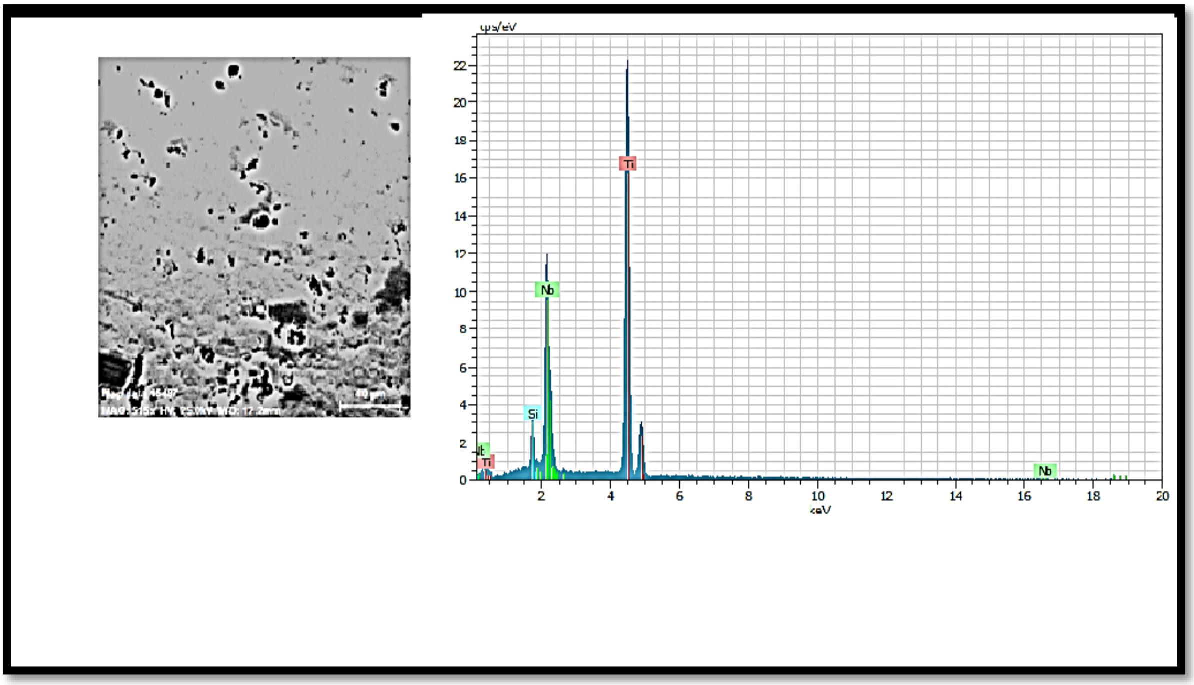

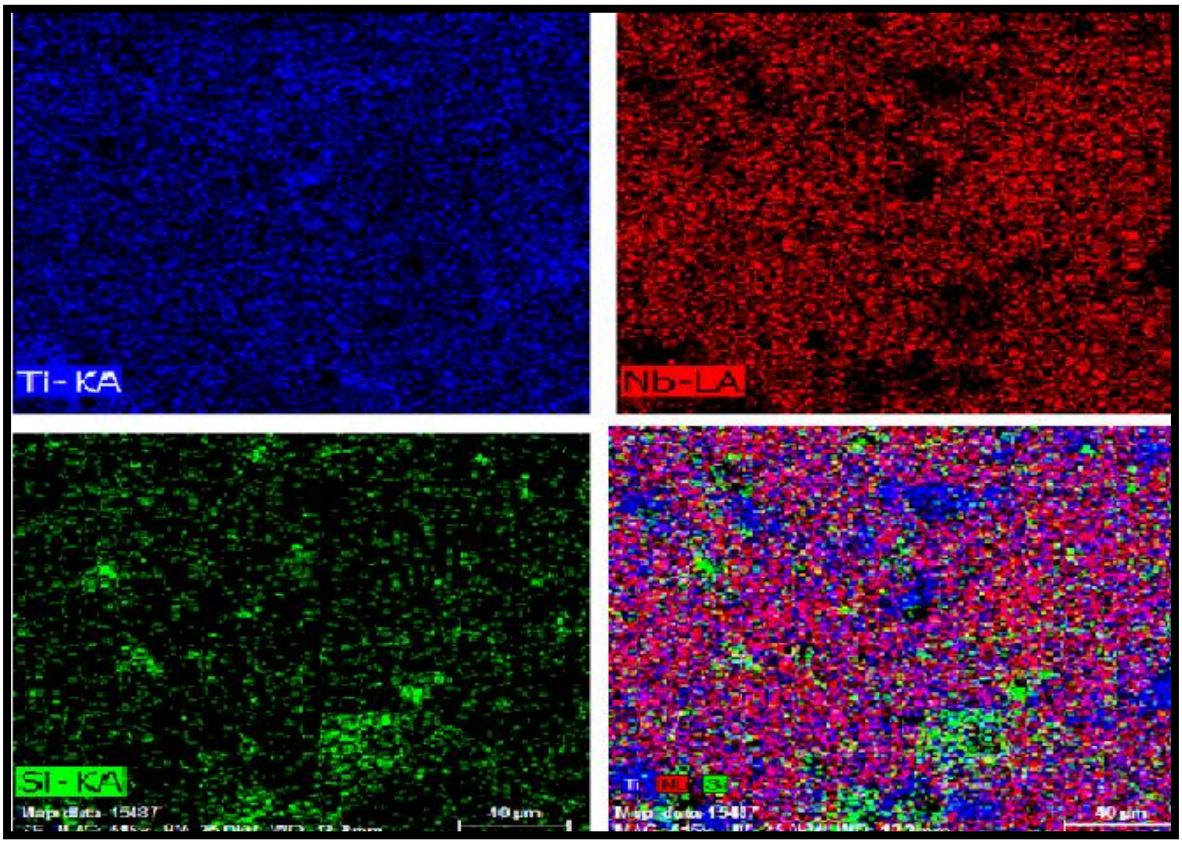

Figure (4.41) a :EDS for **D2** alloy**,** b :mapping for D2 alloy.

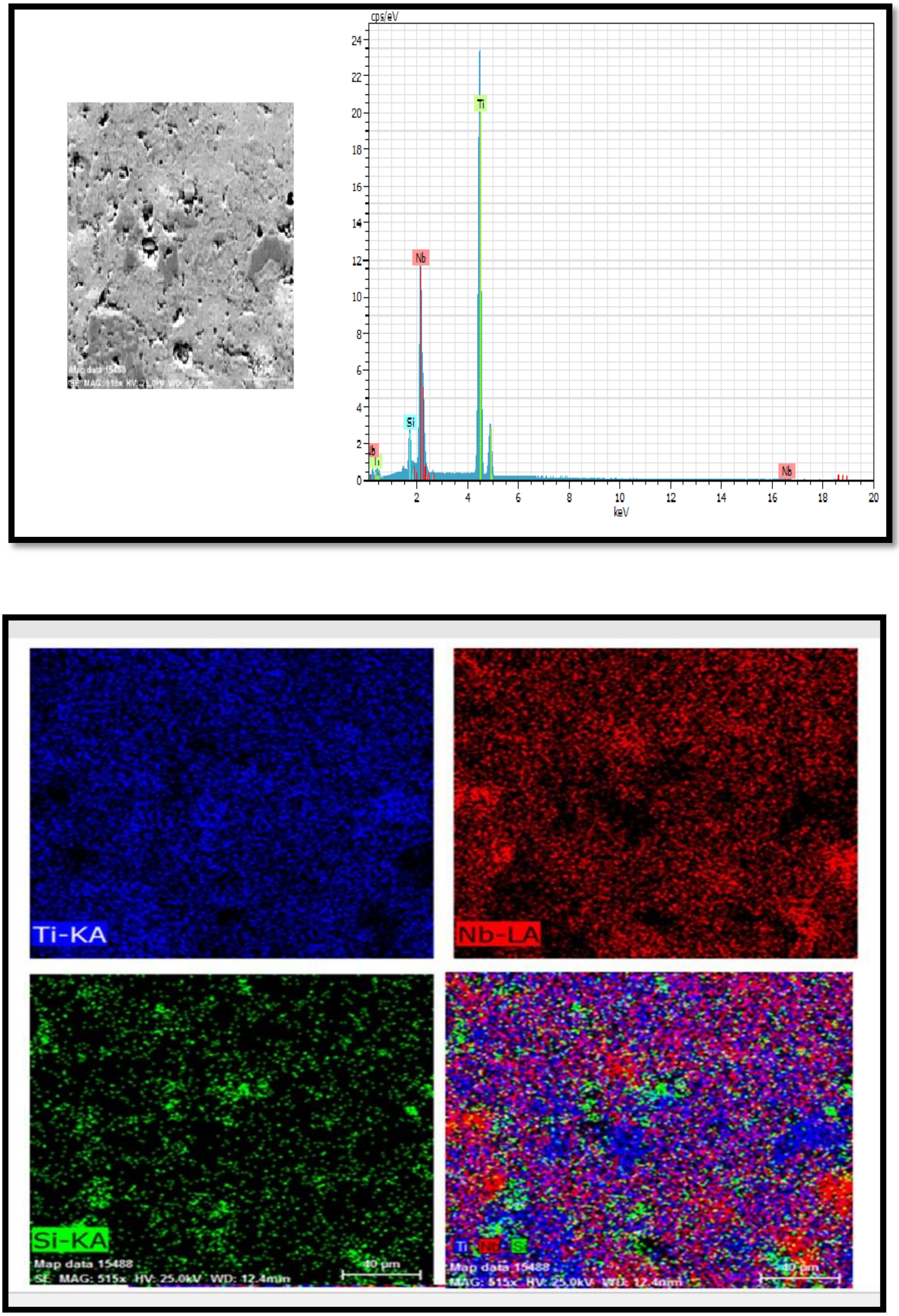

Figure (4.42) a :EDS for **D3** alloy**,** b :mapping for D3 alloy.

4.10. Shape memory properties.

4.10.1 Differential scanning calorimeter (DSC) analysis measurements

DSC measurements were carried out to identify the reversible β-α″ phase transformation in sintered Ti-35 Nb, Ti-Nb-Zr and Ti-Nb- Si alloys as in Figures (4.43),(4.44) and (4.45) respectively, which showed DSC curves of previous alloys. It can be seen that sintered Ti-35Nb, Ti-35Nb-Si and Ti-35Nb-Zr alloys present phase transformation peaks on both heating and cooling curves. The Ms of Ti-35Nb, Ti-35Nb-6.9Zr and Ti-35Nb-0.6Si measured from the cooling curves are 52 °C, -25°C and 2°C respectively. The higher Ms of Ti-35Nb than room temperature explains well the appearance of α″ phase in Ti-35Nb alloy

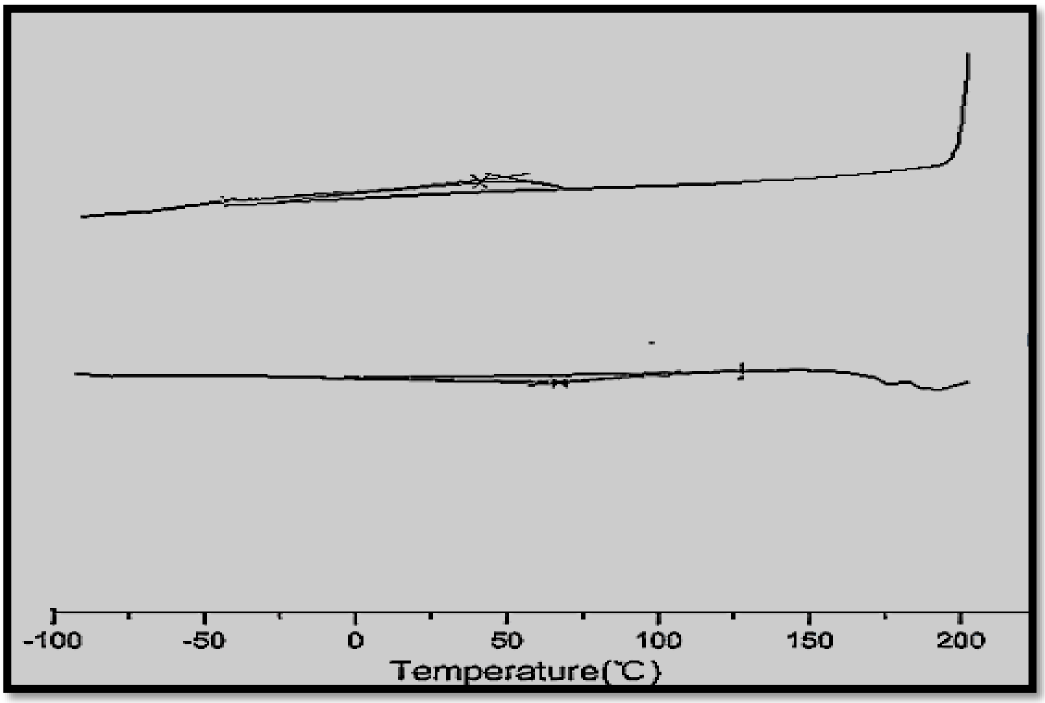

Figure. (4.43) Typical DSC curve obtained for A alloy.

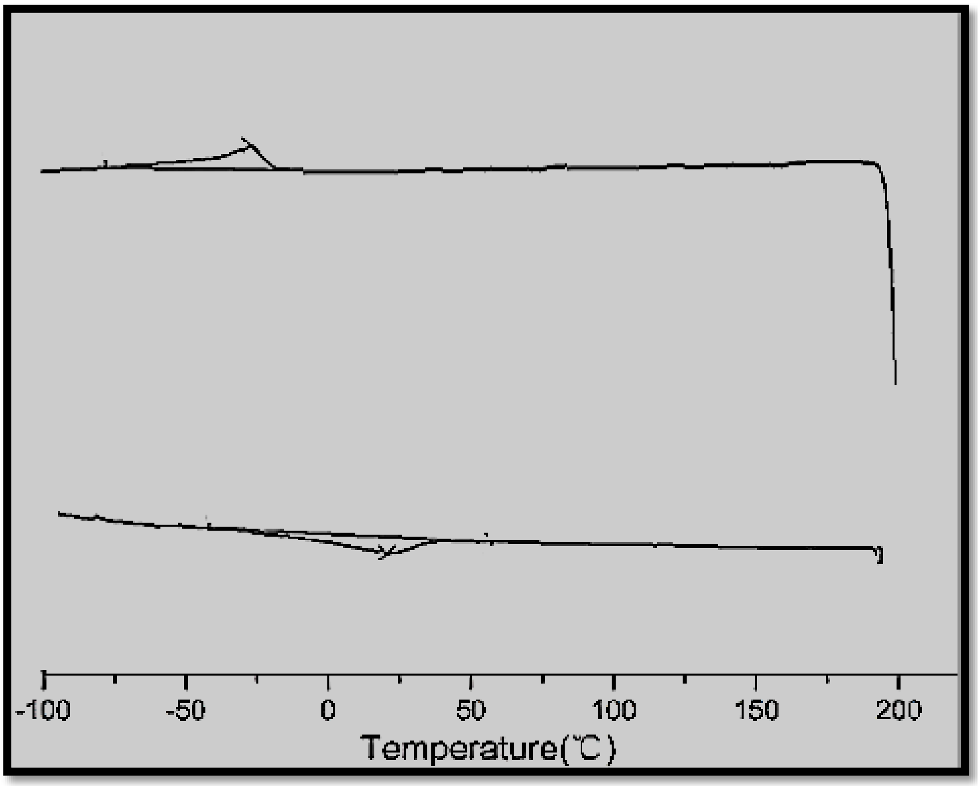

Figure (4.44) Typical DSC curve obtained for C3 alloy.

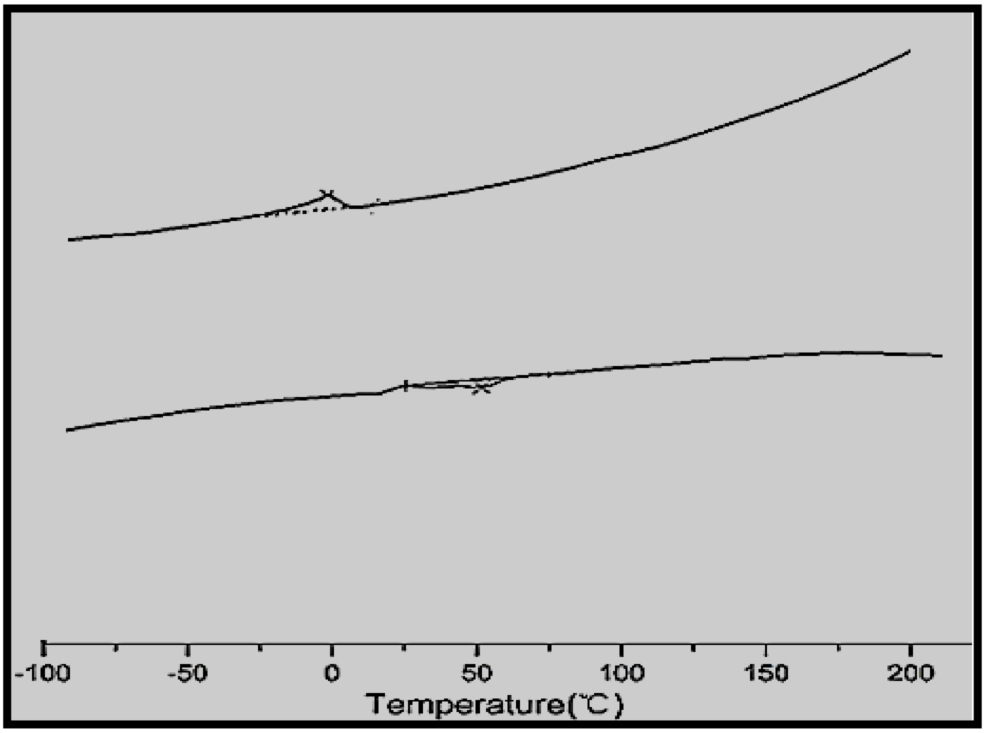

Figure.(4.45) Typical DSC curve obtained for D3 specimen.

The Ms temperature dependence on Zr content of the sintered Ti-35Nb-(6.9)Zr alloys is shown in Figure (4.44) With 6.9wt.% . Zr increase the Ms temperature of Ti-35Nb-6.9Zr alloys decreases to -25°C these result are similar to [145]. Ti-35Nb-(6.9) Zr alloys are mainly composed of β phase at room temperature without the presence of α phase due to its high Nb content which is a β phase stabilizer element. With the increase of Zr content, the extent of Ms decline caused by Zr addition in Ti-35Nb-(6.9) Zr alloys is lowered.

The same behavior were shown for alloys contained silicon addition the Ms temperature dependence on Si content of the sintered Ti-35Nb-(0.6) %Si alloys is shown in Fig. (4.45) With 0.6 wt.% Si increase, the Ms temperature of Ti-35Nb-0.6 Zr alloys decreases to 2°C. Ti-35Nb-(0.6)Si alloys are mainly composed of β phase at room temperature. These results of DSC confirmed the importance of adding elements to Ti-35Nb alloy to improve its overall properties and make it safer for use in medical application.

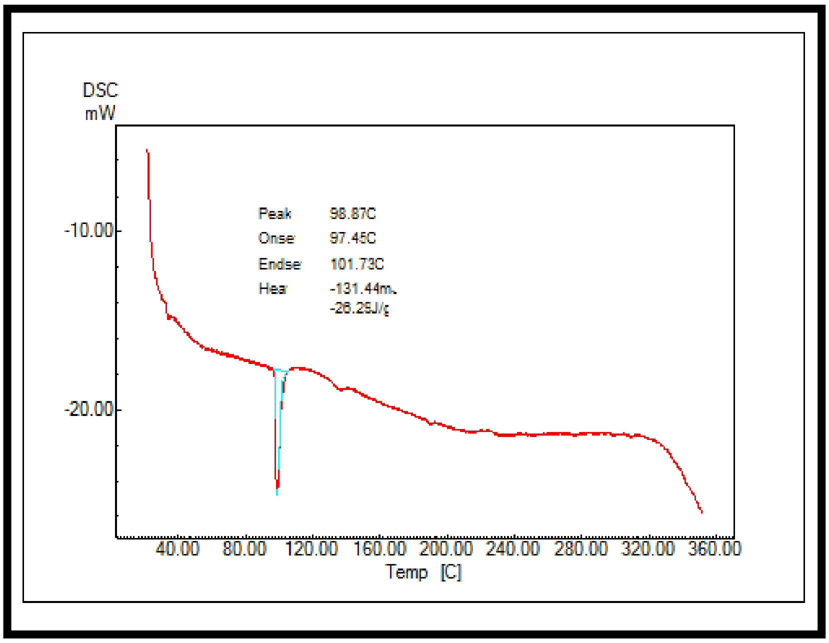

Figure. (4.46) Typical DSC curve obtained for B alloy.

As shown in figure (4.46) of Ti-35Nb after heat treatment, through the heating processes, it was observed that there was a decrease in the transformation temperatures compared to the alloy before the treatment process.

Table (4.4) Results from DSC experimental results.

Alloy	As ºC	Af ºC	Ms ºC	Mf ºC
A	0	110	52	-50
B	97.4	98.87		
C3	-40	30	-25	-75
D3	10	55	2	-20

4.10.2 Shape Memory Effect

The shape memory effect (SME%) of alloys A, B, C3, and D3, treatment was determined by using Brinell hardness by measuring the diameter of ball indenter after and before the heat treatment as shown in table (4.5). Zr and Si are nontoxic elements that can be used as alloying elements to improve the memory effect, which is far less than 5% [136]. The highest shape memory effect was achieved when the addition of 6.9% Zr at. This is because the Zr element easily diffused into the matrix and reacted with the base alloying element to form multi-variant martensite so that the enhancement of shape memory effect has been achieved. Additions of alloying elements exhibited an increase in the SME. This enhancement in the SME was attributed to the existence of the precipitates and grain refinement which was brought about by the addition of alloying element in the parent phase.

Table (4.5): The Influence of alloying elements on SME of Ti-35Nb

Synthesized Composition	Code	SME%	Improving %
Ti-35Nb	A	1.3	
Ti-35Nb	B	4.4	70.44
Ti-35Nb-6.9Zr	C3	3	56.66
Ti-35Nb-0.6 Si	D3	5.5	76.36

4.11. Mechanical Properties

4.11.1 Hardness Test

Brinell hardness was assessed in this research for all alloys (A, B, C1, C2,C3,D1,D2,D3),Figures (4.47) to (4.49) showed the obtained results.

Its clear that the addition of Zr to Ti-35Nb alloy increased the values of hardness. The effect of Zr addition on the rising the hardness values of the specimens is attributed to the role of Zr in reducing porosity and by solid solution hardening from adding more Zr content this result agrees with [145].as depicted in figure (4.47).

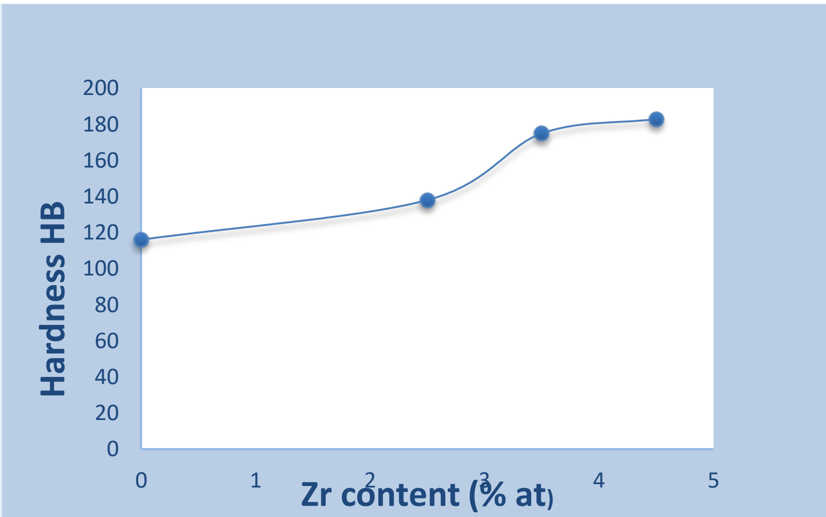

Figure (4.47): Effect of Zr Content on C1, C2, and C3 alloy hardness.

From Figure (4.48) the hardness amounts increases when the amount of Si increased. Attributed the rise in hardness to the fact that silicon is one of the β phase stabilizer element. In addition to the role of Si in reducing porosity as shown in paragraph (4.4). It is reported that hardness of (Ti-Nb) alloys increased with increase of Si content, which belong to the strong Si solid solution strengthening effect, these results agree with [١43].

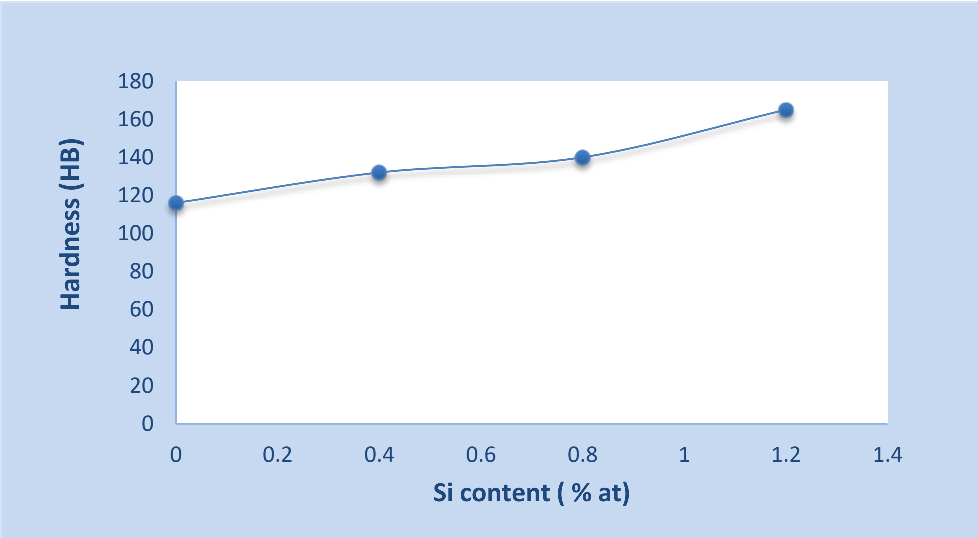

Figure (4.48): Effect of Si Content on D1, D2, and D3 alloy hardness.

After heat treatment for Ti-35Nb alloy hardness value increased as shown in figure. (4.49). This high increase in hardness values is due to a significant decrease in porosity, and the reduction of graine size as seen in the microstructure in (4.8) also played a role.

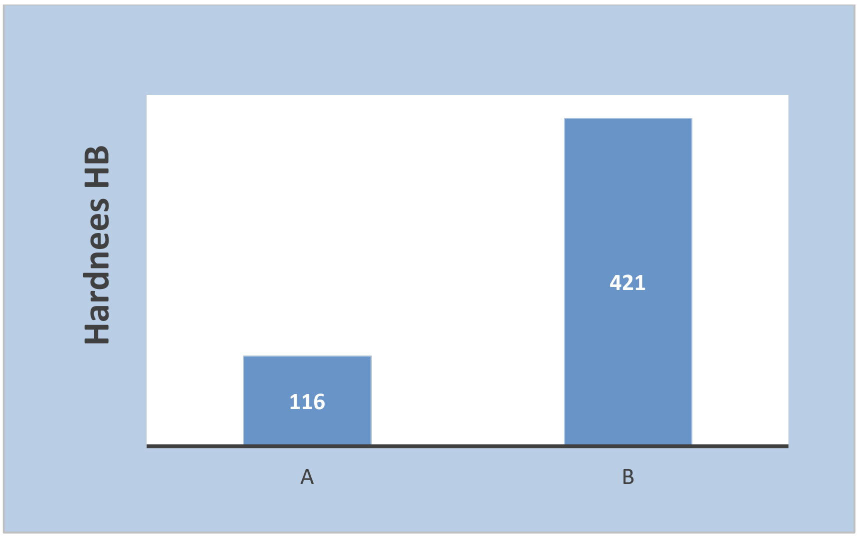

Figure (4.49): Heat treatment effect on hardness of A alloy.

Table (4.6): Shows The Hardness of All Alloys

Specimen code	**Hardness HB**	**Improving %**
A	116	
B	421	72.4
C1	138	15.9
C2	175	33.9
C3	183	48.55
D1	132	12
D2	140	17
D3	165	29.6

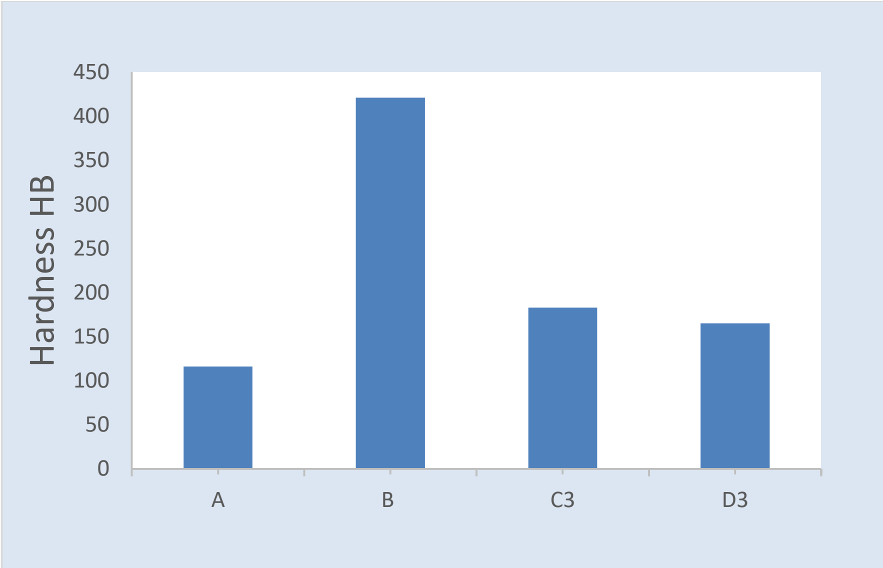

Figure (4.50) comparison of hardness.

4.11.2.Wear Test

Specimens with a diameter of 13.4 mm were put through a wear test at room temperature using varied loads (10 and 15 N) for varying lengths of time (5, 10, 15, 20, 25, and 30 min). The figures from (4. 51), to (4.56) illustrate the wear rate vs time for all used alloys under various loads (10) and (15)N , it can be noted that the wear rate of all tested specimens under 15N load is higher than that under10N.

This variance is caused by an increase in surface friction as the stress on the material rises. [168].

Additionally, the wear rate increases as the time increases for all of the tested specimens. This is undoubtedly due to the fact that friction tends to remove more material from the surface as time goes on, increasing the plastic deformation of the surface material, which causes particles of the material to pull out (debris) [169].

From figures (4.51) and (4.52), it can be noted that the rate of wear decreased drastically with increasing the Zr percentage in the alloy, even it reaches the minimum value at the addition that contained 6.9%at of Zr this may due to the role of Zr addition in reducing porosity of the prepared alloys. In general, the hardness of Ti-35Nb alloys Zr additives increase as the element content increase. Under constant load (10N), (15N) and constant time (30min), the wear rate of TI-35Nb decrease as the Zr increased.

The reason behind this reduction in wear rate is expected since the addition reduce the porosity and increase the friction coefficient, the pores also play a crucial function in preventing the formation of micro cracks and have a favorable impact on wear rate. [168].

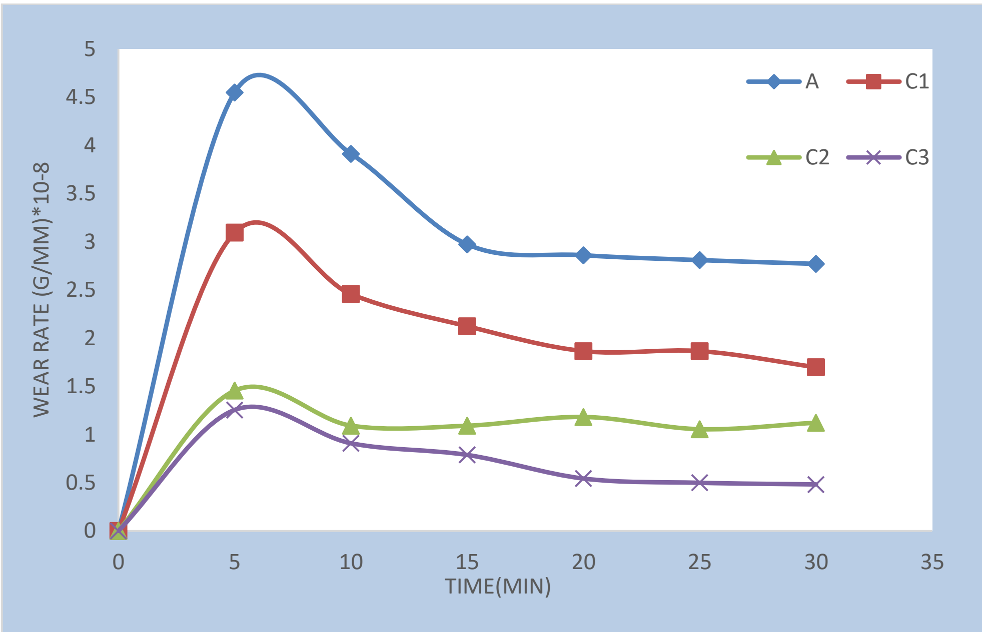

Figure (4.51): For A, C1, C2, and C3 alloy under a 10 N stress, wear rate vs. time.

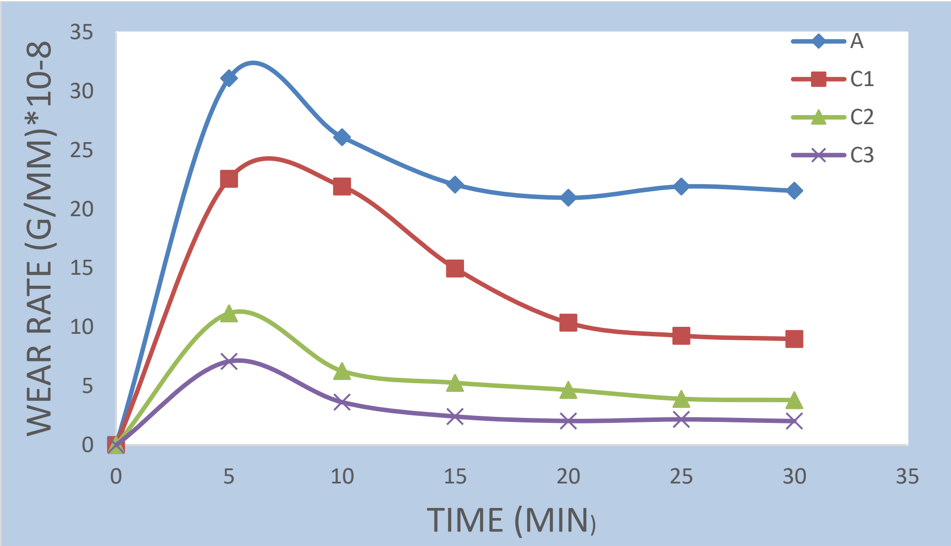

Figure (4.52): For A, C1, C2, and C3 alloy under a 15 N stress, wear rate vs. time.

Figure (4.53) and (4.54) illustrate wear rate for base alloy after heat treatment at 900°C for 30 min where it can be noted that the rate of wear decreased drastically under load (10N) and (15N). After heat treatment because the hardness increased as mention in section (4.11.1) then the wear rate decrease.

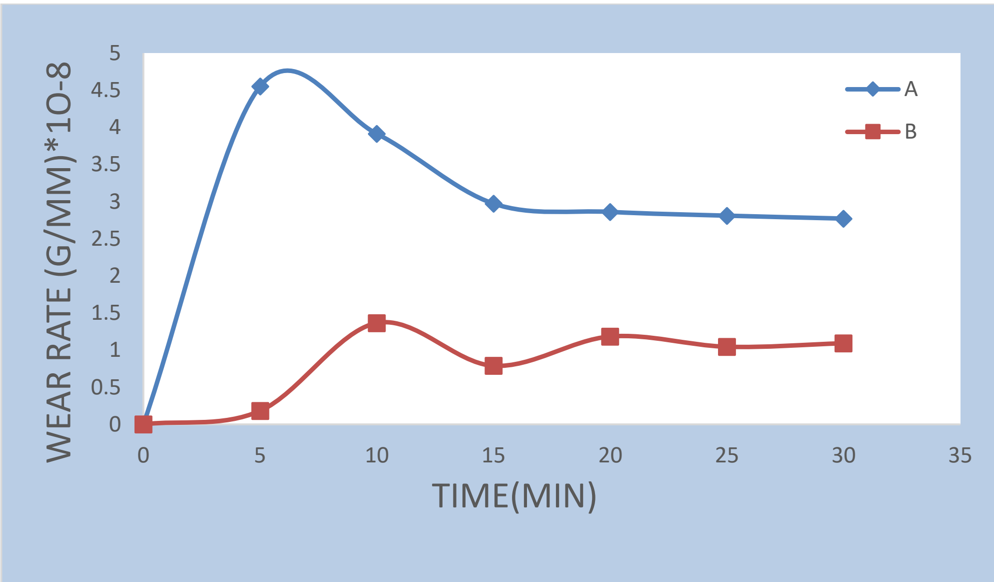

Figure (4.53): Wear rate vs time for A, and B alloy under 10N load.

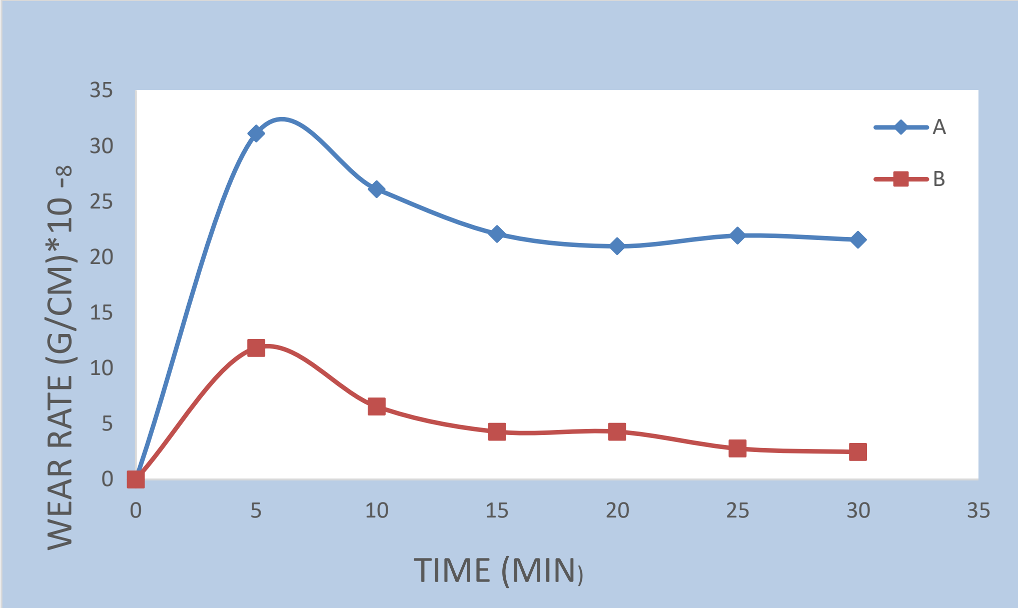

Figure (4.54) Wear rate vs. time for A and B alloy under 15 N.

The addition of silicon increases the hardness as mention in section (4.11.1) then the wear resistance increase as shown in figures below.

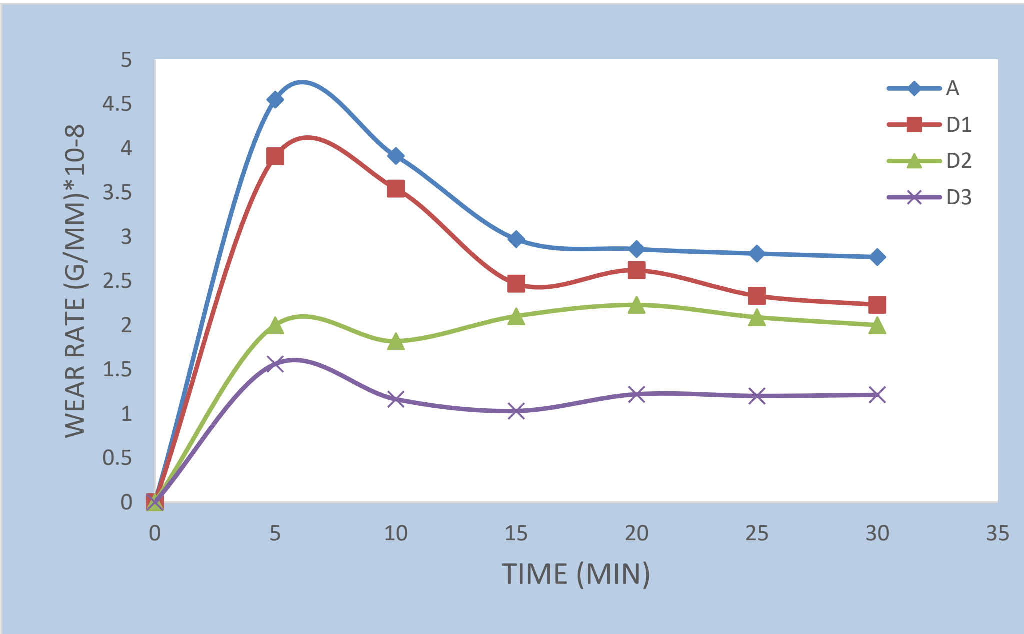

Figure (4.55): Wear rate vs time for A, D1,D2 and D3 alloy under 10N load.

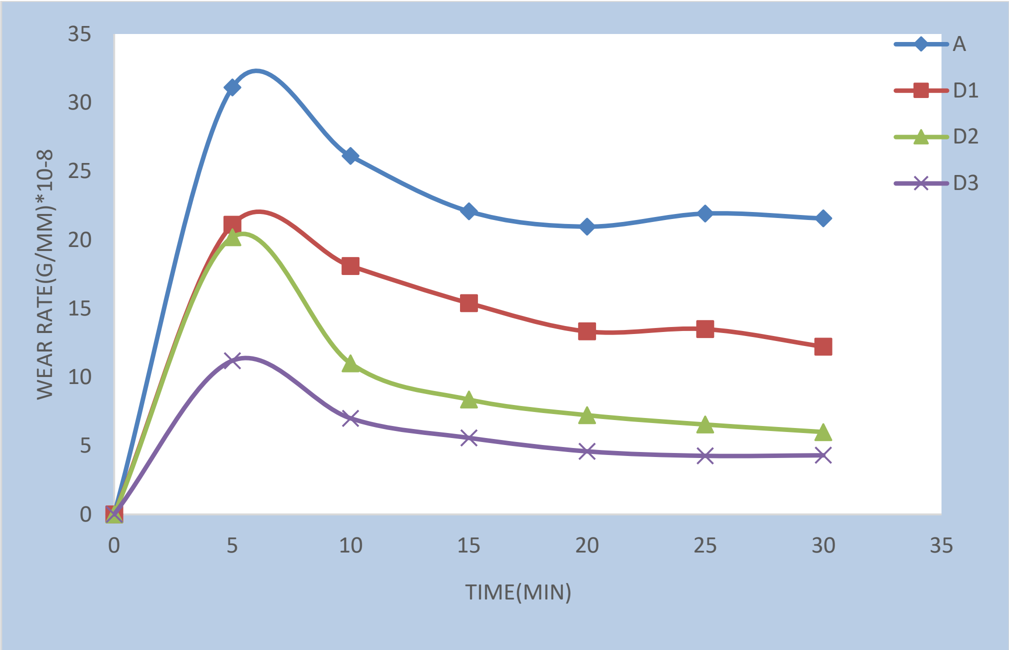

Figure (4.56): Wear rate vs time for A, D1,D2 and D3 alloy under 15N load.

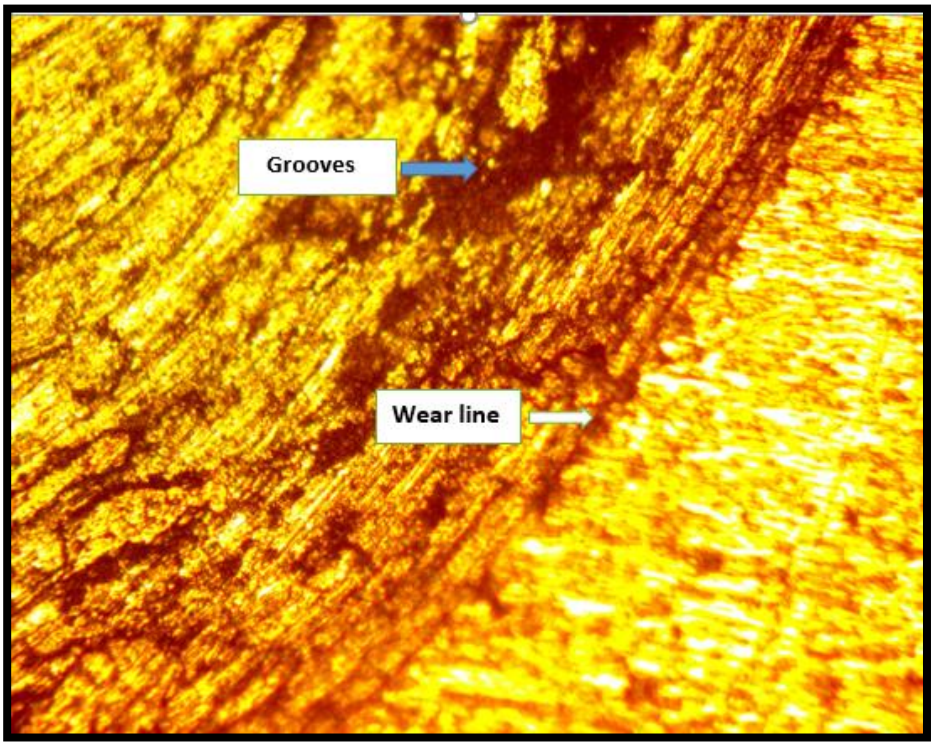

Figure (4.57): Topographic for (A)alloy by use light optical microscope with magnification 100X under(15N) load and (30min) time.

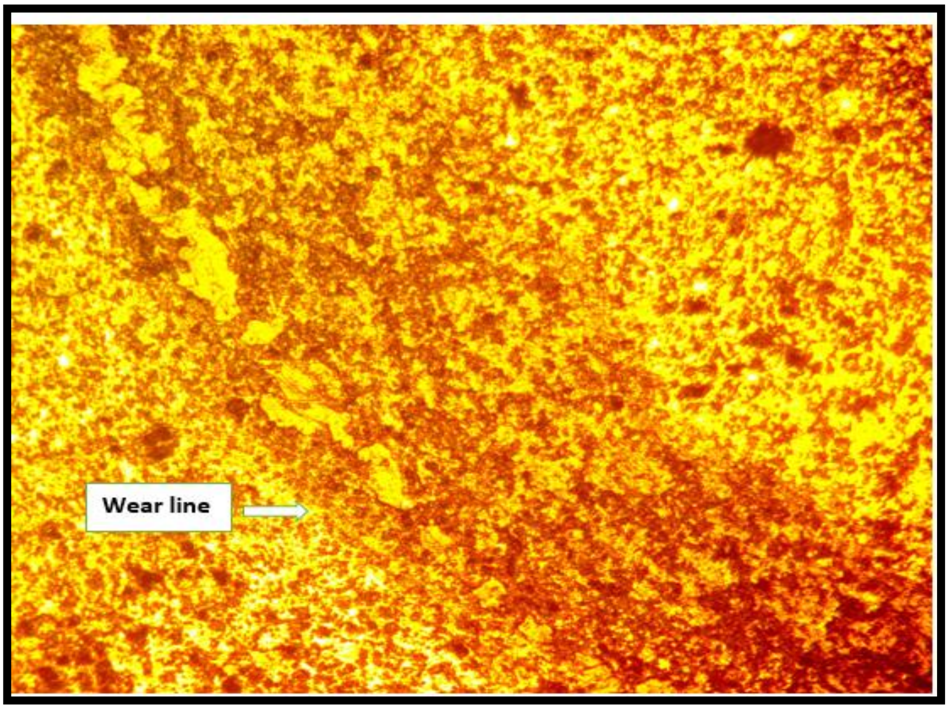

Figure (4.58):Topographic for (B)alloy by use light optical microscope with magnification 100X under(15N) load and (30min) time.

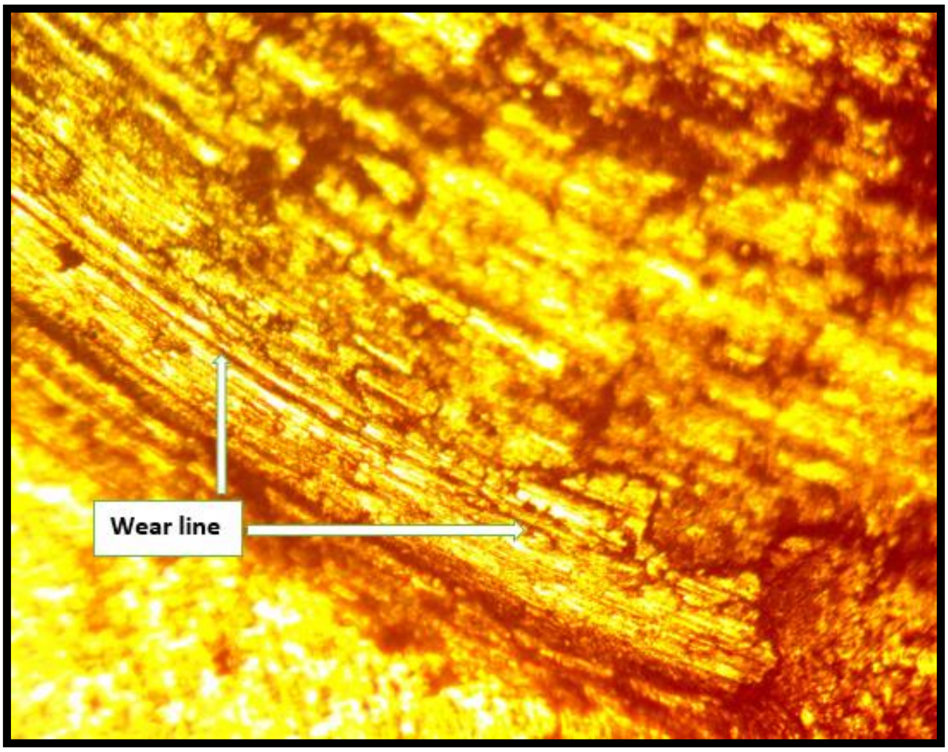

Figure (4.59):Topographic for (C3)alloy by use light optical microscope with magnification 100X under(15N) load and (30min)time.

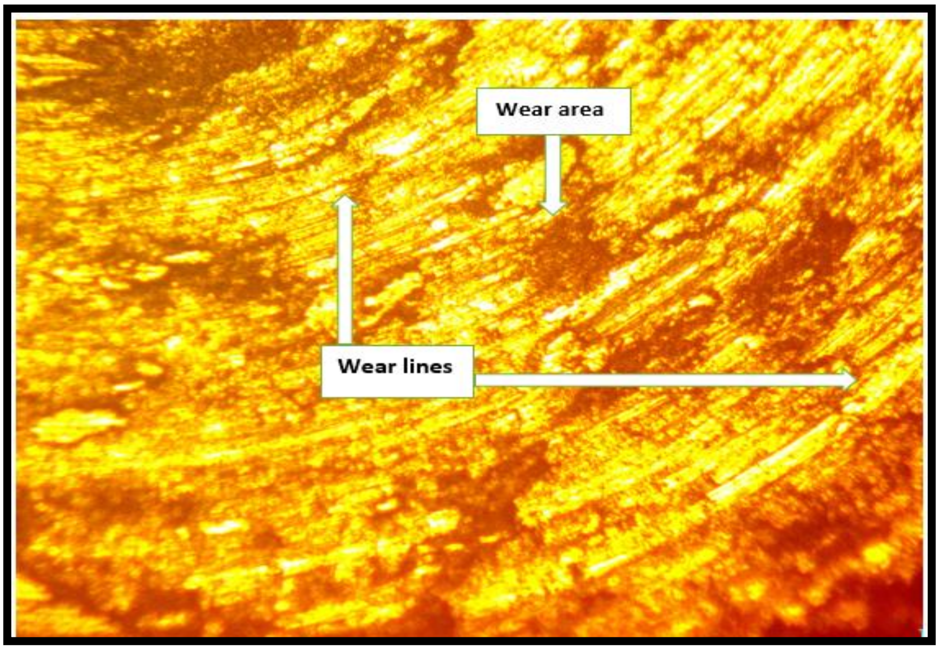

Figure (4.60): Topographic for (D3)alloy by use light optical microscope with magnification 100X under(15N) load and (30min)time.

Figures (4.57),(4.58),(4.59) and (4.60) show an optical microscopy image of the wear tracks of all specimens after the wear test.

Compared with the base specimen (A) an evident groove was observed along the edges of the wear track on the surface of the base specimen. The reason may be due to continuous plastic deformation [170].

Figure (4.58) illustrated that because of the high hardness of base alloy after heat treatment, weight lost with time drastically decreased and decrease in the rate of wear.

From figures (4.59) and (4.60) no clear grooves was formed and observed along the edges of the wear track on the surface of the specimen with different additions. This may be due to the increase in the hardness of the alloy after addition of Zr and Si. This increase led to decrease weight lost with time and a decrease in the rate of wear. The reason may be due to further extrusion deformation becomes more difficult during the wear test [170].

4.11.3 Compression Test.

The results of compression test are cleared for all specimens and illustrated in Figures (4.61), (4.62) and (4.63), figures (4.61) and (4.62) demonstrates that the compression strength value for Ti-35Nb alloy alloys with Zr and Si additions is greater than base alloy, this is because the high hardness and decreased porosity by increasing the percentage of addition. In addition to strength of the specimen improves with decreasing in particle size with increasing amounts of the β phase.

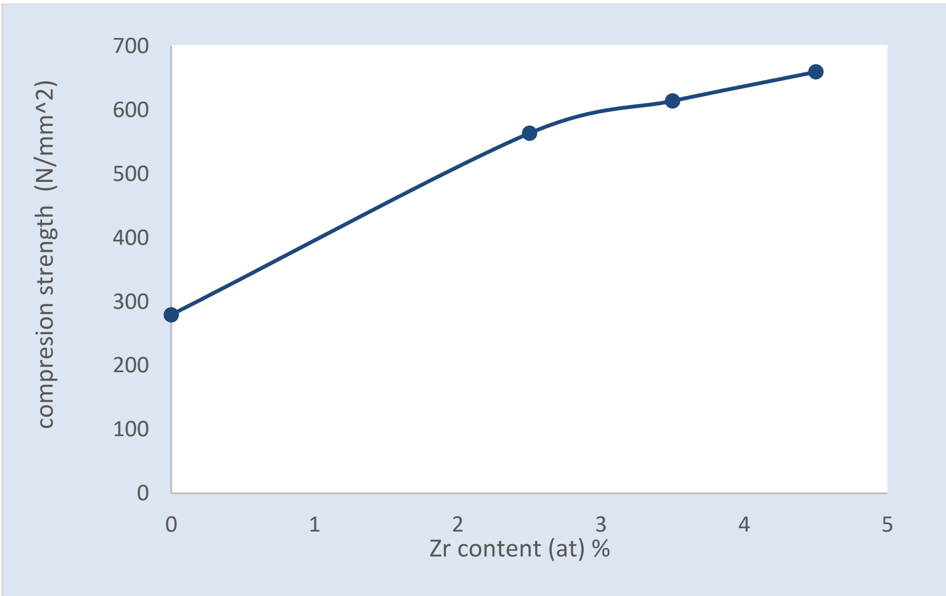

Figure (4.61): Compression strength for A, C1, C2 and C3 alloy.

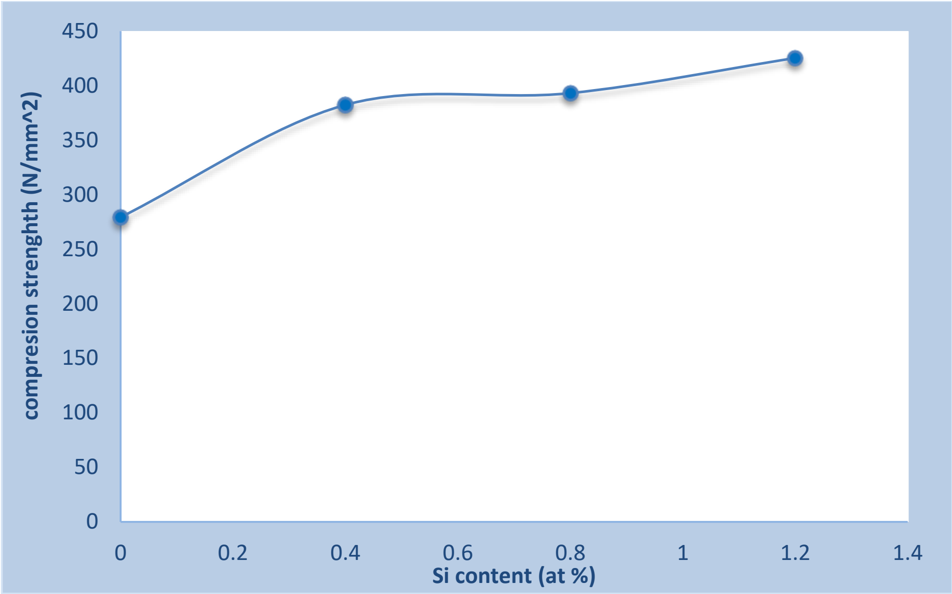

Figure (4.62): Compression strength for A, D1, D2 and D3.

From figure (4.63) it can be noted that the compression strength for base alloy (Ti-35Nb) after heat treatment are more than base alloy before heat treatment, this is because the porosity of alloy is reduced drastically, and the density of the alloy increases.

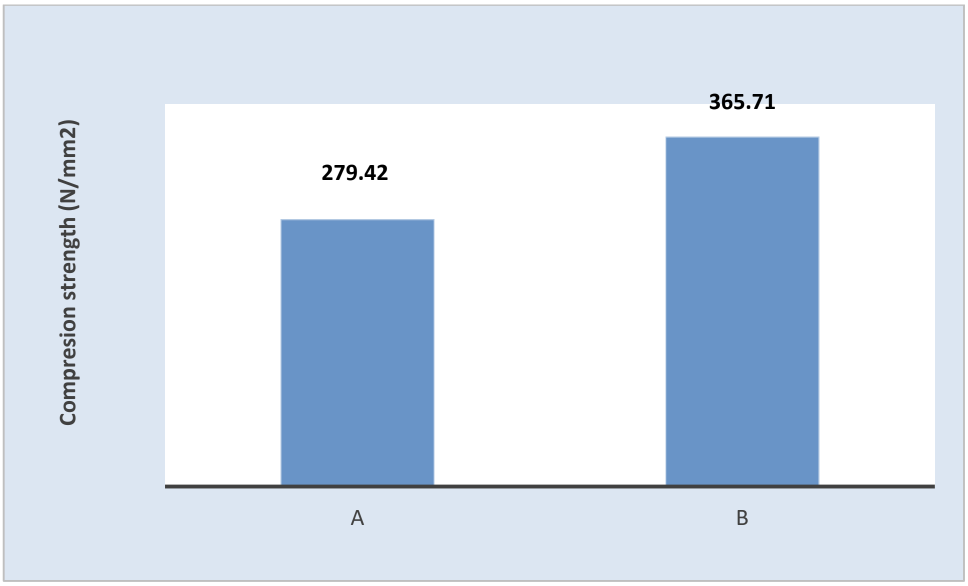

Figure (4.63): Compression strength for A and B alloy.

Table (4.7): shows the Compression Strength of All Alloys.

Specimen code	Compression strength(N/mm2)	Improving
A	279.42	
B	365.71	25.49
C1	563.42	50.40
C2	614.04	54.49
C3	659.4	57.62
D1	382.4	26.9
D2	393.2	28.93
D3	425.4	34.31

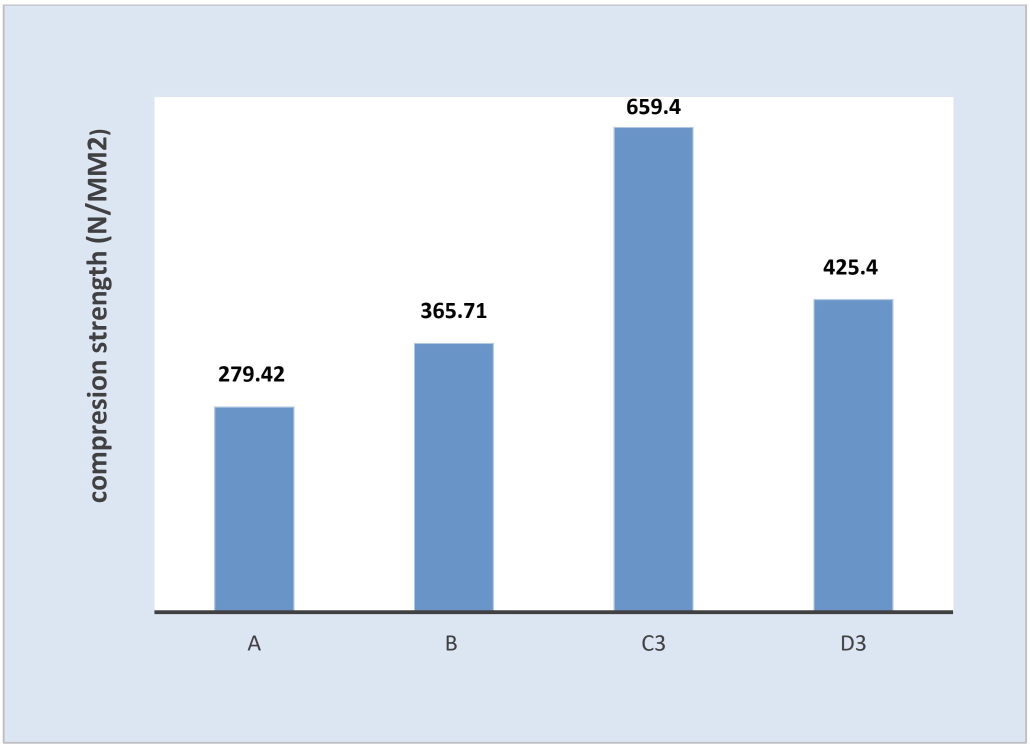

Figure (4.64): Comparison of compression strength of all alloy.

4.11.4 Ultrasonic wave test.

To comprehend the mechanical response of biomedical materials, investigations on elastic deformation behavior are crucial [171]. An ultrasound wave test may be used to assess the elastic modulus, a measure of the material stiffness.

Figure (4.65) (4.66) and (4.67) illustrates the outcomes of using the longitudinal speed and shear speed data to determine the elastic characteristics The Young's modulus drops with increasing Zr concentration between (Ti-35Nb-3.9Zr), (Ti-35Nb-5.4Zr), and (Ti-35Nb-6.9Zr), as seen in Figure (4.65).

Figure (4.66) shows that the elastic modulus fell when the silicon content was raised up to 1 at. %, and subsequently increased as more silicon was added. Unlike alloys that have a Si concentration of less than 1.0 at. percent, the current alloys have a Si concentration of above 1.0 at. percent displayed a high modulus of elasticity, showing that a very stable β-phase causes a rise in the modulus of elasticity with an increase in Si concentration. This results agree with [172]

Figure (4.67) demonstrate the impact of heat treatment on modulus of elasticity where the elastic modulus decreased with value (60.6) where the improvement was (14.8%)

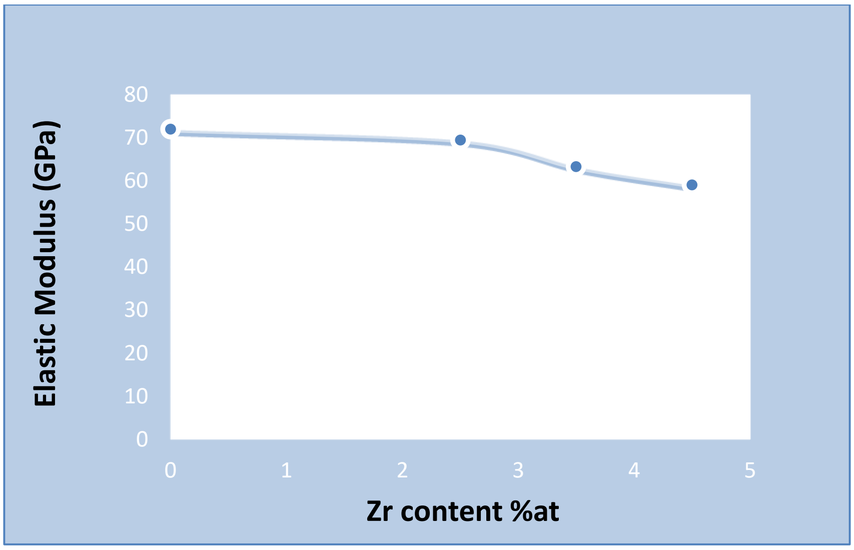

Figure (4.65) Young's modulus of A,C1,C2, and C3 alloy.

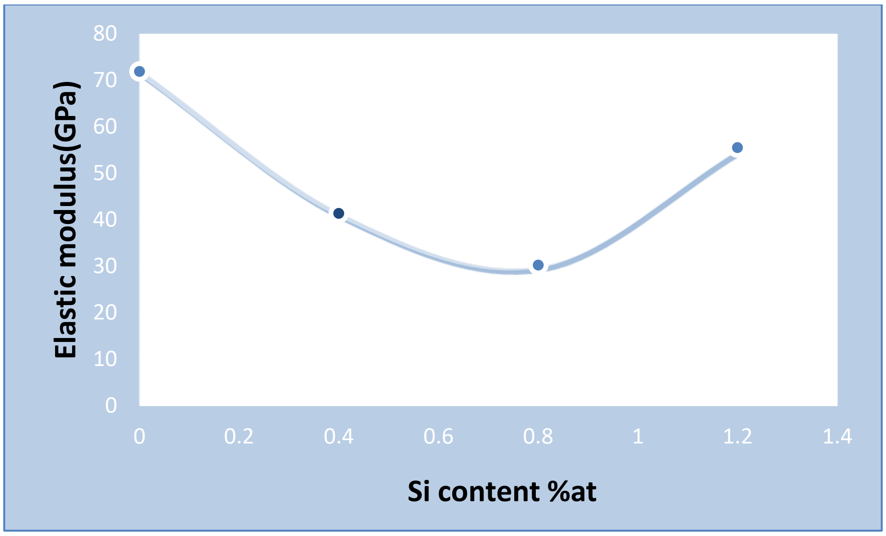

Figure (4.66) Young's modulus of A,D1,D2, and D3 alloy.

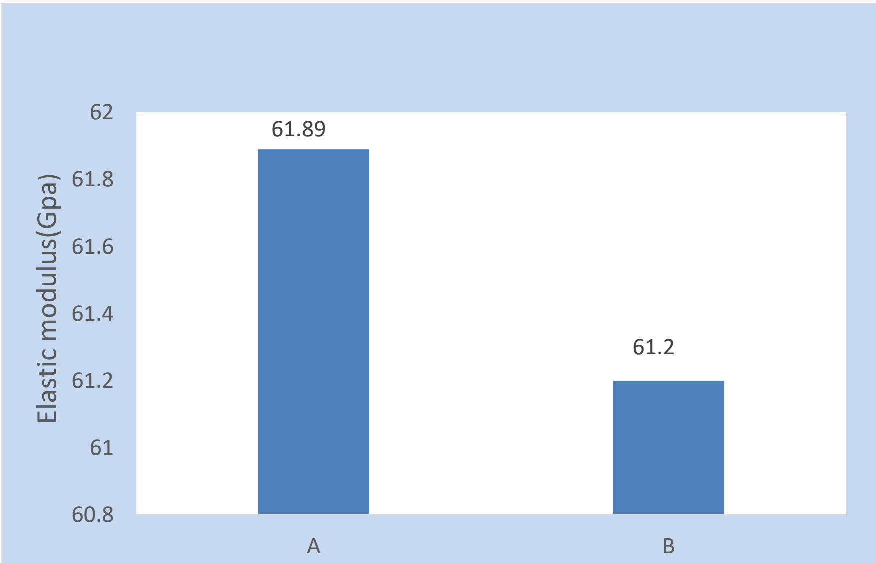

Figure (4.67) Young's modulus of B alloy.

Table (4.8): Ultrasonic Wave Speeds of The Prepared Alloys.

Specimen	**Elastic modulus (Gpa)**	Improving%
A	71.89	
B	60.6	14.8
C1	69.4	3.4
C2	63.20	12.08
C3	58.98	17.95
D1	41.355	42.47
D2	30.23	57.94
D3	55.5	35.7

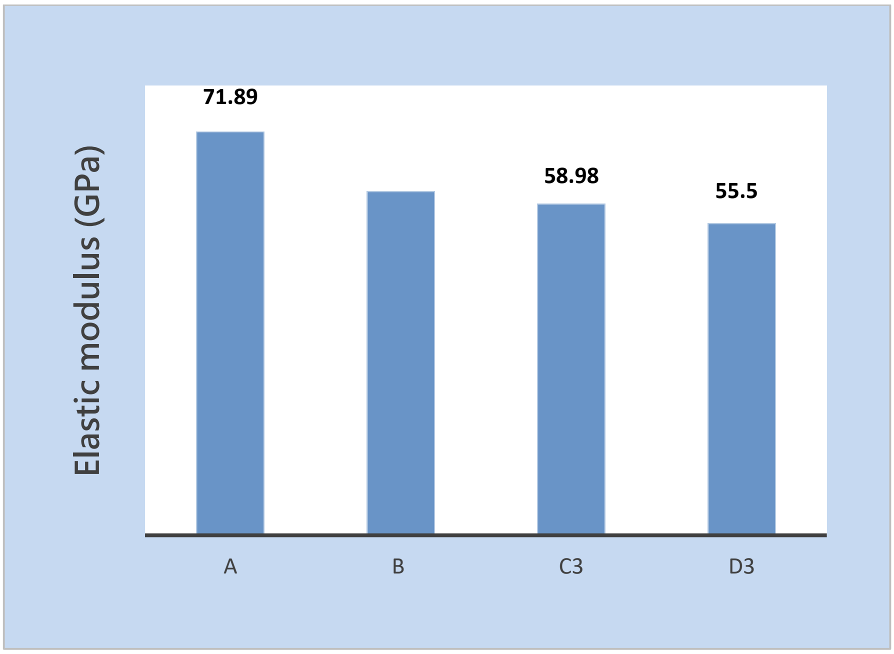

Figure (4.68) Comparison of elastic modulus of all alloys.

4.12. Electrochemical Tests

4.12.1. Open circuit potential Measurement (OCP) .

For all of the investigated alloys, the OCP-time was measured or versus with respect to SCE in Hank and Simulated body fluid solution and at 37 °C. Figures (4.69) and (4.70) depict the changes in the alloys' corrosion potential over time. Potentially reported time ranges from 0 to

150 minutes, with 5-minute intervals. Two specimens of each alloy were used to get the OCP's mean values.

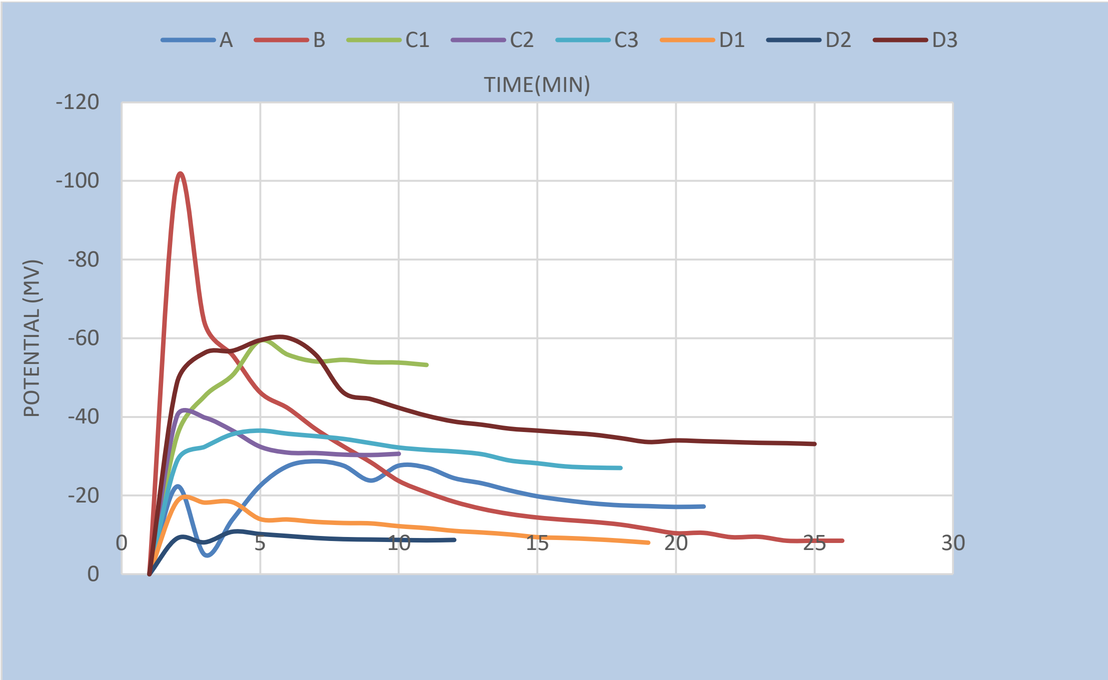

Figure (4.69) :The OCP-time in Hank's solution for all examined alloys at 37 C.

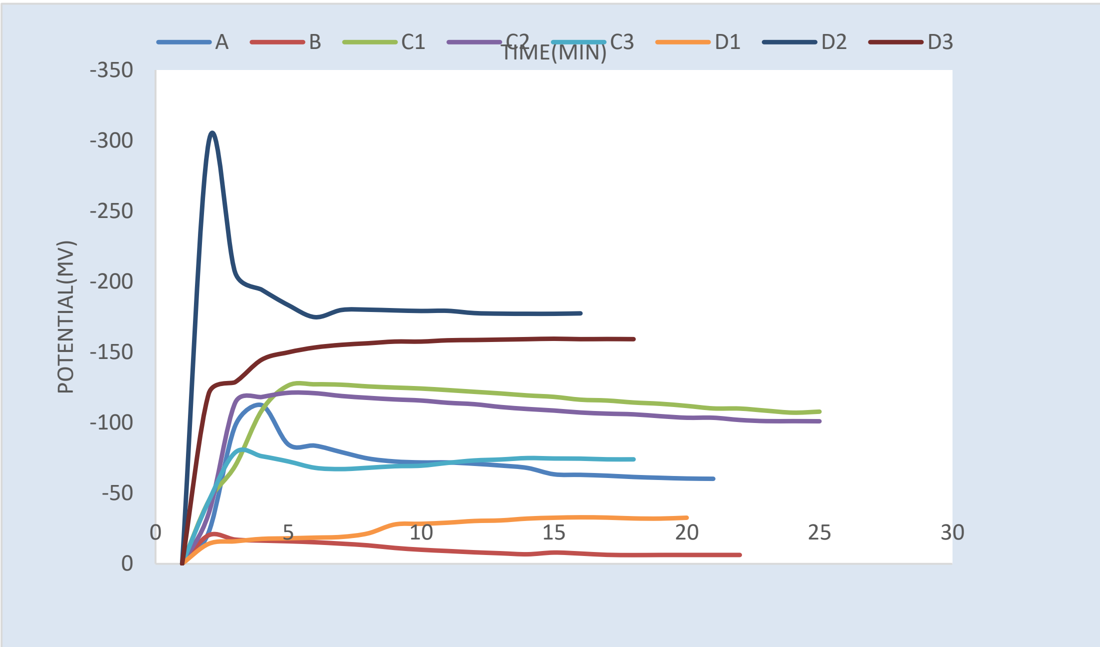

Figure (4.70): The OCP-time in Simulated body fluid solution at 37±1 C° for all examined alloys.

The aforementioned data depict the change in open circuit potential (OCP) with duration, a number of inferences drawn. The initial is that, in the majority of case studies, the corrosion potential grows at a pace that is maximum within the first 30 minutes of research. The creation and oxide film thickness on the surface made of metal which enhances the surface's capacity to ward off corrosion, typically seems to be connected to this initial increase. After then, when the layer grows over the metallic surface, the OCP rises gradually. Another component is that it achieves a high corrosion potential. a point where it starts to stabilize. The constant OCP indicates that deposition and dissolution are in balance. [173].

4.12.2. Potentiodynamic polarization

All specimens' corrosion behavior in Hank's and Simulated body fluid solutions has been investigated. Figures (4.71) and (4.72), which illustrate the corrosion parameters that were obtained from the potentiodynamic polarization test.

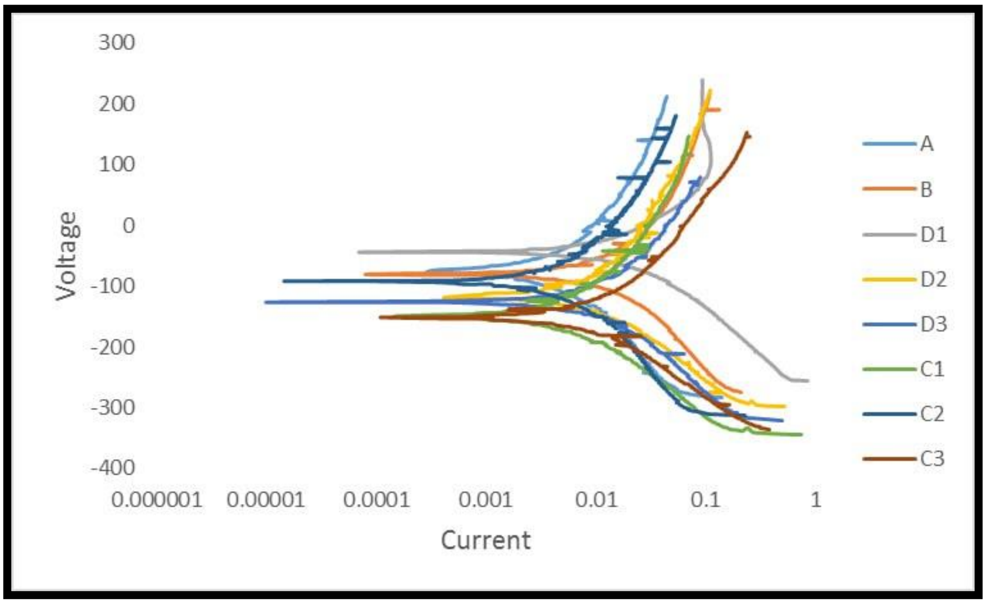

Figure (4.71): Potentiodynamic Polarization for all specimens in Hank's Solution.

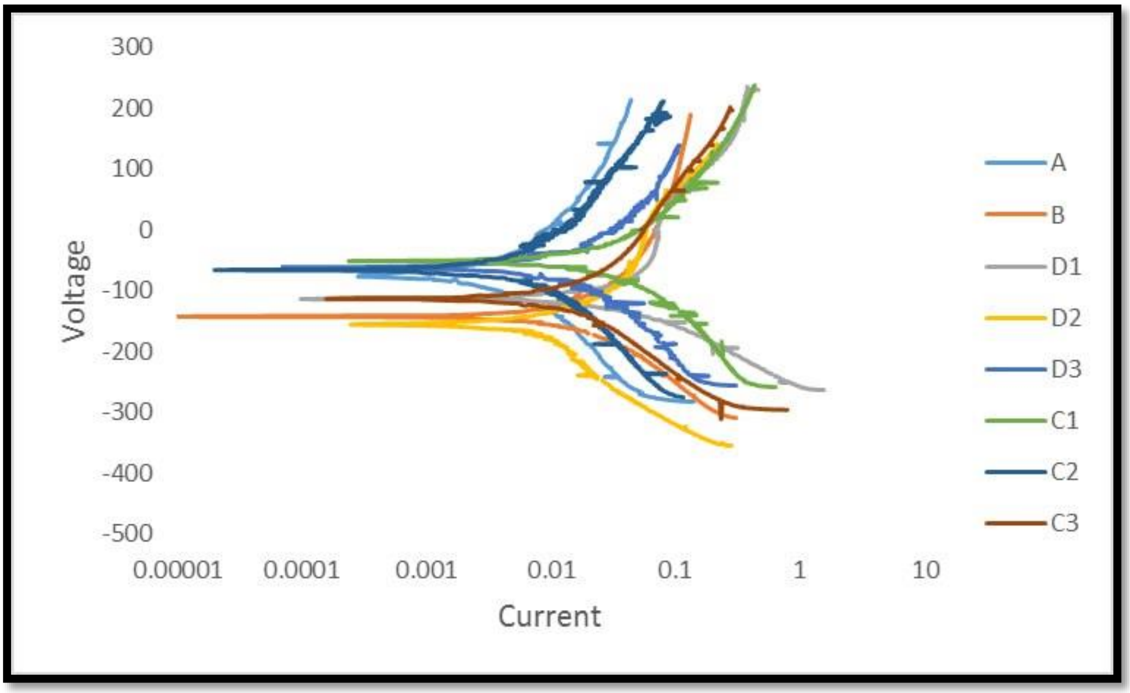

Figure (4.72): Potentiodynamic Polarization for all specimens in Simulated body fluid Solution.

Table (4.9) and (4.10) demonstrates the current of corrosion (I corr), potential of corrosion (E corr), and rate of corrosion (C.R.) for specimens in Hanks and Simulated body fluid solutions at 37°C.

It is clear from Table (4.9) that heat treatment significantly increases the Ti-35Nb alloy's resistance to corrosion in Hank's solutio n. When compared to the base alloy before heat treatment, Icorr is (1.96 µA) displays in Figure (4.73). As shown in figure (4.74), I_{corr}. for B alloys in Simulated body fluid solution is (1.44 A/cm2), which is less than I corr. for A specimen equal (4.64 A/cm^2).

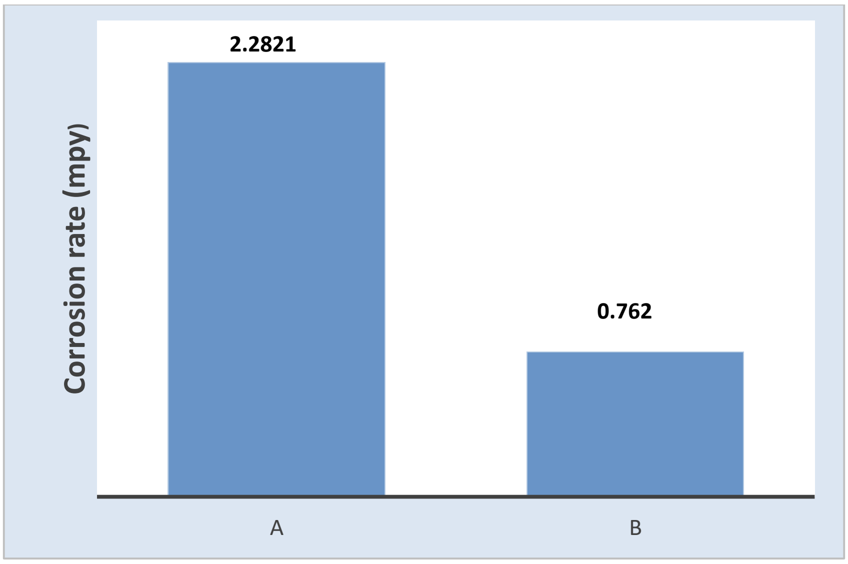

Figure (4.73) Effect of heat treatment on A,B alloy corrosion rate in Hanks solution at 37 °C.

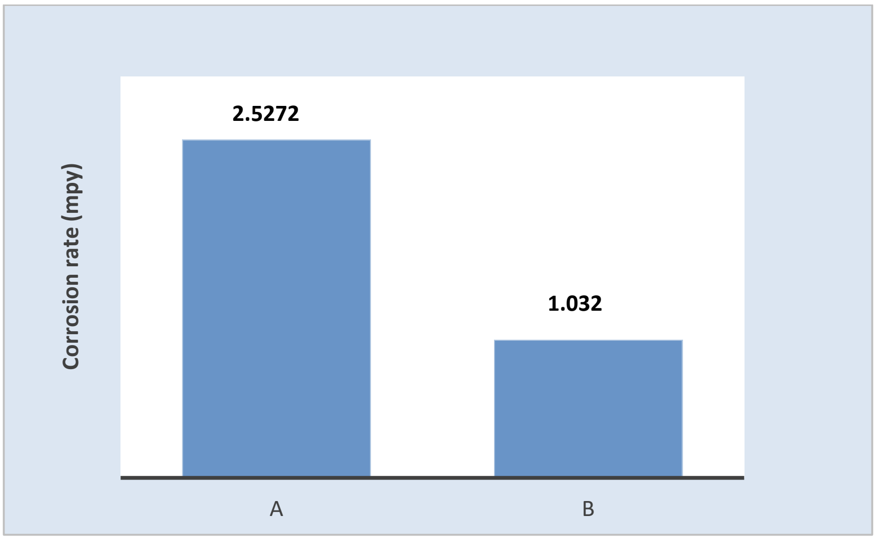

Figure (4.74) : Effect of heat treatment on A,B alloy corrosion rate in Simulated body fluid solution.

at 37 °C I_{corr} for specimens ranges from (1.8 *10-5 A/cm2) for C1 alloy to (1.03 *10-5 A/cm2) for C3 alloy, in comparison to Icorr for A alloy, which is (4.19 A/cm2) for Hanks solution, as shown in to table (4.9). Zr with varied additions of (3.9, 5.4, and 6.9) %at. Also in Simulated body fluid solution With various Zr additions, Ti-Nb alloy's corrosion resistance has improved. (3.9, 5.4 and 6.9) at% as shown in table (4.10) , Icorr. for C alloys is ranged from (2.426*10^-5 μ A/cm2) for C1 alloy to(1.5043*10^-5 μ A /cm2) for C3 alloy in comparison to Icorr for A alloy, which is (4.64*10^-5 μA/cm2).

The addition of Zirconum to Ti-Nb alloy have more homogenous oxide coating on the alloy's surface. Also the corrosion resistance of TiNbZr alloy rises with increasing Zr, because Zirconum addition is added to improve corrosion resistance and speed up blood flow of Ti-Nb alloy, although it does not directly contribute to the development of the phase alone. These results agree with [174].

The Ti-35Nb alloy's corrosion resistance was improved because the Zr addition stabilized β phase, which is essential for this. It can be observed from the polarization curves these alloys displayed a broad un active zone minus the deterioration of the un active coatings as well as low densities of corrosion currents. With the addition of Zr to the Ti-35Nb alloy, the values of the passive current densities and corrosion current densities also dropped. These results have a perfect match with those of [136].

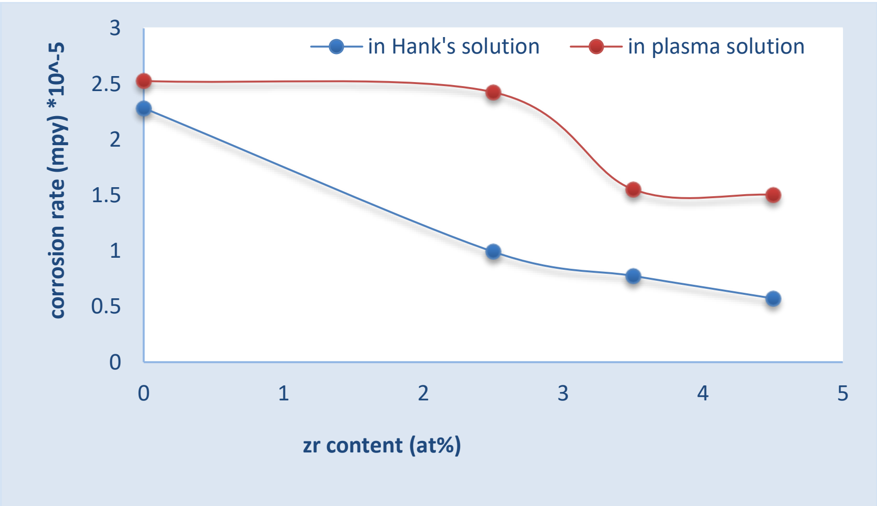

Figure (4.75) The influence of Amount of Zr on rate of corrosion of alloys A, C1, C2, and C3 in Hank and Simulated body fluid solution at 37 °C

Also from Table (4.9), The corrosion resistance can be detected of Ti-Nb alloy in Hanks solution has significantly improved with varying Si additions (0.2 ,0.4and 0.6) wt%, I_{corr}. for specimens is ranged from (3.96*10^-5 μA/cm2) for D1 alloy and (3.3 μA/cm2) for D3 alloy which is less than I corr for the base alloy.

while in Simulated body fluid solution I_{corr}. for D alloys is ranged from (7.598 μA/cm^2) for D1 alloy to (6.9 μA/cm2) for D3 alloy which is more lower than I_{corr} for base alloy. This may be attributed to the collective effect of Si, such as passivity, oxide film, and noble elements which will lead to protection corrosion in the surface layer as shown in Figure (4.76). The two tables show that for specimens A, B, and C in Simulated body fluid solution compared to specimens in Hank's solution, there is a modest increase in corrosion current and corrosion rate. These findings support the idea that the environment to which a metal or alloy is exposed, its chemical makeup, viscosity, and other factors greatly influence how resistant to corrosion it is. [175].

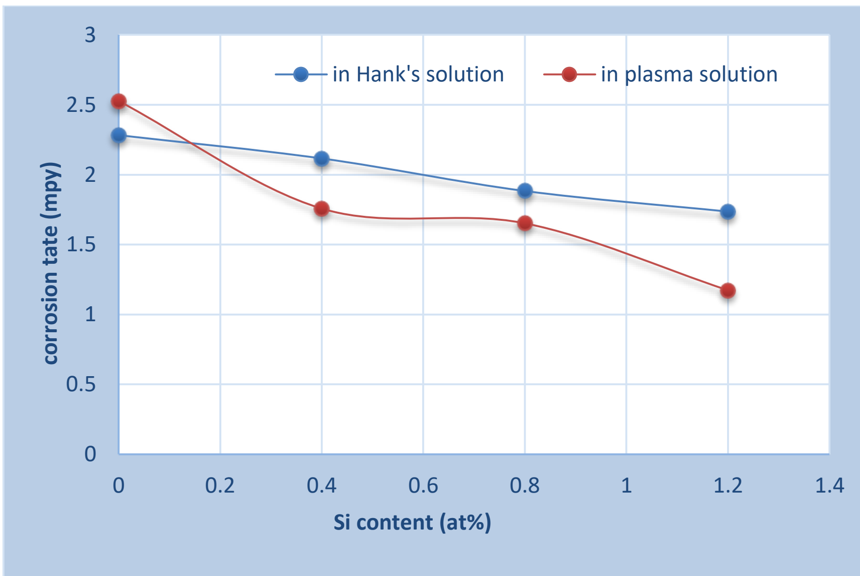

Figure (4.76) The influence of Si content on the corrosion rate of alloys A, D1, D2, and D3 in Hank and Simulated body fluid solution at 37 °C

Table (4.9). All Alloys in Hank's Solution at 37°C: Corrosion Current (Icorr), Corrosion Potential (Ecorr), and Corrosion Rate (C.R).

code Specimen	Icorr (µA)	Ecorr. mV	Rate of Corrosion (C.R.) in mpy	Percentage of improvement
A	4.19	-71.4	2.2821	
B	1.96	-343.3	0.762	66.6
C1	1.8	-151.0	0.99253	56.50
C2	1.4	-90.7	0.7761	65.99
C3	1.03	-149.0	0.573899	170.8
D1	3.6	-95.1	2.11604	7.27
D2	5.4	-114.9	1.88388	17.44
D3	3.3	-127.9	1.7369	56.92

Table (4.10) corrosion current (Icorr), potential (Ecorr), and rate (C.R.) for all alloys in Simulated body fluid solution at 37 °C.

Code Specimen	I corr. µA/cm2	E corr. mV	Rate of Corrosion (C.R.) in mpy	Percentage of improvement
A	4.64	-65.5	2.52735	
B	1.44	-203.3	1.032	54.77
C1	4.4	-50.5	2.4262	3.9952
C2	2.8	-65.5	1.5523	38.5767
C3	2.7	-113.3	1.5043	40.4760
D1	3.24	-113.7	1.7579	30.439
D2	3.07	-157.5	1.6524	34.614
D3	2.23	-62.5	1.17374	56.0545

4.12.3. Metals Ions Release Test

Orthopedic and dental implants can wear and corrode by releasing metal ions into the surrounding tissue through a variety of processes, including corrosion fatigue, stress corrosion, fretting corrosion, etc. [176]. Ti-35Nb, Ti-35Nb-6.9Zr, and Ti-35Nb-0.6 Si alloy immersion tests were done using two solutions (Hank's solution and Simulated body fluid) for get the numerical information required for choosing suitable materials in line a multitude of medicinal applications conditions. The metal ion concentrations discharged into the Hanks solution and Simulated body fluid during a period of 21 days are shown in table (4–11). Ti, Nb, Zr, and Si ions. The Ti ion release from the alloys 6.9 Zr and 0.6 Si was lower with comparable to Ti-Nb base alloy. This is due to the role of silicon and zirconium in the formation of a protective layer after being immersed in the solutions, thus increasing the resistance to corrosion and reducing the release of ions. Table (4-11) show metal ions release concentrations in two different solutions at 37ₒC.

Table (4-11) . Metal Ions Release Concentrations in Two Different Solutions at 37 °C.

Solution	Ti-35Nb		Ti-35Nb-Zr			Ti-35Nb-Si		
	Ti	Nb	Ti	Nb	Zr	Ti	Nb	Si
Hanks	0.550	0.286	0.384	0.183	0.017	0.357	0.12	0.024
Simulated body fluid	0.568	0.190	0.327	0.025	0.012	0.368	0.07	ND

Figures (4.77) to (4.82), shows the quantity of metals ions released after immersion in Hank's and Simulated body fluid solutions for 21 days at 37 C ±2.

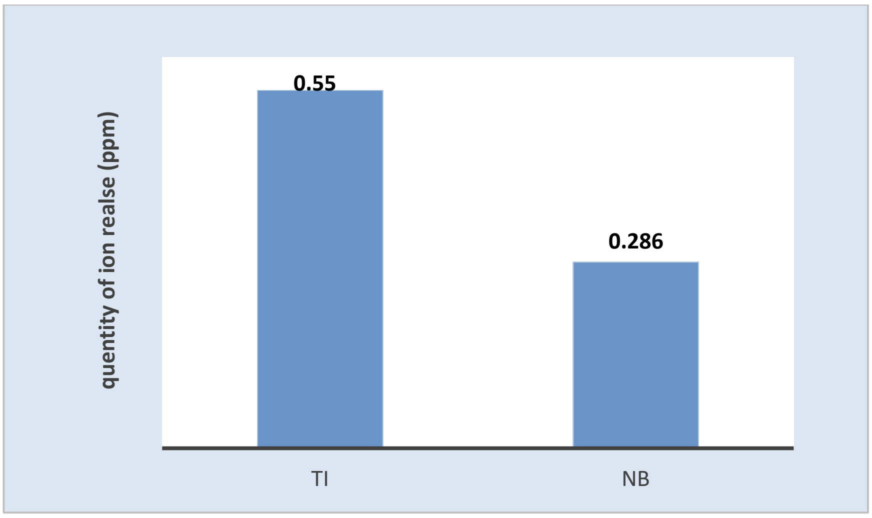

Figure (4.77): Metal ion release values for specimen alloy in Hanks solution.

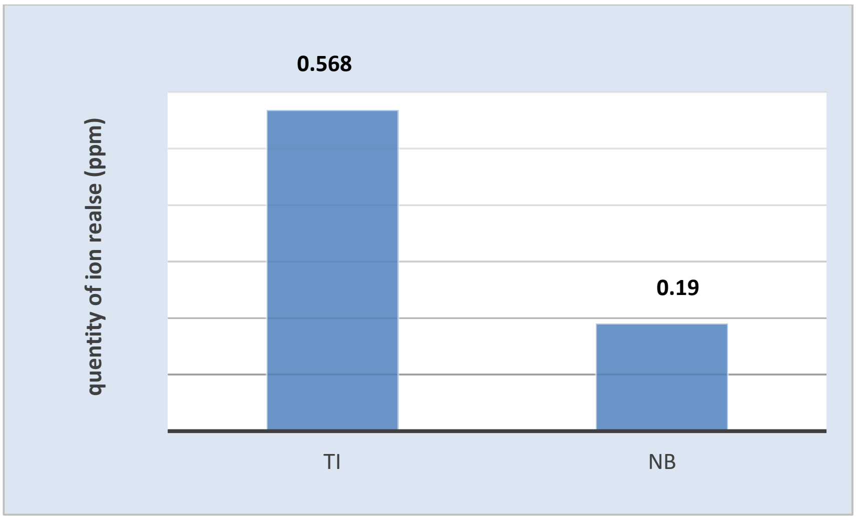

Figure (4.78): Metal ion release values for specimen A, alloy in Simulated body fluid solution.

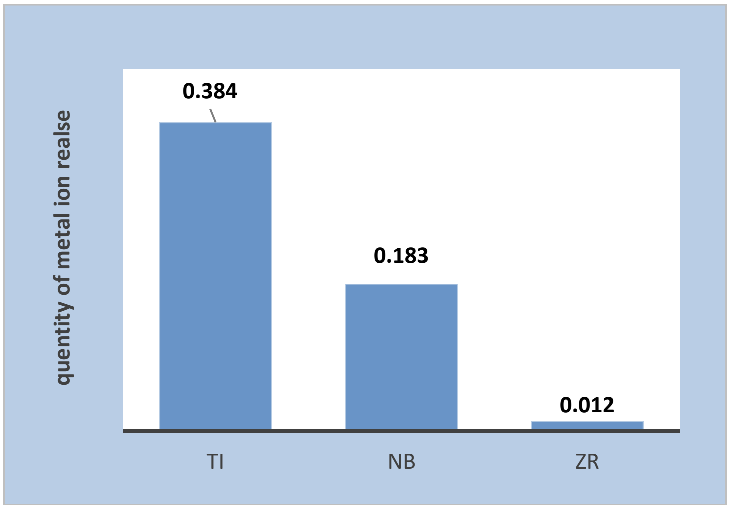

Figure (4.79) metal ion release of C3 alloy in hank Solution.

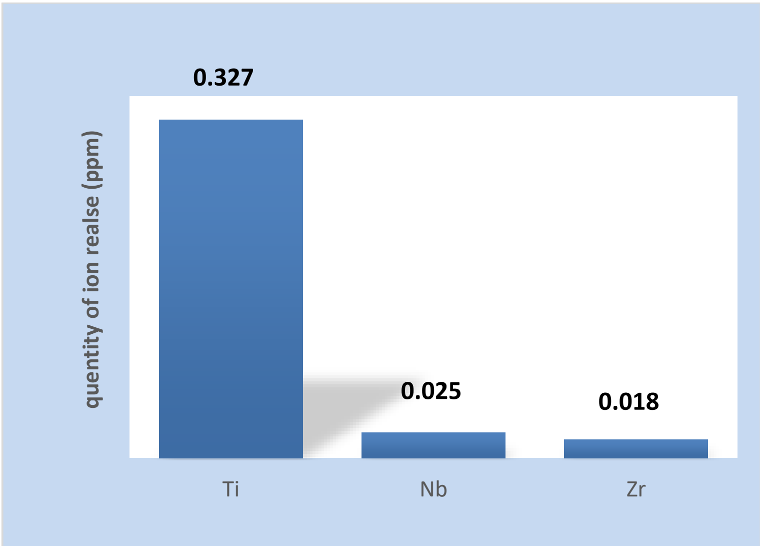

Figure (4.80) metal ion release for C3 alloy in Simulated body fluid solution.

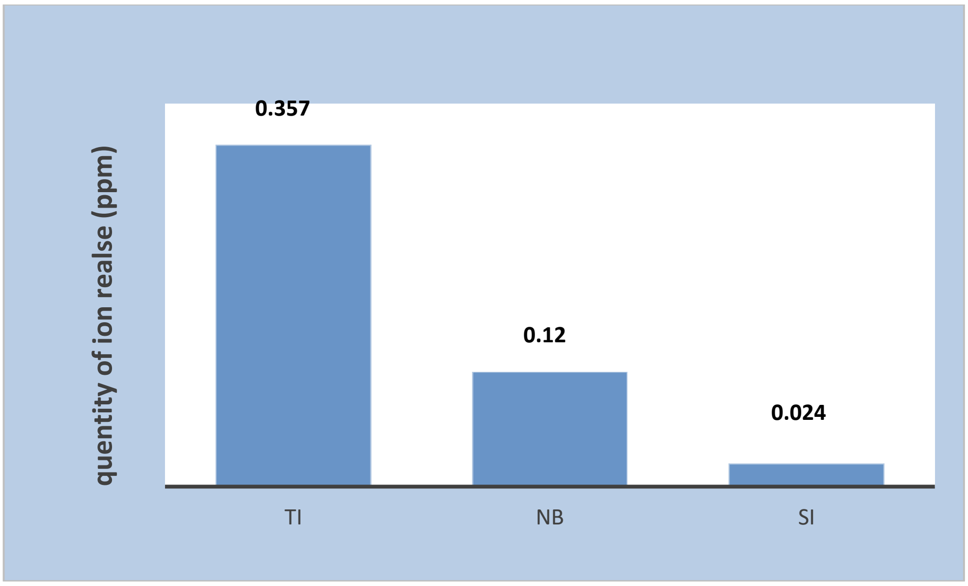

Figure (4. 81) metal ion release for D3 alloy in hanks solution.

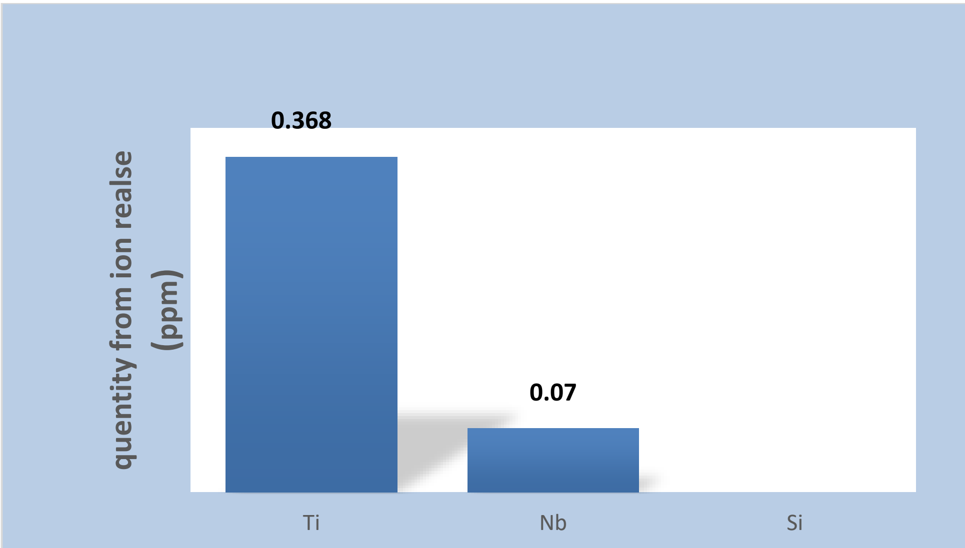

Figure (4.82) metal ion release for D3 alloy in Simulated body fluid solution.

2.13. Contact Angle.

Table (4. 12) Contact angle at different parameters in two solutions

Specimen code	CA/deg. In Hank	CA/deg. In Simulated body fluid
A	60.462	65.480
B	26.588	25.454
C1	37.089	33.768
C2	31.945	29.788
C3	17.099	18.778
D1	33.065	32.568
D2	26.262	26.607
D3	17.099	12.467

Contact angle is an important measurement method to evaluate material surface wettability, and materials with better wettability present lower contact angles in two solutions (hank and Simulated body fluid). Table (4.12) shows the contact angles for all alloys. The contact angle of the specimen decreases dramatically after heat treatment and addition Zirconium and Silicon

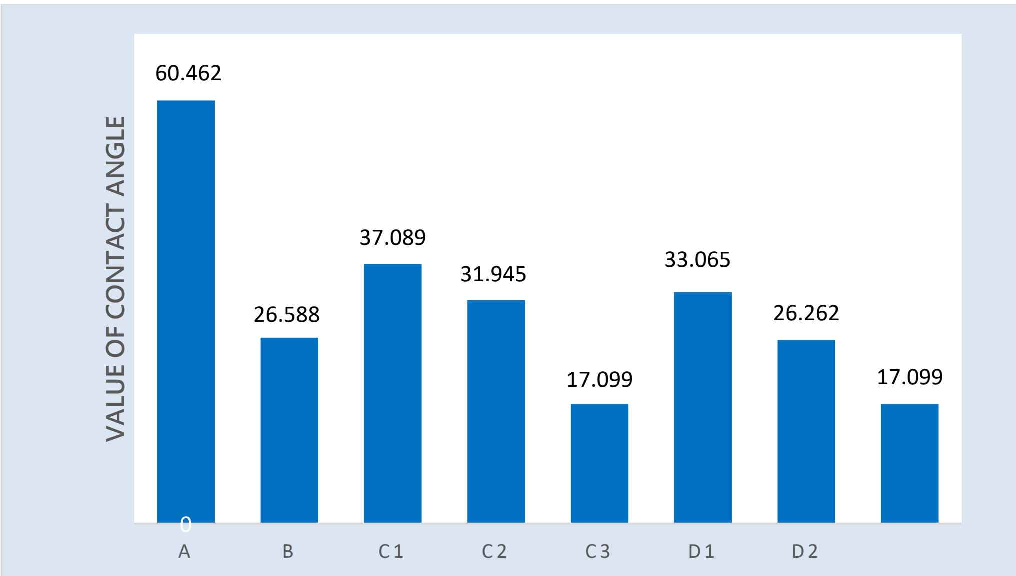

Figure (4.83) contact angle value for all alloys in Hank solution.

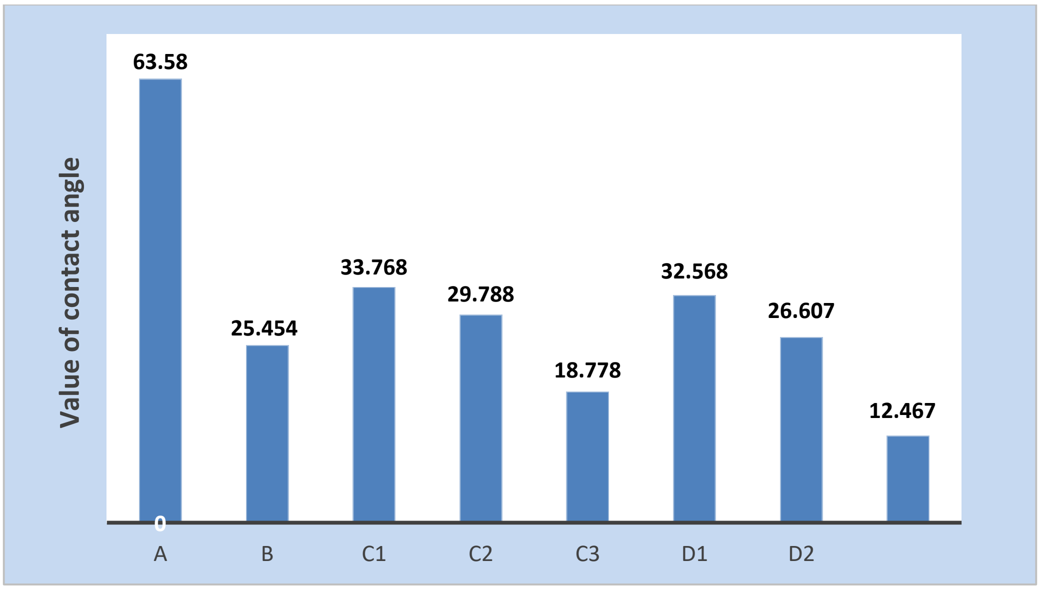

Figure (4.84) contact angle value for all alloys in Simulated body fluid solution.

5.1 Conclusions.

1-XRD results showed that the sintering temperature was 1100°C for 6 hours, sufficient to ensure the transformation of the used elements into alloys structure.

2. The porosity decreases and density increase with increases the addition of elements Zr, and Si, where the improvement ratio of Zr is (54.20%) for C3 alloy while improvement ratio of Si is (31.79%) for D3 alloy and for the density, the percentage of improvement was (64.44% for C3 and 60.59% for D3 alloys). Also after heat treatment operation on the base alloy reduced porosity and increased density where the percentage of improvement of porosity and density is (73.82% and 65.76%) respectively.

3-At room temperature, the Ti-35Nb alloy specimen consists primarily of (α+ß) phases. The Zr and Si specimen addition, however, consists at ambient temperature of a single β phase. After the heat treatment process that there is no change of phases to the base alloy.

4-The addition of zirconium, silicon elements and heat treatment led to a decrease in the temperature of transformation.

5-The increased Si and Zr concentration increased alloys' hardness and was the percentage of improvement after the addition of the values zirconium element (48.55% for C3 alloy) While the percentage of improvement of silicon was (29.6% for D3 alloy) due to solid solution hardening of alloying elements along with a linear behavior. Also after the heat treatment process the hardness improves significantly where the percentage of improvement (72.4%).

6- The values of compression strength increase with an increase in Zr and Si addition compared with the base alloy because of the decrease of porosity, where the improvement ratio is (57.62%) for C3 alloy while it is equal (34.31%) for D3 alloy. After the heat treatment process the compression strength improves significantly where the percentage of improvement (50.40%).

7- The values of elastic modules decrease with an increase in the addition of Zr and Si compared with the Ti-35Nb alloy without additive, where the improvement ratio for C3 Zr alloy is (27.6%) while the improvement ratio of D3 Si alloy equal (22.7%). Also after the heat treatment process on the base alloy, the elastic modules decrease where the percentage of improvement (14.8%).

8- The improvement of wear rate for C3 alloy at 10 N reached 73% and 50 % at load 15 N, respectively, while the improvement percentage for D3 was (86.5%) and (76.5 %) at load (10, 15) N, respectively.

9- The corrosion of Ti-35Nb alloy showed significant improvement with addition of Zr and Si in Simulated body fluid and Hank's solutions. It was shown that higher improvement with the addition of the 6.9 wt% Zr was (170.8%), (40.4760%) in Hank's and Simulated body fluid solutions, respectively. While with addition of 0.6 wt.% of Si, the improvement percentage in Hank's and Simulated body fluid solutions is (54.52%) and (53.55%) respectively. The corrosion resistance after base alloy heat treatment higher than that for base alloy before heat treatment in Hank's and Simulated body fluid Solutions where the percentage of improvement reach to (66.6 %) and (54.77 %) respectively.

10-The ion release results after immersion in solutions, the base alloys with Zr and Si additives exhibited enhances the passive layer to a more area by reduce the ionic release.

11- The contact angle of the specimen decreases dramatically after heat treatment and addition Zirconium and Silicon.

5.2 Recommendations.

1-Study the addition of elements other than Zr and Si other than Ti-Nb Alloy Properties.

2-Study the effect of other heat treatment before age precipitation affects the alloy's mechanical characteristics and microstructure.

٣ - Study other tests such as an antibacterial test.

4-Study the alloys behavior in vivo.

List of Latin Symbols

Symbol	Meaning	units
E	Elastic modulus	GPa
K	Thermal conductivity	W/ m.˚C
n	Spindle speed	rpm
C	Specific Heat	J/kg.°C
T	Temperature	°C
W	Weight	g

List of Greek Symbol

symbol	Meaning	Units
α	alpha Phase	--
β	Beta phase	--
ρ	Density	g/cm^3 + Kg/m^3

List of Subscripts & Superscripts

Symbol	Meaning	Units
D_o	Density of Oil	g/cm^3
DW	Density of Water	g/cm^3
I_{corr}	Corrosion Current Density	$\mu A/m^2$
Ms	Temperature Martensite starts	°C
Mf	Temperature Martensite finished	°C
TB	β transformation temperature	°C
wt	Weight percentage	%

Symbol	Meaning
ASTM	American Society For Testing And Materials
SME	Shape Memory Effect
ATT	Allotropic Transformation Temperature
BCC	Body Centere Cubic
CP	Commercially Pure
HB	Brinell Hardness
BE	Blended Elemental
XRF	X-Ray Fluorescent
EDS	Energy-Dispersive Spectrometry
EW	Equivalent Weight
EIS	Electrochemical Impedance Spectroscopy
HCP	Hexagonal Close Packed
ISO	International Organization for Standardization
MPY	Mils per year
mV	Millivolt
MSCs	Mesenchymal Stem Cells
LOM	Light Optical Microscope
OCP	Open-Circuit Potential
XRD	X-Ray Diffraction

P/M	Powder Metallurgy

List of Abstract Thesis of Higher Education in Iraq University

From No.:	

University: Babylon	Collage: Materials Engineering
Department: Metallurgical Engineering	Accurate Specialization:

Thesis Title: Enhancing the Corrosion Resistance of Ti+35wt%Nb Shape Memory Alloy used for Biomedical Applications.	Thesis Registration:	(1) Nature of Search: Academic	Beneficiary Side: Babylon university Contract Date:

(2)Student Name: Zahraa hussien Khalaf	Date of Birth:29	Gender: female	(4)Assigned Body:
Admission Date:2020-2021	(3)Acceptance Channel: general		

Supervisor Name	Scientific Degree	Gender	Assigned Body	Age
1-Nawal Mohammed Dawood 2- Sundus Abbas Jasim	1- prof 2- Assit prof	1-Female 2-female	**1-Ministry of Higher Education And Scientific Research** **2- Ministry of Higher Education And Scientific Research**	1-47 2-51

1. Specify the nature of academic research or piratical one, in case of research practical mention the beneficiary body and the date of contract.
2. Mention the full name and surname or as it is written in the thesis.
3. Mention acceptance channel (distinct, general acceptance, arrivals, reservation).
4. Assigned body mentions the ministry or the side which the students come from.

Date of Official Letter University		Certificate:	Master	General Specialization:		Accurate Specialization:	

Key Words:	

Abstract of the Thesis

In the present study, Ti-35wt%Nb alloy prepared by powder metallurgy technique, a various amounts of Zirconium (3.9, 5.4, and 6.9 wt%) and Silicon (0.2 ,0.4 ,0.6 wt %) added to the base alloy. The compact pressure was 700 MPa and the green compacts sintered at 1100°C for 6h in inert gas (Argon), then the specimens cooled in the furnace. The effect of heat treatment on the properties of Ti-35Nb shape memory alloy was studied. Also the microstructure was characterized using (scanning electron microscope combined with energy dispersive X-ray spectroscopy, X- Ray Diffraction Analysis, X ray Fluorescent Analysis, Differential Scanning Calorimeter and light Optical microscope). The mechanical properties (Compression, Hardness, and dry wear test), electrochemical (Open circuit, and Polarization tests), and toxicity (Static immersion test) was also study.

Results appear that the porosity percentage decreases gradually with increasing both (Zr and Si) additions. The XRD results show that the base alloys and base alloy after heat treatment consist of two phases (β phase) and (α-phase) at room temperature. The presence of both α and β phase is evident in an alloy with additive Zr and Si. The primary α phase diminishes gradually as the Zr and Si content increases because Zr and Si β stabilizers depress the transition temperature by stabilizing the β phase. The results of transformation temperatures DSC test showed that the transformation temperatures, Ms decreased after adding Zr, Si and after heat treatment for base alloy. The results of shape memory effect showed that the shape effect improved after adding (Zr and Si) and after heat treatment where the improvement ratio is (56.66, 76.36 and 70.44) % respectively.

The addition of Zr, and Si leads to higher values of hardness compared with the master alloy, where the improvement of percentage for highest percentage of addition of Zr, Si and after heat treatment process of base alloy was (48.55%, 29.6%, 72.4%) respectively. The wear resistance increases with the addition of Zr and Si where the improvement of wear rate for C3 alloy at 10 N reached 73% and 50 % at load 15 N, respectively, while the improvement percentage for D3 was (86.5%) and (76.5 %) at load (10, 15) N, respectively. The compressive strength of Ti-35%wt Nb alloy increases with increases Zr, and Si elements addition, but the compressive strength of master alloys with Zr additives is higher compared with master alloys with Si additives, where the improvement ratio is (57.62%) for C3 alloy while it is equal (34.31%) for D3 alloy. After the heat treatment process the compression strength improves significantly where the percentage of improvement (50.40%).

Due to the formation of the inert protective layer on the surface of the metal after the heat treatment process and after the addition of the elements (Zr and Si) it improves in corrosion resistance of Ti-35Nb alloy in Simulated body fluid and Hank's solutions. It was shown that higher improvement with the addition of the 6.9 % wt. Zr, the improvement was reach (176.8%) in Hank's solution, while the higher improvement in Simulated body fluid was (53%) for 0.6 wt.% Si. Also the results of immersion test in Simulated body fluid and hanks solutions showed that the amount of metal ion release significantly decrease after Zr and Si additions and after the heat treatment. The contact angle of the specimen decreases dramatically after heat treatment and addition Zirconium and Silicon.

Signature of scientific supervisor	Signature of supervisor on higher education in the collage

References

[1] Van Humbeeck, J., (1999). \Non-medical applications of shape memory alloys" Materials Science and Engineering: A, 273, pp. 134{148}.

[2] D. Kuroda, M. Niinomi, M. Morinaga, Y. Kato, T. Yashiro, (1998) Design and mechanical properties of new β type titanium alloys for implant materials 244 Mater. Sci. Eng. A 243.

[3] X. Tang, T. Ahmed, H.J. Rack, J. Mater, (2000) Phase transformations in Ti-Nb-Ta and Ti-Nb-Ta-Zr alloys Sci. 35 1805.

[4] D.M. Gordin, T. Gloriant, Gh. Nemtoi, R. Chelariu, N. Aelenei, A. Guillou, D. Ansel, (2005) . Synthesis, structure and electrochemical behavior of a beta Ti–12Mo–5Ta alloy as new biomaterial Mater. Lett. 59 2936.

[5] Y.L. Hao, S.J. Li, S.Y. Sun, R. Yang, (2006). Effect of Zr and Sn on Young's modulus and superelasticity of Ti–Nb-based alloys Mater. Sci. Eng. A 441 112.

[6] M. Niinomi, Metall, (2002) . Recent metallic materials for biomedical applications Mater. Trans. A 33 477.

[7] Bania PJ,(1994).Beta titanium alloys and their role in the titanium industry. JOM ;46:16–9.

[8].Hon YH, Wang JY, Pan YN,(2003). Composition/phase structure and properties of titanium-niobium alloys. Mater Trans ;44:2384–90.

[9] Chang L, Wang Y, Ren Y (2016). In-situ investigation of stress-induced martensitic transformation in Ti–Nb binary alloys with low Young’s modulus Mater Sci Eng A;651:442–8.

[10] Niinomi M,(. 2003) Recent research and development in titanium alloys for biomedical applications and healthcare goods. Sci Technol Adv Mater; 4:445.

[11] Luz AR, Santos LS, Lepienski CM et al (2018). Characterization of the morphology, structure and wettability of phase dependent lamellar

and nanotube oxides on anodized Ti-10Nb alloy. Appl Surf Sci;448:30–40.

[12] [H.Y. Kim, S. Hashimoto, J.I. Kim, T. Inamura, H. Hosoda, S. Miyazaki, (2006) Effect of Ta addition on shape memory behavior of Ti–-22Nb alloy Mater. Sci. Eng. A 417 120–128.

[13] S. Miyazaki, H.Y. Kim, H. Hosoda, Mater. Sci. Eng. A 438-440 (2006)_ Development and characterization of Ni-free Ti-base shape memory and superelastic alloys, 18-24.

[14] Y. Fukui,T. Inamura, H. Hosoda, K. Wakashima, S. Miyazaki, Mater. Trans. 45 (2004) ,Mechanical Properties of a Ti-Nb-Al Shape Memory Alloy, 1077– 1082.

[15] William D. Callister, Jr and David G.Rethwisch ,(2007) Materials Science and Engineering An Introduction', Seventh Edition , John Wiley & Sons, Inc.

[16] S L Angioni, MMeo and A Foreman, (2011), 'Impact Damage Resistance and Damage Suppression Properties of Shape Memory Alloys in Hybrid Composites—A Review', IOP Publishing Smart Materials and Structures, Vol. 20, PP 24, DOI: 10.1088/0964-1726/20/1/013001.

[17] M.S. Alam, M.A. Youssef and M. Nehdi, (2008),'Analytical Prediction of the Seismic Behaviour of Superelastic Shape Memory Alloy Reinforced Concrete Elements', Engineering Structures, Vol. 30, PP. 3399_3411, DOI:10.1016/j.engstruct.2008.05.025.

[18] Kauffman, G,Mayo ,(1993) I. memory metal. Chem matters Oct.

[19] L.G. Machado1& M.A.Savi (2003), "Medical applications of shape memory alloys", Brazilian Journal of Medical and Biological Research 36, pp. (683-691)

[20] Y J Chun, D S Levi, K P Mohanchandra, M C Fishbein and G P Carman, (2010),' Novel Micro-Patterning Processes for Thin Film NiTi Vascular Devices', Smart Materials and Structures, IOP Publishing, Vol.19, PP 9, DOI:10.1088/0964-1726/19/10/105021.

[21] S. Rahimipour, E. Salahinejad, E. Sharifi, H. Nosrati, L. Tayebi, (2020),' Structure, wettability, Corrosion and Biocompatibility of Nitinol Treated by Alkaline Hydrothermal and Hydrophobic Functionalization for Cardiovascular Applications', Journal Pre-proofs, DOI: 10.1016/j.apsusc.2019.144657.

[22] David G. Rabkin, Kevin J. Whitehead, Andrew D. Michaels, Douglas L. Powell and S.V. Karwande, (2009), 'Unusual Presentation of Nickel Allergy Requiring Explantation of an Amplatzer Atrial Septal Occluder Device', Clin. Cardiol. Vol. 32, No.8, E55–E57, DOI:10.1002/clc.20427.

[23] Kazuhiro et.al., (2002). "Scince and Technology of Shape-Memory Alloys: New Developments", MRS Bulletin, February

[24] GF. Andreasen & Fahl JL, (1987), "Shape Memory.In", Encyclopedia of medical devices and instrumentation, Volume 2.Wiley, New York, pp. (15-20).

[25] J. Haasters , G.V Salis –salis and G Bensmann , (1988) Engineering Aspect of Shape Memory alloys.

[26] S.W. Robertson et al ,(2006), "Effect of Product form and heat treatment on the Crstallographic texture of Austenitic Nitinol" Journal Materials Sciences,No.41pp.(621-630).

[27] Al-Humairi, A.N.S., et al.,(2022) BIOMATERIALS: A Multidisciplinary approaches and their related applications. White Falcon Publishing.

[28] Long, M. and H.J.B. Rack, (1998) Titanium alloys in total joint replacement—a materials science perspective.. 19(18): p. 1621-1639.

[29] S. Nmat -Nasser et al (2005),"High Strain-Rate, Small Strain Response of a NiTi Shape-Memory Alloy" Journal of Engineering Materials and Technology JANUARY, Vol. 127, pp (83-89)

[30] Rasha Ali Hussein,(2011),“Preparation and Characterization of NiTi Shape Memory Alloys”, MS.c thesis, University of Technology, Materials Engineering Department

[31] Machado LG & Savi MA (2003) Medical applications of shape memory alloys. Braz J.Med Biol Res 36: 683-691.

[32] Ozeki K, Yuhta T, Aoki H, Asaoka T, Daisaku T & Fukui Y (2003) Deterioration in the superelasticity of Ti sputter coated on NiTi orthodontic wire. Biomed Mater Eng 13:355-362

[33] L. Petrini and F. Migliavacca, (2011)” Biomedical Applications of Shape Memory Alloys” Journal of Metallurgy, Vol. 2011, Article ID 501483, 15 pages,

[34] L.G. Machado and M.A. Savi (2003) “Medical applications of shape memory alloys” Brazilian Journal of Medical and Biological Research , Vol. 36, PP 683-691 ISSN 0100-879 X

[35] Jonathan Black (2006), *Biological Performance of Materials: Fundamentals of Biocompatibility*, Fourth Edition, CRC Press, London

[36] Egon Perilli (2017), ‘Biomaterials, hard tissue’, lecture notes distributed in the topic ENGR7702 Biomaterials, Medical Device Research Institute, Flinders University, Bedford Park, 18 October

[37] Black J, Hastings GW (1998), *Handbook of biomaterials properties*, Chapman and Hall, London UK.

[38] Yuhua Li, Chao Yang, Haidong Zhao, Shengguan Qu, Xiaoqiang Li and Yuanyuan Li,(2014) ‘New Developments of Ti-Based Alloys for Biomedical Applications’, *Materials*, vol. 7, pp. 1709-1800.

[39] Sumner DR, Turner TM, Igloria R, Urban RM, Galante JO (1998), ‘Functional adaptation and ingrowth of bone vary as a function of hip implant stiffness’, *J Biomech*, vol.31, pp. 909–917.

[40] Huiskes R (1990), ‘The various stress patterns of press-fit, ingrown, and cemented femoral stems’, *Clin Orthop Relat Res*, vol. 261, pp.27-38 .

[41] Niinomi M, Hattori T, Morikawa K, Kasuga T, Suzuki A, Fukui H, et al. (2002), ‘Development of low rigidity β-type titanium alloy for biomedical applications’, *Mater Trans*, vol. 43, pp. 2970–7.

[٤2] Mohammed, M.T., Khan, Z.A. and Siddiquee, A.N. (2013) ‘Influence of Microstructural Features on Wear Resistance of Biomedical Titanium Materials’, In Proceedings of World Academy of Science, Engineering and Technology (WASET), Vol. 7, No. 1, pp.49-53.

[43] Tane, L., Cronee, W.C., Wilson, E.H. and Sridharan, K.,(2001) ‘Experimental Investigation of the Wear Behavior in Surface Modified NiTi’, University of Wisconsin, Madison, USA

[44] Fellah, M., Labaïz, M., Assala, O. and Iost, A. (2014) ‘Comparative Tribological study of biomaterials AISI 316L and Ti-6Al-7Nb’, TMS, 237, pp.237-246

[45] Bhushan, B. (2013) ‘Introduction to Tribology’, 2nd ed., John Wiley & Sons, Ltd.: New York, NY, USA.

[46] Valefi, M. (2012). 'Wear and Friction of Self-lubricating CuO-TZP Composites', PhD. Thesis, University of Twente, Enschede, the Netherlands .

.

[47] Aseel safe hemza (2013) ‘study of microstructure, corrosion and dry sliding wear of copper – aluminum- nickel shape memory alloys’, MS.C thesis , materials engineering college , university of Babylon / Iraq.

[48] Bayer, R.G. (2002) ‘Fundamentals of wear failures’, Materials Park, OH: ASM International, pp.901-905.

[49]Williams DF (2008) , ‘On the mechanisms of biocompatibility’, *Biomaterials*, vol. 29, pp. 2941–53.

[50] M. Geetha, A.K. Singh, R. Asokamani, A.K. Gogi (2009), ‘Ti based biomaterials, the ultimate choice for orthopaedic implants – A review’, *Progress in Materials Science*, vol. 54, pp. 397–425.

[51] Arne Biesiekierski, James Wang, Mohamed Abdel-Hady Gepreel, Cuie Wen (2012), ‘A new look at biomedical Ti-based shape memory alloys’, *Acta Biomaterialia*, vol. 8, pp. 1661–1669

[52] Nugroho, A.W. (2013) ‘Investigation of the Production and Mechanical Properties of Porous Beta Titanium Alloy Compacts Prepared by Powder Metallurgy Processes for Biomedical Applications’, Curtin University of Technology.

[53] Bhola, R., Bhola, S.M., Mishra, B. and Olson, D.L. (2011) ‘Corrosion in titanium dental implants/prostheses–a review’, Trends Biomater Artif Organs, Vol. 25, No. 1, pp.34-46.

[54] Qari T., Almadani A. and Bukhary E. (2016) ‘To The Point Review of Implant Materials Corrosion’, EC Dental Science, Vol. 5, No. 2, pp.1025-102

[55] Agarwal, S., Curtin, J., Duffy, B. and Jaiswal, S. (2016) ‘Biodegradable magnesium alloys for orthopaedic applications: A review on corrosion, biocompatibility and surface modifications’, Materials Science and Engineering C, Vol. 68, pp.948-963.

[56] Antunes, R.A. and de Oliveira, M.C.L. (2012) ‘Corrosion fatigue of biomedical metallic alloys: mechanisms and mitigation’, Acta biomaterialia, Vol. 8, No. 3, pp.937-962. 9.

[57] Manivasagam, G., Dhinasekaran, D. and Rajamanickam, A. (2010) ‘Biomedical implants: corrosion and its prevention-a review’, Recent patents on corrosion science, Vol. 2, pp.40-54.

[58] Wang, K.J.M.S. and E. A, (1996) *The use of titanium for medical applications in the USA*.. 213(1-2): p. 134-137.

[59] WJ. Buehler &Wang FE, (1978), "A summary of Recent Rsearch on the Nitinol Alloys and their potential Application in Engineering". Ocean Eng. 1, pp. (105-120).

[60] Kazuhiro et.al., (2002). "Scince and Technology of Shape-Memory Alloys: New Developments", MRS Bulletin, February

[٦1] L.G. Machado1& M.A.Savi, (2003) "Medical applications of shape memory alloys", Brazilian Journal of Medical and Biological Research 36, pp. (683-691)

[62] FJ. Gil &Planell J, (1998), "A In Vitro Thermomechanical Ageing of Ni-TiAlloys", pp. (237-248).

[63] J.T. Hong , T. J. Kim , S. N. Hong , Y.H. Kim , D. K. Chang & E. R. Kim"(2020) "Uncovered self-expandable metal stents for the treatment of refractory benign colorectal anastomotic stricture 10:19841.

[64] E. Darel Hodgoson, ,(1999). "Shape Memory Alloys- Applications and Commercial Aspects", Memory Technologies, shape Memory Alloys

[٦5] A. Verstrynge, J. Van Humbeeck, and G. (2006) Willems, "In-vitro evaluation of the material characteristics of stainless steel and beta-titanium orthodontic wires," American journal of orthodontics and dentofacial orthopedics, vol. 130, pp. 460-470,

[66] C. Leyens and M. Peters, (2003) Titanium and titanium alloys: fundamentals and applications: John Wiley & Sons,.

[67] G. Bedinger, (2014)"Mineral Commodity Summaries: Titanium and Titanium Dioxide," US Geological Survey, Washington DC, USA, pp. 170-171,.

[68] J.R. Davis Davis & Associates (2003). International, Handbook of materials for medical devices.

[69] P. B. Vila, (2015) "Phase transformation kinetics during continuous heating of α+ β and metastable β titanium alloys."

[70]. Niinomi, M.J.M. and m.t. (2002) A, *Recent metallic materials for biomedical applications.*. 33(3): p. 477.

[71] Al-Humairi, A.N.S., et al., BIOMATE RIALS: A Multidisciplinary approaches and their related applications. White Falcon Publishing.

[72]. Manam, N., et al.,(2017) Study of corrosion in biocompatible metals for implants: A review.. 701: p. 698-715.

[73] Guimaraes, Z.A., et al.,(2017) A Novel Porous Diamond-Titanium Biomaterial: Structure, Microstructure, Physico-Mechanical Properties and Biocompatibility. 89(4): p. 3111-3121

[74] Davis, J.R., Handbook of materials for medical devices.(2003).

[75] Pilliar, R. and G.J.C.C.r.i.B. Weatherly, (1986) Developments in implant alloys.. 1: p. 371-403.

[76] Mishra, A.K., et al., (1996) Mechanical and tribological properties and biocompatibility of diffusion hardened Ti-13Nb-13Zr—a new titanium alloy for surgical implants, in Medical Applications of Titanium and Its Alloys: The Material and Biological Issues., ASTM International.

[77]-Long, M. and H.J.B. Rack, (1998) Titanium alloys in total joint replacement—a materials science perspective.. **19**(18): p. 1621-1639.

[78]-Xu, Y., H.J.J.o.t.J.S.o.P. (2001) Nomura, and P. Metallurgy, Homogenizing analysis for sintering of bio-titanium alloy (Ti-5Al-2.5 Fe) in MIM process.. **48**(11): p. 1089-1096

[79]. Fujita, M.J.K.G.z.T.J.o.t.S.S., (1993) Japan, In vitro study on biocompatibility of zirconium and titanium.. **60**(1): p. 54-65.

[80]. Gahlert, M., et al., (2007) Biomechanical and histomorphometric comparison between zirconia implants with varying surface texture and a titanium implant in the maxilla of miniature pigs.. **18**(5): p. 662-668

[81]. Assal, P.A.J.S.M.f.Z.R.m.s.d.o.-s.R.m.s.d.o.e.s.,(2013) *The osseointegration of zirconia dental implants.*. **123**(7-8): p. 644-654.

[82] E.M. Carlisle: Science, (1972), **178**, 619.

[83] E.M. Carlisle: J. Nutr., (1980,) **110**, 1046.

[84] F.H. Nielsen and R. Poellot: J. Trace. Elem. Exp. Med., (2004), **17**, 137.

[85] R. Jugdaohsingh, K.L. Tucker, N. Qiao, L.A. Cupples, D.P. Kiel and J.J. Powell: J. Bone. Miner. Res., (2004), **19,** 297.

[86] D.M. Reffitt, N. Ogston, R. Jugdaohsingh, H.F. Cheung, B.A. Evans, R.P. Thompson, J.J. Powell and G.N. Hampson: Bone, (2003), **32**, 127.

[87] I.D. Xynos, A.J. Edgar, L.D. Buttery, L.L. Hench and .M. Polak: J. Biomed. Mater. Res., (2001), **55**, 151

[88].Zhao S P, Lv S K and Hao W J 2003, ‘Titanium Alloys and Surface Modification’, Harbin: Harbin Institute of Technology Press.

[89]- K.H.Eckelmeyer et al (1984) The effect of quench rate on the microstructure, mechanical properties, and corrosion behavior of U-6 wt pct Nb pages1319–1330.

[٩0] W. L. Downs, J. K. Scott, C. L. Yuile, F. S. Caruso, and L. C. Wong, (1965) "The toxicity of niobium salts," American Industrial Hygiene Association Journal, vol. 26, pp. 337- 346,.

[91]- M. Caicedo, J. J. Jacobs, A. Reddy, and N. J. Hallab, "Analysis of metal ion-induced DNA damage, apoptosis, and necrosis in human (Jurkat) T-cells demonstrates Ni2+ and V3+ are more toxic than other metals: Al3+, Be2+, Co2+, Cr3+, Cu2+, Fe3+, Mo5+, Nb5+, Zr2+," Journal of Biomedical Materials Research Part A, vol. 86, pp. 905 -913,.

[92] Q. Chen and G. A. Thouas, (2015) "Metallic implant biomaterials," Materials Science and Engineering: R: Reports, vol. 87, pp. 1 -57,.

[93]-INAMURA T, HOSODA H, WAKASHIMA K, MIYAZAKI S. (2005) Anisotropy and temperature dependence of Young's modulus in textured TiNbAl biomedical shape memory alloy [J]. Materials Transactions, , 46(7): 1597−1603.

[94] MASAHASHI N, MIZUKOSHI Y, SEMBOSHI S, OHTSU N, JUNG T, HANADA S (2010),. Photo-induced characteristics of a Ti–Nb–Sn biometallic alloy with low Young's modulus [J]. Thin Solid Films, 519(1): 276−283.

[95] MIYAZAKI S, KIM H, HOSODA H. (2006) Development and characterization of Ni-free Ti-base shape memory and superelastic alloys [J]. Materials Science and Engineering A, , 438: 18−24.

[96] HEY J, JARDINE A. (1994) Shape memory TiNi synthesis from elemental powders [J]. Materials Science and Engineering A, , 188(1): 291−300.

[97] MORRIS D, MORRIS M. (1989) NiTi intermetallic by mixing, milling and interdiffusing elemental components [J]. Materials Science and Engineering A, , 110(1): 139−149.

[98] ZHAO D, CHANG K, EBEL T, NIE H, WILLUMEIT R, PYCZAKF. (2015) Sintering behavior and mechanical properties of a metal injectionmolded Ti−Nb binary alloy as biomaterial [J]. Journal of Alloys andCompounds, , 640: 393−400.

[99] KAFKAS F, EBEL T. (2014) Metallurgical and mechanical properties of Ti−24Nb−4Zr−8Sn alloy fabricated by metal injection molding [J]. Journal of Alloys and Compounds, , 617: 359−366.

[100] ALEKSANYAN A, DOLUKHANYAN S, SHEKHTMAN V S, KHASANOV S, TER-GALSTYAN O, MARTIROSYAN M. (2012) Formation of alloys in the Ti−Nb system by hydride cycle method and synthesis of their hydrides in self-propagating high-temperature synthesis [J]. International Journal of Hydrogen Energy, , 37(19): 14234−14239.

[101] MA L W, CHUNG C Y, TONG Y, ZHENG Y. (2011) Properties of porous TiNbZr shape memory alloy fabricated by mechanical alloying

and hot isostatic pressing [J]. Journal of Materials Engineering and Performance, , 20(4−5): 783−786.

[102] WEN M, WEN C, HODGSON P, LI Y. (2014) Fabrication of Ti−Nb−Ag alloy via powder metallurgy for biomedical applications [J]. Materials & Design, , 56: 629−634.

[103] TERAYAMA A, FUYAMA N, YAMASHITA Y, ISHIZAKI I, KYOGOKU H. (2013) Fabrication of Ti−Nb alloys by powder metallurgy process and their shape memory characteristics [J]. Journal of Alloys8−s412. and Compounds, , 577: s40

[104] WANG X, CHEN Y, XU L, LIU Z, WOO K D. (2013) Effects of Sn content on the microstructure, mechanical properties and biocompatibility of Ti−Nb−Sn/hydroxyapatite biocomposites synthesized by powder metallurgy [J]. Materials & Design, , 49: 511−519.

[105] OGHBAEI M, MIRZAEE O. (2010) Microwave versus conventional sintering: A review of fundamentals, advantages and applications [J]. Journal of Alloys and Compounds, , 494(1): 175−189

[106] ROY R, AGRAWAL D, CHENG J, GEDEVANISHVILI S. (1999) Full sintering of powdered-metal bodies in a microwave field [J]. Nature399(6737): 668−670.

[107] DAS S, MUKHOPADHYAY A, DATTA S, BASU D. (2009) Prospects of microwave processing: An overview [J]. Bulletin of Materials Science,32(1): 1−13.

[108] MOUR M, DAS D, WINKLER T, HOENIG E, MIELKE G, MORLOCK M M, SCHILLING A F. (2010) Advances in porous biomaterials for dental and orthopaedic applications [J]. Materials, 3(5): 2947−2974

[109] RYAN G, PANDIT A, APATSIDIS D P. (2006), Fabrication methods of porous metals for use in orthopaedic applications [J]. Biomaterials, 27(13): 2651−2670.

[110] XU J, BAO L, LIU A, JIN X, TONG Y, LUO J, ZHONG Z,(2015) biomedical porous NiTi alloy prepared by microwave sintering [J]. Materials Science and Engineering C, , 46: 387−393.

[111] GEETHA M, SINGH A, ASOKAMANI R, GOGIA A. (2009) Ti based biomaterials, the ultimate choice for orthopaedic implants—A review[J]. Progress in Materials Science, , 54(3): 397−425.

[112] NIINOMI M. (2008) Metallic biomaterials [J]. Journal of Artificial Organs, , 11(3): 105−110.

[113] H.S. Kim, S.H. Lim, I.D.Yeo,W.Y. Kim, Mater. Sci. Eng. 449–451A (2007) 322.

[114] C.R.M. Afonso, G.T. Aleixo, A.J. Ramirez, R. Caram, Mater. Sci. Eng. 27C (2007) 908–913

[115] J.R. Newman, D. Eylon, J.K.(1988) Thorne, Titanium and Titanium Alloys, Metals Handbook, ASM International, Metals Park, OH, USA, , p. 824.

[116] A. Choubey, R. Balasubramaniam, B. Basu, J. Alloys Compd (2004),. 381 288.

[117] C.J. Boehlert, C.J. Cowen, J.P. Quast, T. Akahori, M. Niinomi, (2008) Mater. Sci. Eng. 28) 323–330.

[118] L.J. Xu, Y.Y. Chen, Z.G. Liu, F.T. Kong, J. (2006) Alloys Compd. 453
١١٩] Y. Mantani, M. Tajima, (2006) , Mater. Sci. Eng 43–440A 315.

[120] E.B. Taddei, V.A.R. Henriques, C.R.M. Silva, C.A.A. (2004) Cairo, Mater. Sci. Eng. 24C 683.

[121] Y.H. Hon, J.Y. Wang, Y.N. Pan, (2003) . Metall. Mater. Trans. 44 2384.

[١٢2] Vinarcik, E.J ,(2002) *High integrity die casting processes*.: John Wiley & Sons.

[١٢3] Callister, W.D. and D.G. (2011) Rethwisch, *Materials science and engineering*. Vol. 5.: John wiley & sons NY.

[١٢4] Erdem,O.J.U.M.A.v.G.D.,(2017)The Development and Applications of Powder Metallurgy Manufacturing Methods in Automotive Industry**9**(3): p. 100-112.

١25] Kipouros, G., et al., (2006) On the advantages of using powder metallurgy .

[126] Groover, M.P., Introduction to manufacturing processes. (2011): Wiley Global Education.

[127] Sharma, P.J.S.C. and Co. Ltd. (2004) Publications, Production Technology. 58.

[128] Rajput, R.,(2007) A textbook of manufacturing technology: Manufacturing processes.: Firewall Media.

[129]. Hammi, Y., et al. (2010) Fatigue Modeling of a Powder Metallurgy Main Bearing Cap. in SIMULIA Customer Conference..

[١٣0] Rao, K.V., (2002) Manufacturing Science And Technology- Manufacturing Processess And Machine Tools.: New Age International

[١٣1]Sinka, C.J.K.P. and P. Journal, (2007) Modelling powder compaction. **25**: p. 4-22.

[١٣2] Groover, M.P,(2007) Fundamentals of modern manufacturing: materials processes, and systems.: John Wiley & Sons.

[١٣3] Shatokha, V, (2010)., Sintering: Methods and products.: BoD– Books on Demand.

[١٣4] Meluch, L., (2010) Warm compaction of aluminium alloy Alumix, , University of Birmingham. 123.

[135] Fang, Z.Z., *Sintering of advanced materials*.: Elsevier.

[136] B. L. Wang, Y. F. Zheng* and L. C. (2009) Electrochemical corrosion behavior of biomedical Ti–22Nb and Ti–22Nb–6Zr alloys in saline medium 60, No. 10

[137] L.W. Ma, C.Y. Chung, Y.X. Tong, and Y.F. Zheng, (2011).Properties of Porous TiNbZr Shape Memory Alloy Fabricated by Mechanical Alloying and Hot Isostatic Pressing 20:783–786

[138] Eliene Nogueira de Camargo, et al ,(2012) Production of Ti-22Nb-6Zr Shape Memory Alloy by Powder Metallurg -36-0467

[139] Ana L´ ucia Roselino Ribeiro1, (2013) TiNbZr alloys potential substitutes of the Ti6Al4V alloy for dental applications? An electrochemical corrosion study 065005 (11pp).

[140] Terayamaa,∗, N.Fuyamaa, Y.Yamashitab, I.Ishizaki b, H.Kyogokuc. (2013) . Fabrication of Ti–Nb alloys by powder metallurgy process and their shape memory characteristics Department of Mechanical Engineering, Faculty of Engineering, Kinki University 577S S408–S412

[141] M Lai, Y Gao, (2014) Indirect determination of martensitic transformation temperature of sintered nickel-free Ti–22Nb–6Zr alloy by low temperature compression test. https://doi.org/10.1016/j.matdes.2014.03.067.

[142] Bai Y, Deng Y, Zheng Yet al. (2014) Characterization, corrosion behavior, cellular response and in vivo bone tissue compatibility of titanium–niobium alloy with low Young's modulus. Mater Sci Eng C;59:565–76.

[143] A. M. G. Tavaresa, W. S. Ramosa, J. C. G. de Blasb, E. S. N. Lopesc, R. Caramc, W. W. Batistaa, S. A. Souzaa. (2015), Influence of Si addition on the microstructure and mechanical properties of Ti-35Nb alloy for applications in orthopedic implants Department of Materials Science and Engineering, Federal University of Sergipe, 49100-000

[144] Mazyan Yahaya1,2,a, Salhana Sahidin@Salehudin2 et al ,(2016) Microstructures and Mechanical Properties Of Ti-Nb Alloy at Different Composition of Nb Produced Via Powder Metallurgy Route Materials Science Forum Submitted: ISSN: 1662-9752, Vol. 863, pp 14-18

[145] Jie Wu, Hua Li, Bin Yuan, Yan Gao (2017) High Recoverable Strain Tailoring by Zr adjustment of sintered Ti-13Nb-(0-6)Zr biomedical

alloys School of Materials Science and Engineering, South China University of Technology Guangzhou 510641, PR China

[146] E. Yilmaza;*, A. Gökçeb, F. Findika;b and H.Ö. Gülsoyc (2018) Powder Metallurgy Processing of Ti–Nb Based Biomedical Alloys Sakarya University, Sakarya, 54187.

[147] Mustafa K. IBRAHIM1, E. HAMZAH1, Safaa N. SAUD2, E. M. NAZIM1, A. BAHADOR1 (2018) Parameter optimization of microwave sintering porous Ti−23%Nb shape memory alloys for biomedical applications , Management & Science University, 401 00 Shah Alam, Selangor, Malaysia

[148] Yuqing Zhang ,Danni Sun et al (2019) Mechanical and biological properties of Ti–(0–25 wt%)Nb alloys for biomedical implants Application .doi: 10.1093/rb/rbz042

[149] Elena O. Nasakina et al (2020) Obtaining a Wire of Biocompatible Superelastic Alloy Ti–28Nb–5Zr Institution of Russian Academy of Sciences, Leninsky Prospect, 49, 119991 Moscow, Russia

[150] Kyong Min Kim 1, Hee Young Kim et al (2020) E_ect of Zr Content on Phase Stability, Deformation Behavior, and Young's Modulus in Ti–Nb–Zr Alloys University of Tsukuba, Tsukuba, Ibaraki 305-8573, Japan

[151] Yuya Ishiguro , Yuhki Tsukada, Toshiyuki Koyama. (2020), Phase-field study of the spinodal decomposition rate of β phase in oxygenadded Ti–Nb alloys Department of Materials Design Innovation Engineering, Nagoya University, Furo-cho, Chikusa-ku, Nagoya 464-8603,

[152] H.-W. Liu, D.P. Bishop, K.P. Plucknett (2013)"Effect of processing variables on production of powder metallurgical titanium Can. Metall. Q. 52, 39.

[153] de Oliveira CSS, Griza S, de Oliveira MV, Ribeiro AA, Leite MB (2015) Study of the porous Ti35Nb alloy processing parameters for implant applications, Powder Technol. 281: 91–98

[154] ASTM B-328 (2003) Standard Test Method for Density, Oil Content, and Interconnected Porosity of Sintered Metal Structural Part and Oil –Impregnated Bearing, ASTM international

[155] M. H. Wu, T.W Duerig , K.N. Melton , D. Stockel and C. M. Wayman , [1990] Cu-based shape memory alloys , In Engineering Aspects of shape memory alloys , ,P.96.

[156] Khilfa, A. H. (2015) "Effect of Y and Ge addition on Mechanical properties and Corrosion behavior of Biomedical CoCrMo Alloy (F75) ", MSc thesis, University of Babylon, Iraq.

[157] Jawad, M. S., (2015) "Effect of (Cu & Cr) Additives on Corrosion and Dry Sliding Wear of NiTi Shape Memory Alloy", MSc thesis, Submitted to the Council of the College of Materials engineering /University of Babylon

[158]-Sasmita, F., Wibisono, G., Judawisastra, H., & Priambodo, T. A. (2018), Determination of elastic modulus of ceramics using ultrasonic testing. In AIP Conference Proceedings (Vol. 1945, No. 1, p. 020017).

[159] Tkacz, J.; Slouková, K.; Minda, J.; Drábiková, J.; Fintová, S.; Doležal, P.; Wasserbauer, J. (2016) Corrosion behavior of wrought magnesium alloys AZ31 and AZ61 in Hank"s solution. Koroze a Ochrana Materiálu, 60, 101–10.

[160] Y.W.GU, et al .(2003) In vitro studies of plasma-sprayed hydroxyapatite/Ti-6Al-4V composite coatings in simulated body fluid (SBF) Pages 1603-1611

[161] Jaber, H.H. (2014) " The Effect of Addmixed Ti on Corrosion Resistant of High Copper Dental Amalgam" journal of Babylon University, Vol. 22, No.2, pp.413-421.

[162] Hanawa, T. (2004) 'Metal ion release from metal implants', Materials Science and Engineering: C, Vol. 24, No. 6-8, pp.745-752.

[163] A Lakshmanan ,(2012) "sintering of ceramics –New emerging techniques " in tech web .org. Croatia.

[164] L.E. Penrod, ,dx(2003) Fabrication and characterization of porous shape memory alloys , Master diss., Texas A& M university ,.

[165]-Niinomi M. Biomaterials (2003);.Mechanical, physical, and chemical characterization of Ti–35Nb–5Zr and Ti–35Nb–10Zr casting alloys.24:2673–83

[166] Won-Yong Kim et al (2007) Microstructure and Pseudoelasticity of Ti-Nb-Si Based Alloys with Biocompatible Alloying Elements doi:10.4028/www.scientific.net/MSF.546-549.2151.

[167] Nawal M. D.,(2014) "Preparation And Characterization Of Bio Nitinol With Addition Of Copper" PhD. thesis, materials engineering department , university of technology/ Iraq.

[168] Wagner, W.R., Sakiyama-Elbert, S.E., Zhang, G. and Yaszemski, M.J. eds., (2020). "Biomaterials science: An introduction to materials in medicine". 4th ed, Academic Press ,Elsevier.

[169] Tripathy, I., (2011), "Effect of Microstructure on Sliding Wear Behaviour of Modified 9Cr-1Mo steel" , MS.C thesis , Metallurgical and Materials Engineering, National Institute of Technology, Rourkela.

[170] Li, L., Kim, M., Lee, S., Bae ,M.,& Lee, D.,(2016) "Influence of multiple ultrasonic impact treatments on surface roughness and wear performance of SUS301 steel", Surface and Coating Technology, Vol.307, pp.517-524.

[171]. Nie, L., Zhan, Y., Hu, T., Chen, X., & Wang, C. (2014). β-Type Zr–Nb– Ti biomedical materials with high plasticity and low modulus for hard tissue replacements. Journal of the mechanical behavior of biomedical materials, 29, 1-6.

[172] Sun-Ki Kim et al (2008). Dry Sliding Wear Characteristics of Ti-Nb-Si Alloys for Biomedical Application, Materials Science Forum Vol 569 pp 149-152. doi:10.4028/www.scientific.net/MSF.569.149

[173] R. Singh And N. B. Pahotre ,(2007) " Corrosion Degradation And Prevention By Surface Modification Of Bio Metallic Materials" , J Mat. Sci: Mater, Vol. 18, , pp. 725 – 751.

[174] Mehmet Kaya et al (2019) Microstructure characterization and biocompatibility behaviour of TiNbZr alloy fabricated by powder metallurgy https://doi.org/10.1088/2053-1591/ab58a5

[175] Sarkar, N.K. and Greener, E.H., (1974) "Corrosion behavior of the tin-containing silver-mercury phase of dental amalgam". *Journal of dental research*, Vol.*53,* No.4, pp.925-932.

[176] Hansen, D. C. (2008). Metal corrosion in the human body: the ultimate bio-corrosion scenario. The Electrochemical Society Interface, 17(2),31.